Copyright

by

Raymond Charles Zowarka, Jr.

2003

**The Dissertation Committee for Raymond Charles Zowarka, Jr. Certifies that this is the approved version of the following dissertation:**

# Electrodynamics of a Hypervelocity Surface Conversion Process Using Electromagnetic Accelerators

**Committee:**

Mircea D. Driga, Supervisor

Ross Baldick

Martin L. Baughman

William M. Grady

Henry G. Rylander, Jr.

# Electrodynamics of a Hypervelocity Surface Conversion Process Using Electromagnetic Accelerators

by

**Raymond Charles Zowarka, Jr., B.S.E.S., M.S.E.E.**

**Dissertation**

Presented to the Faculty of the Graduate School of

The University of Texas at Austin

in Partial Fulfillment

of the Requirements

for the Degree of

**Doctor of Philosophy**

**The University of Texas at Austin**

**December 2003**

## Dedication

This dissertation is dedicated to my parents,

Raymond, Sr. and Mary Lou Zowarka,

for their support and love.

## Acknowledgments

I would like to thank my advisor, Dr. Mircea Driga for his guidance and support during my graduate studies in electrical engineering. I have known Dr. Driga since 1974 and he has given constant encouragement for me to pursue an advanced degree. I also want to thank Drs. Ross Baldick, Martin Baughman, Mack Grady, and Grady Rylander for serving on my committee.

Many colleagues at The University of Texas at Austin Center for Electromechanics (UT-CEM) made contributions to this research. I want to thank Dr. John Uglum who participated in the theoretical work and developed many of the system simulations for analyzing the process: Mr. James Bacon who was project engineer during the development and construction of the pulsed power supply; Mr. Bobby Sledge, mechanical engineer, performed many of the tests on the plasma arc starter and constructed the square bore launcher; Mr. Darwin Davis, control engineer, was instrumental in designing and constructing the repetitive control system; Mr. Ben Rech, mechanical engineer, constructed the augmented railgun; and Mr. Bob Polizzi who is an excellent technician and knowledgeable in all aspects of the system helped conduct experiments and manufactured many system components.

Many of the critical components were built in our laboratory at UT-CEM. I want to thank machinist Del Beltran for his expert craftsmanship and dedication to this project. This research was sponsored by the United States Air Force, Tinker Air Force Base at Oklahoma City through a contract administered by

ARINC Corporation. Special thanks go to Mr. Thanh Nguyen of ARINC Corporation for preparing the metallurgical samples.

Finally, I want to thank Lori Moore and Patrice Palmer of UT-CEM for their help with graphics and word processing software.

**Electrodynamics of a Hypervelocity Surface Conversion Process Using Electromagnetic Accelerators**

Publication No. _____

Raymond Charles Zowarka, Jr., Ph.D.

The University of Texas at Austin, 2003

Supervisor: Mircea D. Driga

The U.S. Government and commercial entities are dependent on chemical plating and coating processes to replace worn or eroded material on damaged parts. Logistics Centers have been forced to consider replacement materials for repair operations due to tightening of government regulations on the use of toxic and hazardous materials.

Existing state of the art thermal spray processes (HVOF, D-gun, Plasma Spray) are limited to powder velocities of about 1 km/s because they rely on the thermodynamic expansion of gases. Because these methods rely on the mechanical bonding of the powder to the substrate the coatings and their bonds are a fraction of the parent material strength. To make full use of this repair process the coating has to bond to substrate with near parent material strength and coating has to build with good strength layer to layer. A new thermal spray process using

electromagnetic forces can accelerate powder particles to a final velocity in excess of 2 km/s. At this velocity powder particles have sufficient kinetic energy to melt their own mass and an equivalent substrate mass on impact. The kinetic energy of the process allows fusion bonding of greater strength than that created by low velocity processes as well as improved coating density.

This dissertation describes the invention of the Electromagnetic Powder Deposition (EPD) process. The railgun process is combined with a gas dynamic mechanism, called a snowplow, to produce controllable bursts of gas with the speed and duration required to accelerate finite segments of dispersed powder to the conditions required for plating purposes. The physics of the railgun and snowplow process are presented and proof of principle experiments is described. A method to start a planar arc in repetitive fashion had to be developed. An added complexity was that the source had to be stable at atmospheric pressure. A repetitive discharge power supply, instrumentation and control system had to be developed. To industrialize the process it had to be demonstrated that the process could build multiple layers with good bond strength layer to layer.

# TABLE OF CONTENTS

# LIST OF TABLES

# LIST OF FIGURES

# CHAPTER 1: INTRODUCTION

## Electromagnetic Powder Deposition: Background

The U.S. Government and commercial entities are dependent on chemical plating and coating processes to replace worn or eroded material on damaged parts. Logistics Centers have been forced to consider replacement materials for repair operations due to tightening of government regulations on the use of toxic and hazardous materials.

Existing state of the art thermal spray processes (HVOF, D-gun, Plasma Spray) are limited to powder velocities of about 1 km/s because they rely on the thermodynamic expansion of gases. State of the art processes are described in [1]. Because these methods rely on the mechanical bonding of the powder to the substrate the coatings and their bonds are a fraction of the parent material strength. To make full use of this repair process the coating has to bond to substrate with near parent material strength and coating has to build with good strength layer to layer. A new thermal spray process using electromagnetic forces can accelerate powder particles to a final velocity in excess of 2 km/s. At this velocity powder particles have sufficient kinetic energy to melt their own mass and an equivalent substrate mass on impact. The kinetic energy of the process allows fusion bonding of greater strength than that created by low velocity processes as well as improved coating density.

This dissertation describes the invention of the Electromagnetic Powder Deposition (EPD) process [2]. The railgun process is combined with a gas dynamic mechanism, called a snowplow [3], to produce controllable bursts of gas with the speed and duration required to accelerate finite segments of dispersed powder to the conditions required for plating purposes. The physics of the railgun and snowplow process are presented and proof of principle experiments is described. A method to start a planar arc in repetitive fashion had to be developed. An added complexity was that the source had to be stable at atmospheric pressure. A repetitive discharge power supply, instrumentation and control system had to be developed. To industrialize the process it had to be demonstrated that the process could build multiple layers with good bond strength layer to layer.

The Electromagnetic Powder Deposition (EPD) process was developed at Center for Electromechanics (CEM) as a method of imparting high velocities to powder particles [4]. Figure 1 compares several thermal spray processes in terms of particle velocity and gas temperature and shows how EPD performs. What is unique to the EPD approach is that the use of electromagnetic railgun force means that the gas flow velocity can be as high as desired, and is not limited by any chemical or thermodynamic constraints. The process has promise of greatly improving bond strength and coating density if empirical scaling trends continue with increasing velocity.

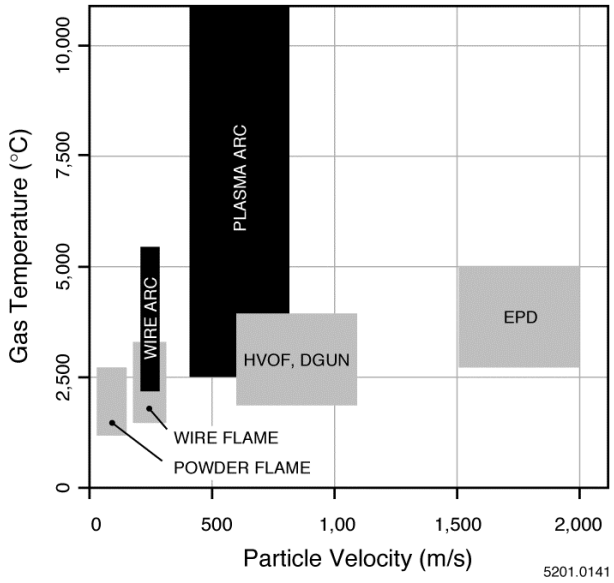


Figure 1. Comparison of conventional thermal spray process to the EPD method

The railgun is filled with an ionizable gas, and a radio frequency (RF) excited cavity at the breech of the accelerator provides a line source of plasma. A high energy electrical pulse, provided by a pulsed energy source, expands the line source into a planar arc which is driven forward by electromagnetic forces. The arc is an efficient snowplow sweeping the gas in the bore to a final velocity approximately twice desired powder velocity. Figure 2 shows such a snowplow system operating in ½ atmosphere Xenon from work done in the late 1970s.

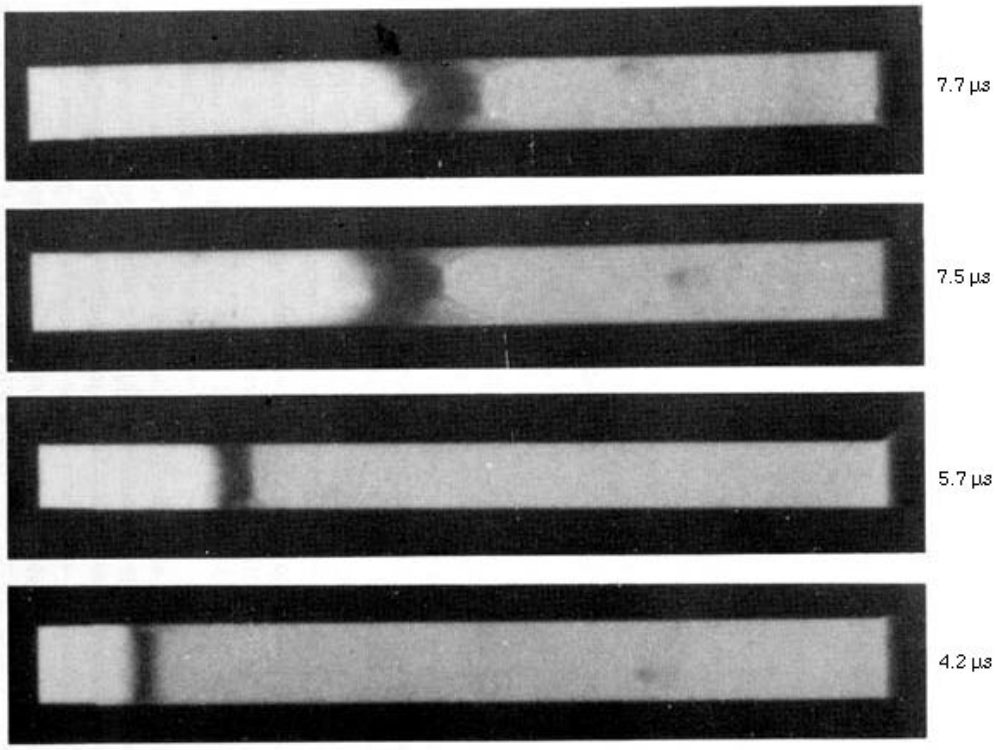


Figure 2. Shearer demonstrated the snowplow process in 1970

The gun length and current pulse is tailored such that the plasma arc is extinguished as the gas column reaches the powder ports into the railgun bore. The hot plasma does not interact with the powder or the substrate surface. The shocked gas passes over a powder cloud introduced near the end of the gun and accelerates the powder through drag forces. The electrical and powder discharge frequency can be adjusted so that the deposition rate and thermal input to the substrate can be controlled (fig. 3).

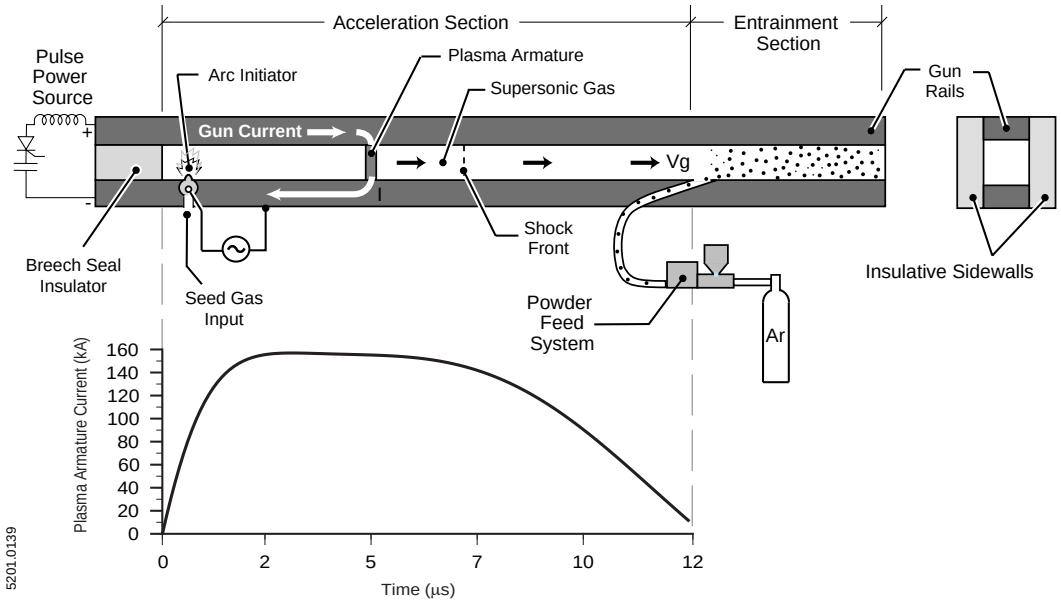


Figure 3. The EPD process utilizes an electromagnetic accelerator to form a dense, high velocity gas column that passes over injected powder to produce spray product

The process has the ability to control the thermal input to the substrate because it is pulse driven as opposed to continuous. The process of forming and accelerating the snowplow arc can be unstable. A special current pulse to drive the process has been specified to avoid plasma instabilities. The process has been designed to operate at atmospheric pressure for ease of use and cost savings. A special RF excitation source and arc generation cavity have been designed to allow the initiation plasma to form at atmospheric pressure. A special manifold has been designed for the end of the gun to keep the substrate flooded with inert gas thereby preventing target oxidation. Because the process uses a snowplowed gas

column to accelerate the powder with drag forces, both conducting and nonconducting powders may be sprayed.

This process can be used to build up coatings of parent material strength because it has the potential to create a fusion bond with the substrate. It can build up the material with less heat input than a welding process therefore mitigating substrate warpage. The more energetic impact will create denser coatings. It can be used to apply chrome to substrates therefore avoiding the generation of environmentally hazardous hexavalent chrome, a byproduct of electroplating. Insulating materials may also be sprayed. Due to the improved bond strength material build up may be possible allowing the formation of macro structures.

### *Arc Starter*

One of the most challenging aspects of the research was to create a continuous source of plasma in the breech of the gun in order to make the process rep-ratable. Previous plasma driven railguns had clamped a fuse material between the rails and exploded the fuse as a planar source of plasma. To implement this in the EPD process would have required an automated fuse loader. This was deemed complex and unreliable. In addition, the arc products would have been metallic in nature and held the prospect of contaminating the coatings. It was understood that a plasma source could be created, but the experience base was in creating plasma in partial pressures. Glow discharges were familiar in different lamps and vacuum tubes. For the process to be versatile it would have to operate at atmospheric pres-

sure. An experimental program was undertaken where familiar glow discharges in vacuum were created with ac and dc sources and then the pressure increased to observe if the discharge could be maintained at atmospheric pressure. All combinations of gas and electrical sources failed as the pressure was raised. The arc would collapse to a filament which was not the correct source geometry for creating a planar arc to drive the snowplow process. The search was started for an electrical source that would provide the correct energetics to maintain a diffuse arc as the pressure increased. The search narrowed to radio frequency (RF) sources. An RF source was procured and it was determined that at 150 MHz, line source of argon plasma could be reliably sustained at 1 atmosphere pressure.

***Proof of Principle Experiments***

With a reliable constant source of plasma in the breech of the gun focus changed to demonstrating the snowplow process. A highly instrumented proof of principle experiment was designed to verify the process operation. A ½ m long square bore railgun with a transparent sidewall was designed and manufactured. The transparent sidewall allowed for high speed photography of the plasma armature to verify stability and velocity. In addition to photography, the experiment was instrumented with electromagnetic b-dot probes, fiber optics, and pressure transducers. The b-dot probes respond to the magnetic signature of the arc and are a reliable gauge of the arc position in time. The fiber optic probes sense the light emitted by the plasma and also record the arc position as a function of time. The pressure transducers sense the gas pressure of the snowplow column and confirm the ability of the arc to sweep up and accelerate the gas. The photography not only

confirms arc position as a function of time it also allows evaluation of the viscous drag acceleration of micro particles. Operating the high speed instrumentation in the presence of the RF source and pulsed power supply required special attention to shielding and grounding techniques. A single shot capacitor bank was used as the pulsed power source to drive the railgun. Chapter 4 presents a description of the experiment, diagnostic results and comparison to simulation.

***Rep-rate System and Controls***

Once the proof of principle experiments yielded encouraging results attention moved to the rep-rate system. The purpose of the rep-rate system was to:

- demonstrate the arc starter would supply plasma reliably
- design a robust gun with integrated arc starter and powder delivery
- design a rep-rate pulsed power source and a process control system
- demonstrate that multiple spray events would create bonded coating

The top level detail of the rep-rate system is shown in figure 4. The main pulse forming bank and switches discharge into the railgun. A large lower voltage capacitor bank recharges the pulse forming network (PFN). This bank stores enough energy for 10 consecutive railgun discharges. The IGBT switches close to charge the energy storage inductor. At peak current the SCR switch block closes and the IGBTs open to develop voltage across the inductor that charges the pulse forming network. After full charge is sensed by the control system the power switches close the PFN into the railgun. The arc starter is supplying a continuous line source of plasma at the breech of the gun. The electric field established by the

PFN voltage stretches the line source into a planar arc that snowplows the prefill of argon gas into a dense gas column. The column then sweeps across the powder supplied by a continuous duty powder feeder accelerating the powder to target. The top level control blocks are also shown in figure 4. The control system is all fiber optically isolated to break any ground loops that are readily influenced by the strong RF content of the arc starter.

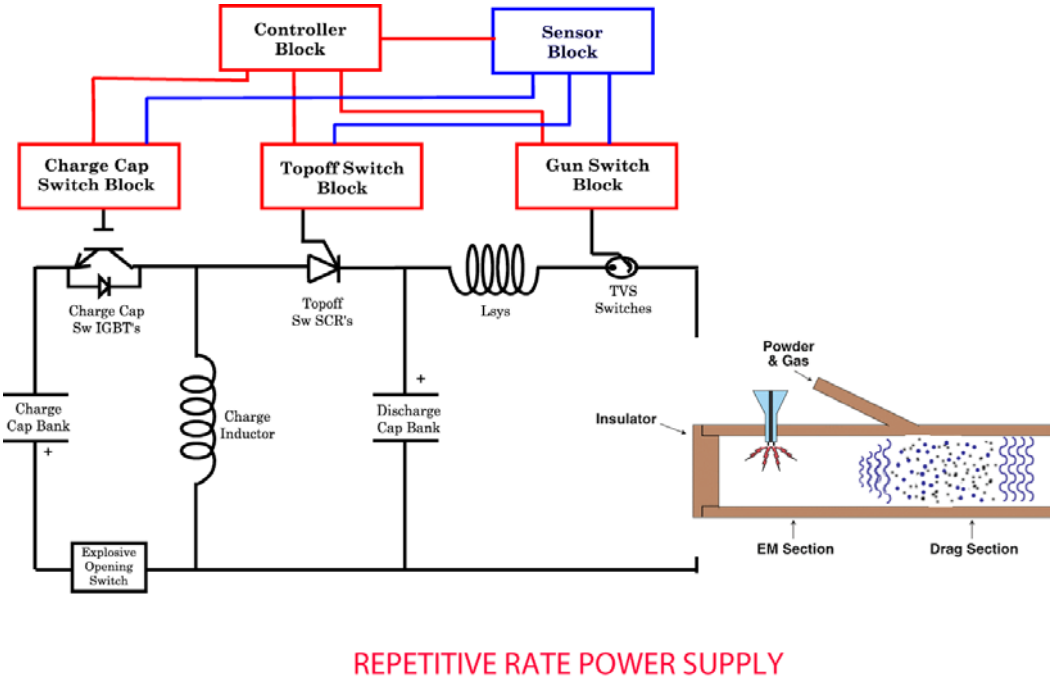


Figure 4. The elements of the rep-rate system and its top level control architecture

The railgun was a very robust design which evolved from 15 years of experience in the design and fabrication of electromagnetic launchers. It used refractory materials for the sidewalls and used high melting point, high strength material for the rails. The coaxial cavity arc starter with integrated argon gas de-

livery was designed into the breech of the launcher. Supply tubes to connect to a commercial powder feeder were provided at the entrainment section of the gun. The rails were fabricated with a unique laminated structure to increase the inductance gradient while maintaining mechanically stiff appendages to clamp ceramic sidewalls.

***Coatings and Commercial Systems***

The last part of the dissertation presents results from the spray process and description of work completed toward identifying an industrial system. One of the most exciting results was the ability to create fusion bonded coatings. This opens a whole new capability for this industry. The grain growth across the substrate coating interface pictured in figure 5 demonstrates that the powder is striking and fusing to the substrate. The irregular shape of the top of the coating layer will diminish as multiple passes are made on the substrate and will be eventually ground smooth in finishing processes. In addition to the fusion coatings realized with Inconel powder an interesting interlocking bond was demonstrated layer to layer.

After testing of the 10 shot rep-rate system, a better understanding of system operation was obtained and attention turned to identifying components that would eventually lead to an industrial system. It was realized that a higher inductance gradient in the railgun would lower the operating current and power required of the process. An augmented railgun was built and demonstrated on the 10 shot system. This achieved two goals. First, it lowered the power rating and size of the PFN and, second, reduced the heating in the railgun.

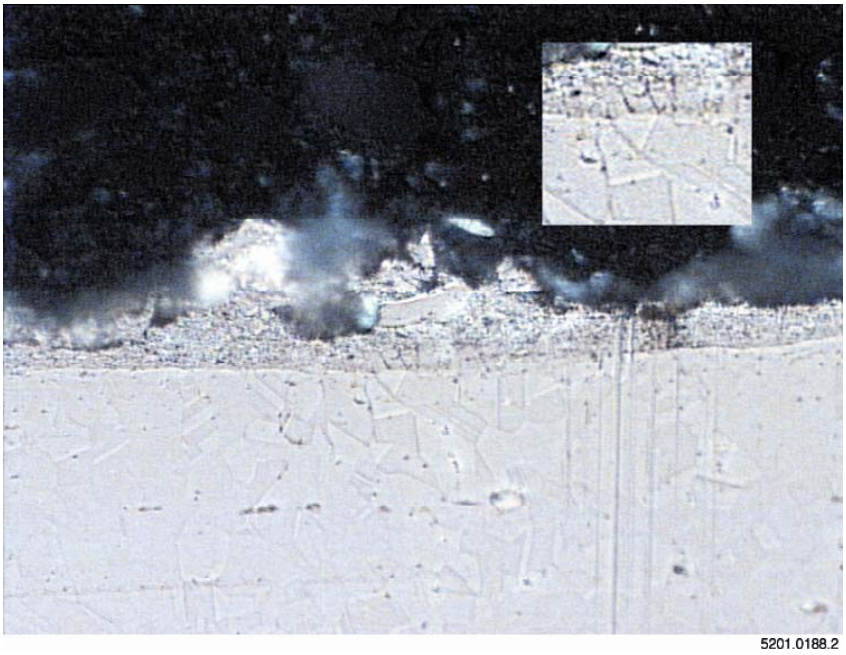


Figure 5. Micrograph of EPD coating demonstrating grain growth across substrate to coating interface

Life of components was also a concern in an industrial system. Capacitors required of the industrial PFN were ordered and life tested to 1 million discharges. Once the efficiency of the system was increased with the augmented railgun, the system power requirements was met with a standard 440 V, 200 A disconnect. A high voltage power supply that could recharge the PFN at the desired rep-rate was identified. The power switches between the PFN and the railgun could remain the triggered vacuum switches or change to high power SCRs. Either technology was sufficiently robust to switch the process. In conclusion there did not appear to be any technology hurdles that would have prevented an industrial grade system from being realized.

# CHAPTER 2: ELECTROMAGNETIC POWDER DEPOSITION SYSTEM OPERATING PRINCIPLES

Early research in powder spray attached powder material to the face of a fuse clamped between accelerator rails. The discharge current exploded the fuse, and the powder and fuse plasma accelerated down the gun. Early descriptions of the process assumed the arc would attach to the powder particles and the JxB magnetic body force would accelerate the powder. It was the observation of this author that the acceleration mechanism was due to viscous drag of the plasma over the powder particles, not a body force.

The next generation of accelerators attempted multiple discharges to sweep several arcs past the powder during the dwell time in-bore in order to discretely increment the powder velocity. The timing of closely spaced discharge events, coupled with the requirement for a mechanism to rapidly reestablish a diffuse arc at the breech of the gun yielded a complex operation. A more elegant solution was proposed by Dr. John Uglum when he suggested the use of the snowplow mechanism originally described by Shearer. In the snowplow process, a planar arc filling the cross section to the bore is accelerated by the JxB force. The plasma efficiently accelerates the gas and shock compresses it into a short column. The densified column sweeps over the powder, and only requires one event to accelerate the powder to target. This will be demonstrated in the analysis presented in the following sections [5].

**Railgun Equations**

The dominant force acting on the combined arc/gas column system arises from the JxB magnetic forces in the arc. As the arc accelerates down the launch tube, compression waves will coalesce to form a normal shock wave ahead of the arc. According to Siegel [6], the normal shock wave forms almost immediately after the onset of arc motion. The pressure and velocity of the argon directly behind the shock, and of the argon in front to the arc, equalize very quickly. Thus, the pressure which occurs on the face of the arc may be approximated by the pressure which exists immediately behind the normal shock wave.

Volume integrating the local force balance equation gives the "railgun equation" for the system

$$\frac{d}{dt}(M_{gas} V_{gas}) = \frac{1}{2} L' I^2 \tag{1}$$

For calculation purposes let the current driving the arc be given by the relation

$$I = I_0 \sin \omega t \tag{2}$$

Integrating equation (1) and using equation (2) for current gives the gas momentum relation

$$M_{gas}\ \frac{dZ_{arc}}{dt} = \frac{1}{4}\frac{L'I_0^2}{\omega}(\omega t - \frac{1}{2}\sin 2\omega t) \tag{3}$$

$Z_{arc}$ is displacement from the arc initiation point and the snowplow relation has been used to define

$$V_{gas} = \frac{dZ_{arc}}{dt} \tag{4}$$

The continuity relation requires

$$M_{gas} = \rho_0 A_B Z_{arc} \tag{5}$$

where

$A_B$ = area of the bore

$\rho_0$ = the initial gas density

Substituting equation (5) in momentum equation (3) and integrating gives the arc displacement

$$Z_{arc} = \frac{1}{2}\frac{I_0}{\omega}\sqrt{\frac{L'}{\rho_0 A_B}}\sqrt{\omega^2 t^2 - \frac{1}{2}(1-\cos 2\omega t)} \tag{6}$$

The gas velocity is derived by taking the derivative of the arc displacement.

$$V_{gas} = \frac{1}{2} I_0 \sqrt{\frac{L'}{\rho_0 A_B}} \frac{\omega t - \frac{1}{2}\sin 2\omega t}{\sqrt{\omega^2 t^2 - \frac{1}{2}(1 - \cos 2\omega t)}}$$

$$= \frac{1}{2} I_0 \sqrt{\frac{L'}{\rho_0 A_B}} F(t) \qquad (7)$$

The time function modifying the peak velocity is presented in figure 6. It is seen that the gas column quickly comes to final velocity and the rest of the time is spent sweeping new gas into the snowplow column.

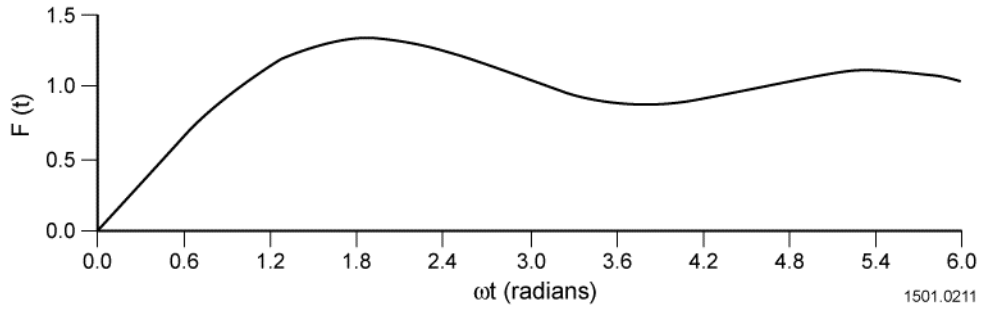


Figure 6. The time dependence of the velocity, F(t), demonstrates that the gas column quickly comes to final velocity

Conditions must now be found for the gas properties in order to analyze the powder acceleration portion of the sprayer. Pressure gradient terms appear as shock jump conditions. The relation which defines this is

$$P_{gas} = P_0[1 + \left|\frac{V_{gas}}{a_1}\right|^2 \frac{\gamma(\gamma+1)}{4} + \frac{\gamma V_{gas}}{a_1}\sqrt{1 + \left|\frac{\gamma+1}{4}\right|^2 \left|\frac{V_{gas}}{a_1}\right|^2}\,] \tag{8}$$

where

$P_0$ = initial gas pressure in bore

$a_1$ = sound speed in argon

$\gamma$ = specific heat ratio of argon

Other gas properties associated with a normal shock have been presented in Plapp [7]. The temperature change across the shock front is given by

$$T_{gas} = T_0[\frac{2 + (\gamma-1)(\frac{V_{gas}}{a_1})^2}{(\gamma+1)(\frac{V_{gas}}{a_1})^2}][(\frac{2\gamma}{\gamma+1})(\frac{V_{gas}}{a_1})^2 - (\frac{\gamma-1}{\gamma+1})] \tag{9}$$

where

$T_0$ = the temperature of the fill gas in-bore

Of importance to the snowplow process is the density increase across the shock boundary.

$$\rho_{gas} = \rho_0 \frac{(\gamma+1)(\frac{V_{gas}}{a_1})^2}{2+(\gamma-1)(\frac{V_{gas}}{a_1})^2} \tag{10}$$

The continuity equation requires

$$\rho_0 Z_{arc} = \rho_{gas} L_{gas} \tag{11}$$

Rearranging gives

$$Z_{arc} = \frac{\rho_{gas} L_{gas}}{\rho_0} \tag{12}$$

The variables introduced in the previous equations are identified in figure 7.

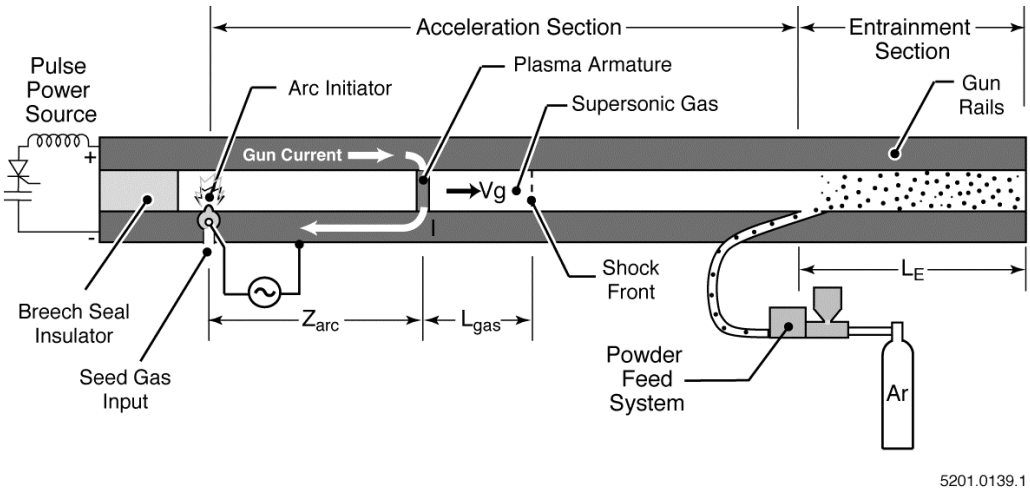


Figure 7. Identification of variables used in the railgun and snowplow theory

Once the length of the gas column accelerating the powder is known the length of the railgun and its operating parameters may be established from these equations, but first it is necessary to examine the deposition requirements of the system.

**Deposition Rate**

Leading industrial coating processes were investigated to establish a goal deposition rate for the EPD process. A deposition rate of 100 g/min was selected as competitive. As presented earlier, a commercial powder feeder delivers powder to the entrainment section of the gun. The mass flow rate into the entrainment section of the gun is

$$\frac{dM_E}{dt} = \overline{\rho}_E A_B v_E \tag{13}$$

where

$\overline{\rho}_E$ = average powder density in the entrainment section

$v_E$ = output velocity of the powder feeder

$$\overline{\rho}_E = \frac{\frac{dM_E}{dt}}{A_B v_E} \tag{14}$$

Commercial powder feeders have mass flow rates in the 30 – 100 g/min regime and velocities on the order of 3 – 7 m/s for powder sizes of interest 60 – 100 $\mu m$ . The entrainment length of the gun is given by

$$L_E = v_E t_{reprate} \tag{15}$$

where

$t_{reprate}$ = the time between railgun discharges

**Viscous Drag Acceleration of Powder with Snowplow Process**

The force acting on each powder particle is generated by the viscous drag produced by high velocity gas flowing past it at a speed equal to $V_{gas.}$ The force equation for each particle is

$$Mp\frac{dV_p}{dt} = C_D A_{eff} P_{kinetic} \tag{16}$$

where

$M_p$ = mass of particle = $\frac{\pi}{6}\rho_p d^3 = 3.77x10^{-6}$ g, ( $\rho_p = 7.2 g/cm^3$, $d = 100 \mu m$ )

$d$ = diameter of the powder particle

$V_p$ = velocity of particle

$$A_{eff} = \text{effective area of particle} = \frac{\pi d^2}{4}$$

$$P_{kinetic} = \text{kinetic pressure of gas} = \frac{1}{2}\rho_{gas}(V_{gas} - V_p)^2$$

$$C_D = \text{viscous drag coefficient}$$

Substituting these terms into equation (16) and rearranging, gives

$$\frac{d(\frac{V_P}{V_{gas}})}{dt} = \frac{1}{2}\frac{A_{eff}}{M_P}C_D\rho_{gas}V_{gas}(1-\frac{V_p}{V_{gas}})^2 \qquad (17)$$

Equation (16) assumes that an individual sphere is in the flow field with little disturbance from neighbors. This assumption may be checked by inserting typical powder feeder parameters and railgun bore area into equation (14), (mass rate of 30 g/min, bore area of 1.5 $cm^2$, velocity of 3 m/s).

$$\overline{\rho}_E = \frac{\frac{30g}{60s}}{1.5cm^2\,300\frac{cm}{s}} = 1.11x10^{-3}\frac{g}{cm^3} \qquad (18)$$

Once the average density is calculated an individual powder particle can be placed at the center of an imaginary cube and the cube dimension found that produces the average density.

$$\overline{\rho}_E = \frac{M_p}{\lambda^3}$$

where

$\lambda$ = powder particle spacing in the entrainment section

$$\lambda = \left(\frac{M_p}{\rho_E}\right)^{\frac{1}{3}} = \left(\frac{3.77\text{x}10^{-6}\,\text{g}}{1.11\text{x}10^{-3}\,\frac{\text{g}}{\text{cm}^3}}\right)^{\frac{1}{3}} = 0.15\text{cm} \tag{19}$$

This means that the individual powder particles are spaced by an average separation of 15 diameters. The assumption of little influence from neighboring spheres is valid.

Equation (17) may be rewritten as

$$\frac{d\left(\frac{V_P}{V_{gas}}\right)}{\left(1-\frac{V_p}{V_{gas}}\right)^2} = \frac{dt}{\tau} \tag{20}$$

where

$$\tau = \frac{2M_P}{A_{eff} C_D \rho_{gas} V_{gas}} = \frac{4d\rho_P}{3C_D \rho_{gas} V_{gas}}$$

At the end of the railgun process a gas column of near constant speed and density is delivered to the entrainment section. Figure 8 indicates that for Mach numbers of interest the drag coefficient is also constant and near unity.

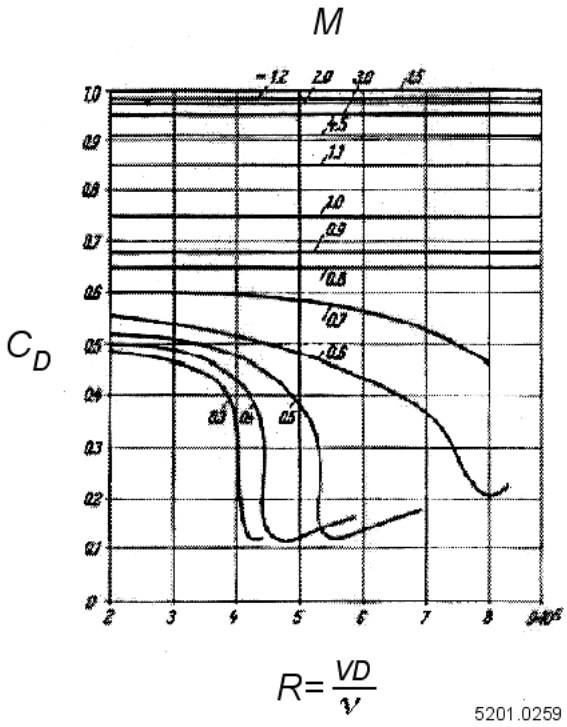


Figure 8. For Mach numbers of interest the drag coefficient is constant and near unity [8]

Equation (20) may be integrated directly and with the initial condition that the powder velocity is negligible at time zero the solution is

$$\frac{t}{\tau} = \frac{\frac{V_P}{V_{gas}}}{1 - \frac{V_P}{V_{gas}}} \tag{21}$$

Rearranging yields

$$\frac{V_P}{V_{gas}} = \frac{(\frac{t}{\tau})}{1+(\frac{t}{\tau})} \tag{22}$$

This equation indicates that the powder gains ½ the gas velocity in a time $\tau$. The force has fallen to ¼ its initial value and the snowplow mechanism yields diminishing returns beyond this increment.

The total length of gas flow needed to reach a given velocity is found by integrating the differential speed between the gas column and the powder particle. Then

$$L_{gas} = \int (V_{gas} - V_P)dt = V_{gas}\tau \int (1 - \frac{V_P}{V_{gas}})\frac{dt}{\tau} \tag{23}$$

Substituting equation (20) into equation (23) and integrating

$$L_{gas} = V_{gas}\tau \ln(\frac{1}{1-\frac{V_P}{V_{gas}}}) \tag{24}$$

**Coating Considerations**

The advantage of the EPD process is the ability to accelerate powder to very high velocity. The desire to create a fusion bond with the substrate requires that the powder strike with enough velocity to melt the powder particle plus an

equivalent mass of substrate. As an example, the energy per unit mass required to heat and melt chromium starting at room temperature is

$$\frac{E}{M} = c_p \Delta T + E_{melt} = 1.106 \text{x} 10^6 \frac{J}{kg} \tag{25}$$

Equating the energy required to melt plating powder, plus an equal mass of substrate, to the kinetic energy of the powder gives.

$$\frac{1}{2} V_P{}^2 = 2 \frac{E}{M} \tag{26}$$

Solving for the powder velocity yields

$$V_P = 2.1 \frac{km}{sec} \tag{27}$$

It turns out that for most metals, $V_P$ falls in the 2 km/s regime to meet the requirement of melt on impact. Earlier it was shown that the snowplow is efficient in accelerating the powder to one half gas velocity. For this reason the working velocity of the railgun is chosen to be 4.2 km/s. Once $V_{gas}$ is known, then all the operating parameters for the process are established.

A consistent set of design parameters are given in table 1

Table 1. Consistent set of parameters defining EPD operation

| Parameter | Value |
|---|---|
| Vpowder | 2100 m/s |
| $d_{powder}$ | 100 μm |
| $V_{gas}$ | 4200 m/s |
| $\rho_{powder}$ | 8913 kg/m$^3$ |
| $a_1$ | 319 m/s |
| $\rho_0$ | 1.783 kg/m$^3$ |
| $\gamma$ | 1.4 |
| $\rho_{gas}$ | 10.4 kg/m$^3$ |
| $C_D$ | 1 |
| $\tau$ | 27.2 μs |
| $L_{gas}$ | 0.0792 m |
| $Z_{arc}$ | 0.462 m |
| $L_E$ | 0.2 m |
| $I_{gun}$ | 200,000A |
| $P_{gas}$ | 29.7x10$^6$ N/m$^2$ (4311 psi) |
| T | 10,325 K |

# CHAPTER 3: ARC STARTER

It was realized early in the research effort that a reliable means of starting the arc at the breech of the gun was imperative [9]. The possibility of rapidly loading foil fuses in the breech of the gun was considered, but quickly dismissed for its complexity and the possibility of contaminating the coating surface with fuse by-products. An additional constraint placed on the plasma source was its ability to operate at atmospheric conditions. Lamps and vacuum tubes were known to produce diffuse plasmas at partial pressures, but the prospect of operating the spray system at partial pressure was not attractive to industry. Industrial sprayers used Argon as a cover gas due to its inert properties. Argon is readily available at a reasonable cost, therefore it was studied as the carrier gas for the EPD process.

**Experiments to Create Diffuse Stable Plasma**

The starting point was to try a simple concept and configuration in an attempt to establish the planar arc. An electrical stress riser was designed into the breech of the gun (fig. 9). The theory was the electric field introduced by the pulsed power supply would break down the bore in this high field region and initiate a traveling arc. An advantage of this concept was that it could be advanced into the bore as the electrode wore for ease of maintenance and long life. The

concept was tested in a railgun, but failed to create a planar arc which filled the entire cross section of the bore.

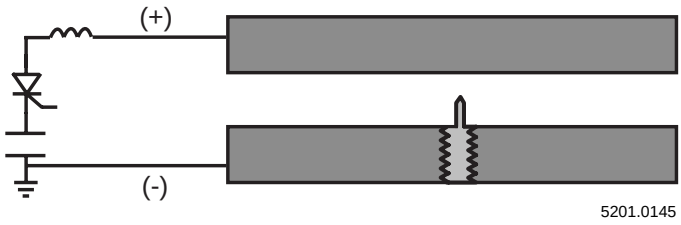


Figure 9. Railgun rails with stress riser concept for arc initiation

Attention then turned to creating a line source of plasma across the bore that would then be stretched into a planar arc when the high electric field of the PFN was applied to the gun. Testing started in partial pressure with conventional ac power sources to understand the behavior of these plasmas. To minimize the effect of electrode shape smooth cylindrical electrodes specified by ASTM 149 were used, figure 10a. A neon sign transformer was used as the excitation source. The transformer operated at 60 Hz and was capable of 7500 V open circuit with a current limit of 20 mA. The vacuum chamber was evacuated and then back-filled with argon gas at 0.5 torr. Excitation testing at this level produced a glow discharge around both electrodes, figure 10b. As the pressure was increased to 2 torr the discharge centered on the electrodes and filled the 4 mm gap between electrodes, figure 10c. Further increasing the pressure to 70 torr constricted the dis-

charge into multiple filamentary arcs, figure 10d. Raising the pressure to 1 atmosphere caused the arc to become stationary in one filamentary discharge, figure 10e.

The glow discharge testing confirmed the difficulty in creating a diffuse arc at atmospheric pressure. This initial testing led to a search for different electrode geometries and power sources capable of sustaining a diffuse arc at atmospheric conditions in argon.

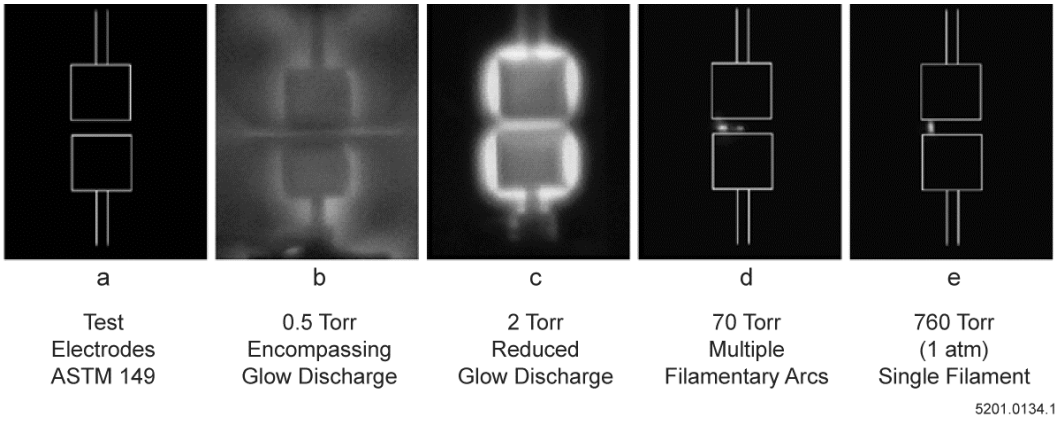


Figure 10. Diffuse arc testing

It is known that higher frequency sources can break down air even at higher pressures. An ENI model A-300 radio frequency amplifier with the following specifications: 300 kHz-35 MHz, 300 W, 55 dB gain, and 200 V peak was borrowed as a source for further testing. The plasma source was changed to a cylindrical cavity with coaxial electrodes. If stable diffuse plasma could be created

at atmospheric pressure then one edge of the cavity would be open to the railgun bore to introduce a line source of plasma to the bore, figure 11. The slot would act as an ideal armature initiator providing a full-width voltage stressor and a starter quantity of conductive gas.

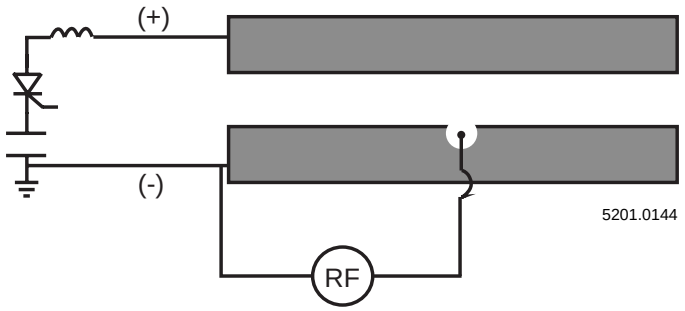


Figure 11. Coaxial cavity arc starter concept with an RF source

Experimental hardware was produced to test in the vacuum chamber. The first variants were full cavities without the slot in order to determine if stable diffuse plasma could be created at elevated pressure. The first test articles were 3 mm and 7 mm diameter cavities with a 2.7 electrode to cavity diameter ratio, figure 12. These devices were assembled in the vacuum chamber and the camber was back-filled with Argon gas. The first electrodes were conventional spark plugs that would screw into the copper rail material and the center electrode was extended with a piece of tungsten to form the inner electrode. At 35 MHz excitation this configuration was able to sustain a diffuse arc in the coaxial cavity up to

a pressure of 600 torr. With this success an ENI model 3200L RF amplifier was purchased that had the capability of 120 kHz – 150 MHz, 175 W, 55 dB gain, and 200 V peak. With 150MHz excitation stable diffuse arcs were demonstrated at atmospheric pressure in argon.

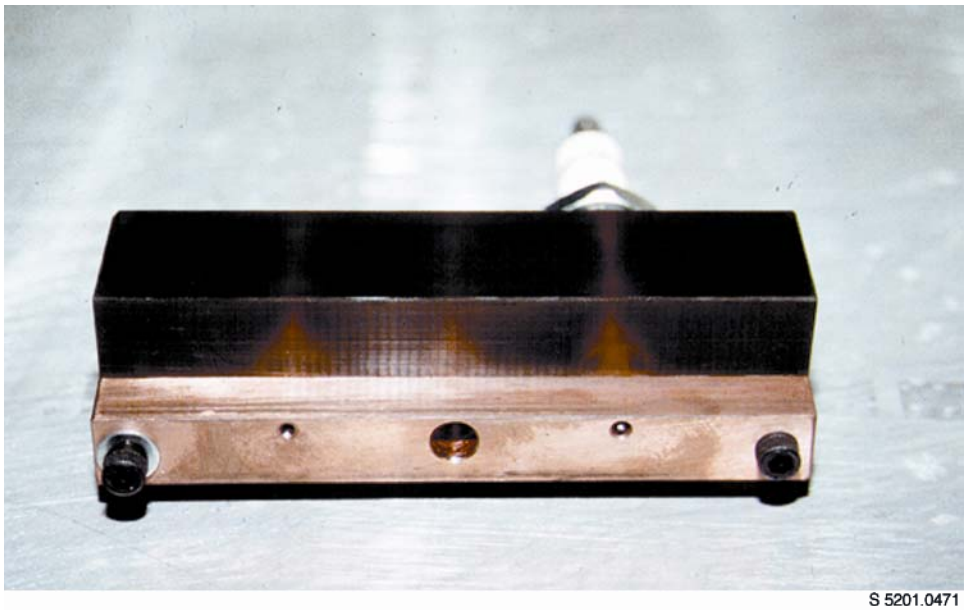


Figure 12. First test article for evaluation of coaxial cavities

Once stable plasmas were produced the test fixture was modified to open the coaxial cavity at the rail surface to create the linear source, figure 13. The configuration was retested in the presence of this perturbation to evaluate its influence. The cavity performed well and once again stable, diffuse plasma which would bulge slightly from the linear slot was demonstrated.


Figure 13. The surface of the rail material was milled to expose the coaxial cavity to the bore

The final step to the process was to insure that the line source of plasma would react to the electric field supplied by the pulsed power supply and stretch across the bore to form a planar arc. To assess this behavior a proof of principle railgun experiment was designed and the arc starter was integrated into the breech of the gun. In figure 14 the line source of plasma is viewed through a glass side-wall of the test railgun. Assessment of the arc starter is presented in Chapter 4.

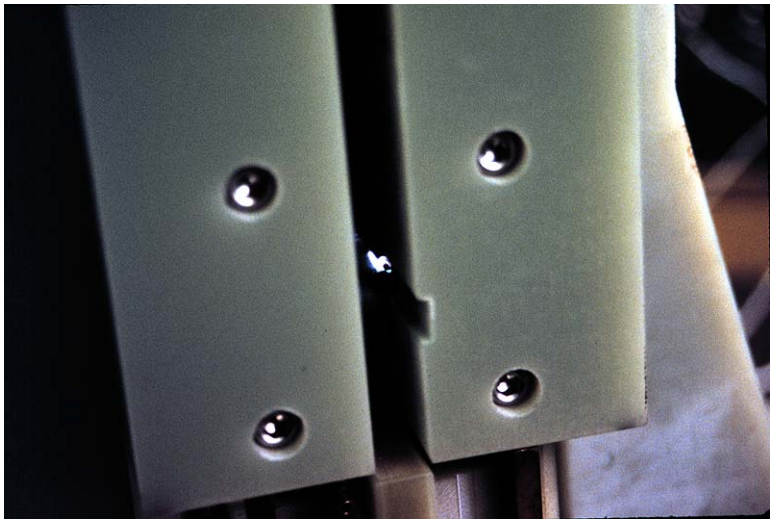

Figure 14. Arc starter integrated into the breech section of the proof of principle railgun

**Transmission Line Considerations**

Once the high frequency source was introduced attention had to be paid to the transmission line effects and the characteristic of the termination of the line at the plasma cavity.

Consider the voltage difference between two neighboring points on the line located a positions x and $x+\delta x$, respectively. The self-inductance of the portion of the line lying between these two points is $L\delta x$. This small section of line can be thought of as a conventional inductor, and therefore obeys the equation

$$V(x,t) - V(x+\delta x,t) = L\delta x \frac{\partial I(x,t)}{\partial t} \tag{28}$$

In the limit $\delta x \to 0$, the above equations reduces to

$$\frac{\partial V}{\partial x} = -L\frac{\partial I}{\partial t} \tag{29}$$

Consider the difference in current between two neighboring points on the line, located at positions x and $x+\delta x$, respectively. The capacitance of the portion of the line lying between these two points is $C\delta x$. This small section of the line can be thought of as a convention capacitor, and therefore obeys the equation

$$\int_0^t I(x,t)dt - \int_0^t I(x+\delta x,t) = C\delta x V(x,t) \tag{30}$$

In the limit $\delta x \to 0$, the above equations reduces to

$$\frac{\partial I}{\partial x} = -C\frac{\partial V}{\partial t} \tag{31}$$

Differentiating equation 29 with respect to x yields

$$\frac{\partial^2 V}{\partial x^2} = -L\frac{\partial^2 I}{\partial x \partial t} \tag{32}$$

Differentiation equation 31 with respect to t yields

$$\frac{\partial^2 I}{\partial x \partial t} = -C\frac{\partial^2 V}{\partial t^2} \tag{33}$$

Combining equation 32 and 33 gives

$$LC\frac{\partial^2 V}{\partial t^2} = \frac{\partial^2 V}{\partial x^2} \tag{34}$$

This is the wave equation with wave velocity, $v = \frac{1}{\sqrt{LC}}$.

Considering the general solution

$$V(x,t) = V_0 \exp[i(\omega t - kx) + KV_0 \exp[i(\omega t + kx)] \quad (35)$$

where

$V_0$ = amplitude of the RF source

$\omega$ = frequency of the source

$k = \omega\sqrt{LC}$

This corresponds to a voltage wave of amplitude $V_0$ which travels down the line and is reflected, with reflection coefficient K, at the end of the line. Substituting 35 into 31 yields

$$I(x,t) = \frac{V_0}{Z_0}\exp[i(\omega t - kx)] - \frac{KV_0}{Z_0}\exp[i(\omega t + kx)] \quad (36)$$

where

$$Z_0 = \sqrt{\frac{L}{C}}$$

If the line is terminated by a resistance R at x=0 we have, from Ohm's law,

$$\frac{V(0,t)}{I(0,t)} = R \quad (37)$$

This yields an expression for the coefficient of reflection,

$$K = \frac{R - Z_0}{R + Z_0} \quad (38)$$

To evaluate the ability to deliver sustaining power to the plasma in the starter cavity a RF power meter was connected to the amplifier. Results of the testing are shown in figure 15. It can be seen that of the 100 W supplied by the amplifier that

25 W enter the cavity to sustain the plasma. In the course of railgun testing it was observed that the energetic event of stretching the arc across the bore and the plasma sheet accelerating away from the slit in the cavity would on occasion extinguish the arc starter. To address this situation a carrier wave was introduced on top of the 150 MHz signal. At discrete intervals the carrier would double the voltage output of the amplifier creating a short burst of full voltage from the device. If the cavity had extinguished, the elevated voltage spike would cause the plasma to re-initiate. The power spike can be seen in figure 15 and occurs at a much greater rate than the inter-shot time of the railgun assuring the plasma is restarted before a discharge is required.

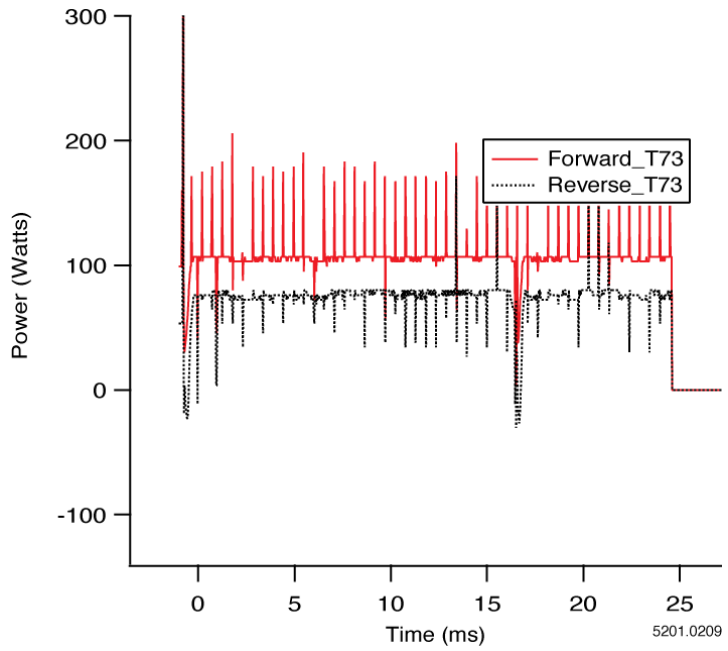


Figure 15. Forward and reverse power measured in arc starter system

It became obvious in testing with the high frequency RF that there would be a significant interference problem with control systems and instrumentation. Grounding and shielding techniques required to operate in this environment as well as control system isolation guidelines are discussed in Chapters 4 and 6.

# CHAPTER 4: PROOF OF PRINCIPLE RAILGUN EXPERIMENTS

With the theory developed and a reliable arc starter demonstrated a set of experiments were designed to determine the feasibility of the EPD approach. A highly instrumented [10] glass sidewall railgun was designed to confirm operation of the snowplow process and its ability to accelerate micro spheres to velocity of interest.

## Instrumented Railgun

The Bench Test Railgun (BTR) was designed with an instrumentation suite that would allow mapping of the position of the arc in bore as a function of time, measurement of the pressure of the compressed gas column formed in front of the snowplow, and finally high speed photographic confirmation of the viscous drag mechanism for accelerating micro particles, figure 16. The resolution of arc position in time was accomplished with electromagnetic sensors known as b-dot probes and fiber optic transducers that recorded the passage of light in bore. The pressure ahead of the arc was measured with fast response piezoelectric pressure transducers mounted in the railgun rails.

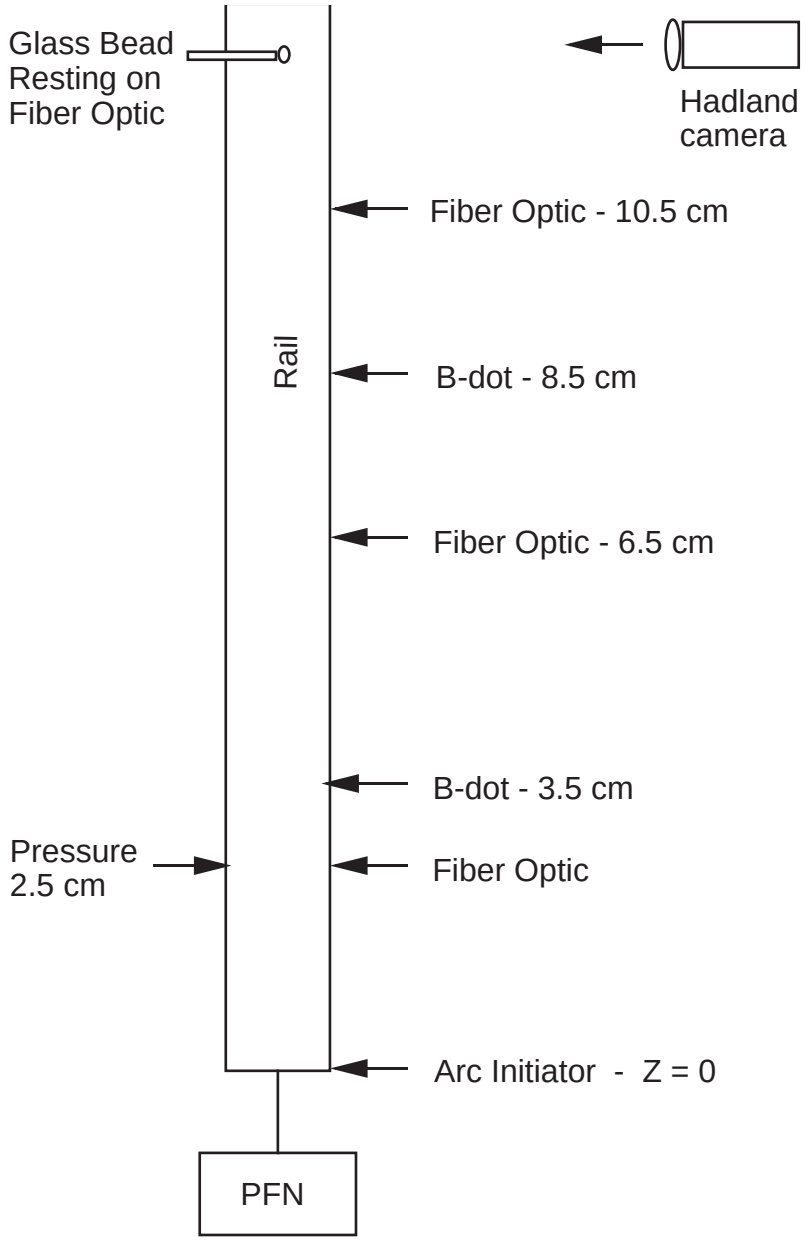


Figure 16. Definition of instrumentation proposed to confirm snowplow process and micro sphere acceleration

The railgun was manufactured with a transparent sidewall, figure 17, to allow in bore high speed photography of the arc acceleration and form as well as the confirmation of micro particle acceleration.

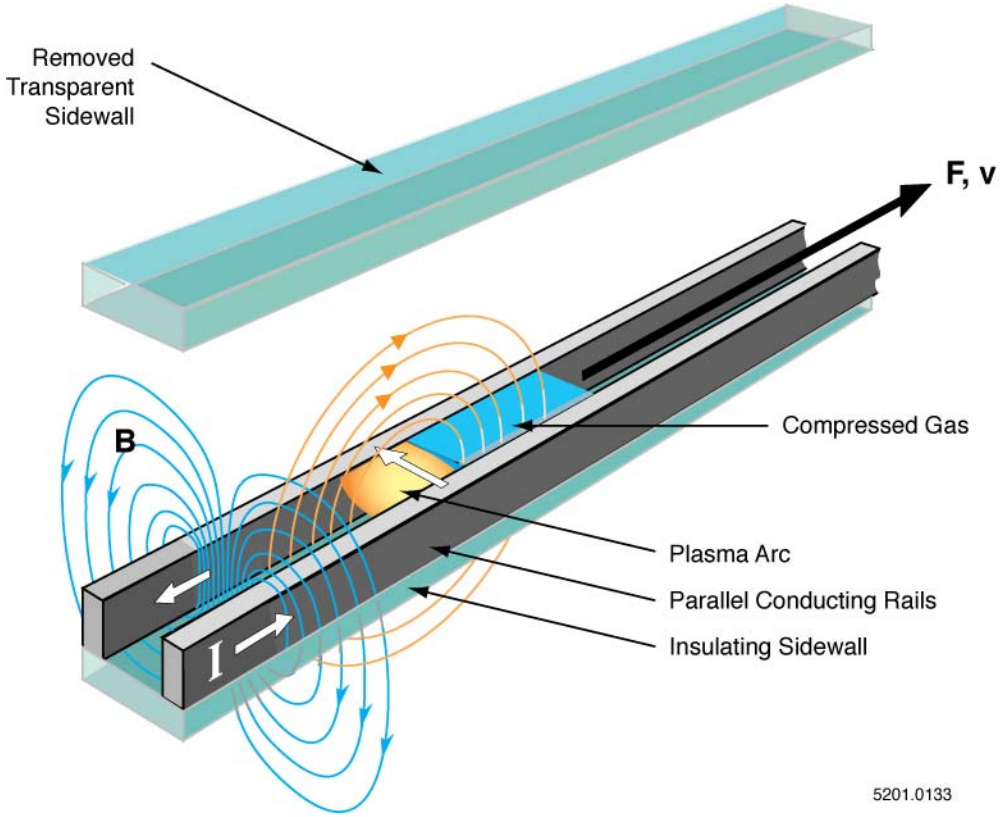


Figure 17. The railgun was manufactured with a transparent sidewall to allow high speed photographic observation of the arc and accelerated micro particles

A photograph of the railgun hardware is shown in figure 18. It was mounted vertically to allow for ease of access due to the large number of diagnostics on the gun. The rails were made from ETP copper and the major structural

components of the gun were manufactured from G10. The front pieces of G10 are robust and clamp the polycarbonate sidewall. The gun was fired with a 400 μF capacitor bank that could be charged to 8 kV.

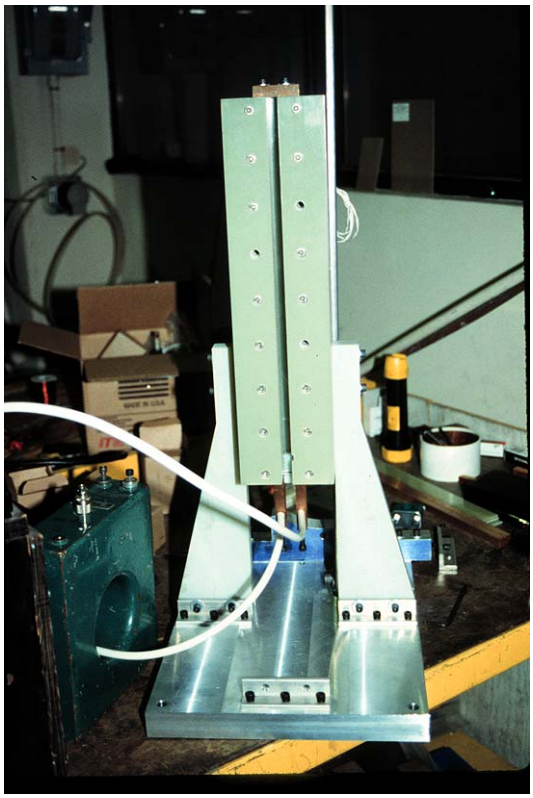

Figure 18. BTR with the bore axis mounted vertically for ease of diagnostic access

### *B-dot Probe Position Sensors*

B-dot probes are diagnostics that measure the passage of magnetic field. There are two popular versions of this probe; one for measuring the field produced by the rail current and the second for measuring the field produced by the

armature current. The orientation of the coil diagnostic and its interaction with the magnetic field is illustrated in figure 19. The radial b-dot probes are so named because they measure the time rate of change of flux emanating radially from the gun centerline. This field is produced by the rail conductors. The rail flux at any instant of time is proportional to the current entering the breech of the gun. The voltage signal measured from a radial b-dot may be integrated to give rail current at the time the plasma armature is passing the probe. These probes are useful if there is a suspicion that more than one arc is forming in the railgun. When the first arc passes the probe some fraction of the total current entering the breech of the gun will be measured with the probe. When the second arc passes, the integrated signal from the probe will match the current waveform measured at the input to the gun. The second type of probe is the axial b-dot. It is so named because it measures the time rate of change of axial flux in the gun. It can be seen from the figure that this flux comes from the armature. This diagnostic is useful in determining the time at which the plasma passes the location of the probe. It can be seen in figure 19 that the voltage goes through a current zero just as the maximum flux distribution is passing under the probe. Because these probes determine position in time an average velocity may be determined by using two of these devices spaced along the railgun axis. Measuring the time between zero crossing of the probe voltage output and dividing it into the spacing produces the average velocity of the armature between the locations.

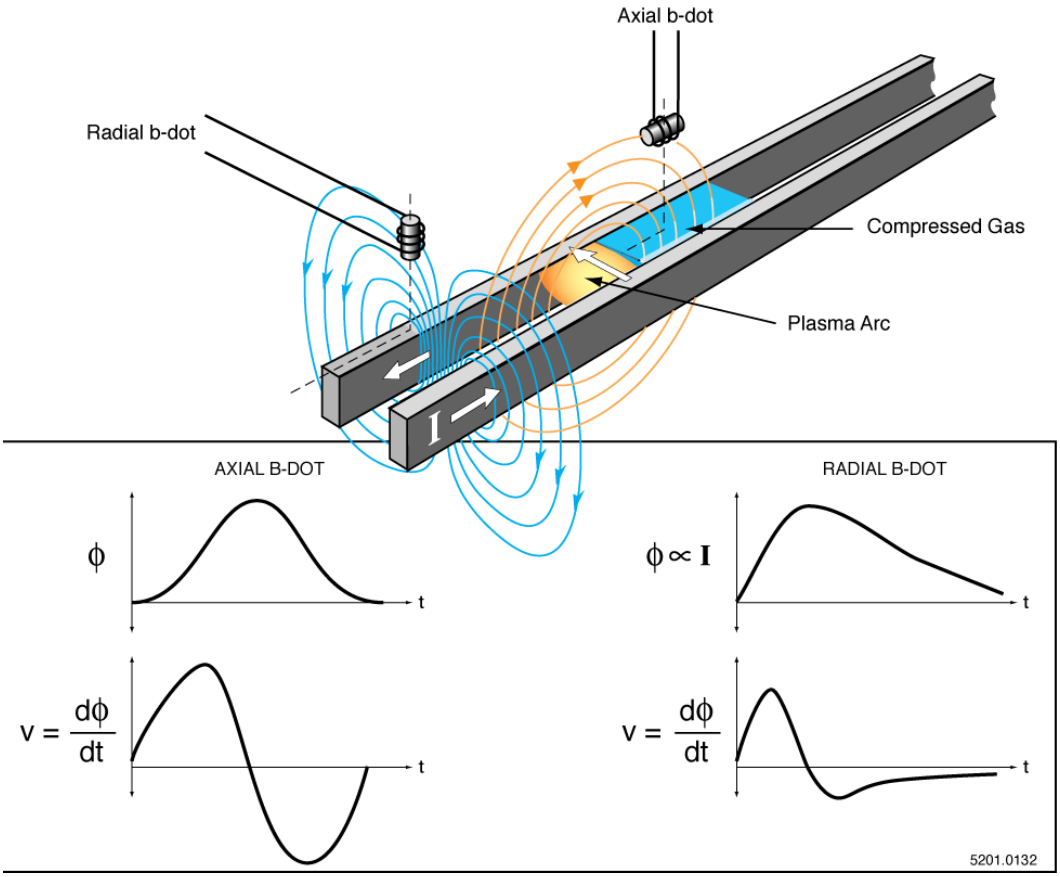


Figure 19. Explanation of the function of a b-dot magnetic probe diagnostic

B-dots for analyzing the plasma armature motion were designed for the BTR. An expression for voltage induced in a coil of wire by a moving sheet current is presented in the literature [11].

$$\dot{\phi}_p^A(t) = \frac{\mu_0 NAI}{4\pi w} z_p H\left[\frac{1}{[(D+\frac{W}{2})^2 + z_p^2]\sqrt{(D+\frac{W}{2})^2 + z_p^2 + (\frac{H}{2})^2}}\right. \\ \left. - \frac{1}{[(D-\frac{W}{2})^2 + z_p^2]\sqrt{(D-\frac{W}{2})^2 + z_p^2 + (\frac{H}{2})^2}}\right] \quad (39)$$

where

$\dot{\phi}_p^A$ = rate of change of the field at the location of the probe over its cross sectional area, A.

I = railgun current

N = number of turns in the b-dot coil

$z_p$ = position of the probe relative to the arc sheet in the direction of the axis of the gun

H = bore height

W = bore width

D = distance to the probe relative to the centerline of the gun

The parameters that define the geometry of the gun rails and the diagnostic coil are identified in figure 20.

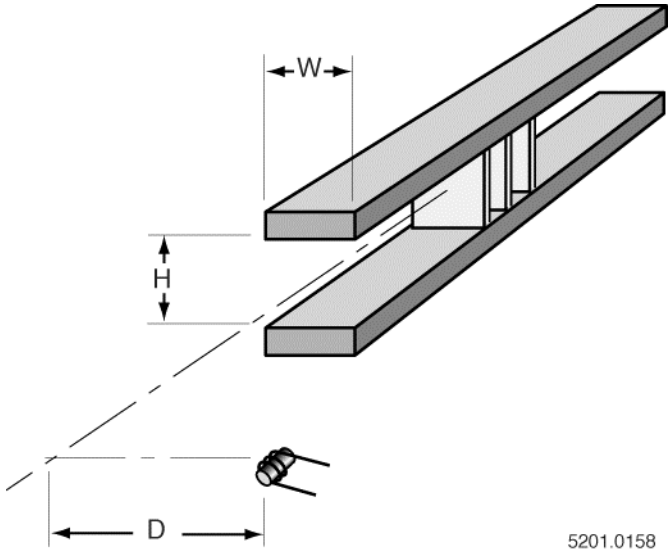


Figure 20. Geometry factors considered in the design of an axial b-dot

A Basic program was written which divided the plasma armature up into 10 discrete sheets of current and then calculated the b-dot coil output based on the superposition of the literature formulas. The literature was also searched for a good approximation to the current distribution within and length of a plasma armature and estimates were developed [12]. The ten sheets are assumed to contain current in the following percentages starting at the front of the armature and working backward, 50, 14, 8, 7, 6, 5, 4, 3, 2, 1. The b-dot coils in that experiment were 30 turn devices wrapped on a 1.5 mm diameter form. The coils were located 0.5 in. (dimension D) from the centerline of the gun which had a bore dimension of 0.5 in. (dimension W) 0.5 in. (dimension H). As mentioned in the previous chapter it was a challenge to design diagnostics that would work reliably in the

presence of the RF source at the arc starter. It can be seen in figure 21 that the signal output strength of the b-dot was designed to surpass any noise component. In addition the connection wires to the b-dot were made of twisted shielded cable to prevent spurious signals from coupling to the output.

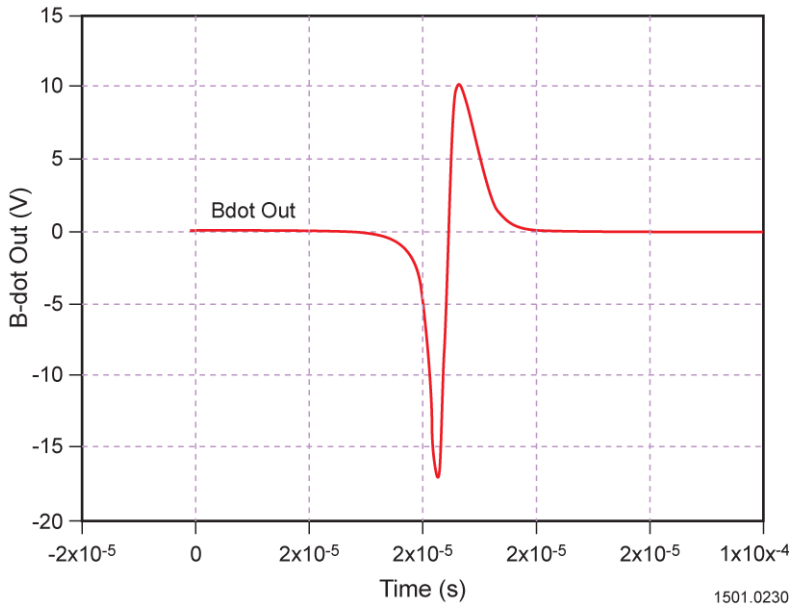


Figure 21. Predicted b-dot output signal

An actual b-dot coil terminated to its cable is shown in figure 22. These coils were then place in protective holders that could be mounted to the experiment. The positioning of the b-dot probes on the BTR is shown in figure 23. They are the three equally spaced holders along the length of the BTR just above the copper breech buswork.

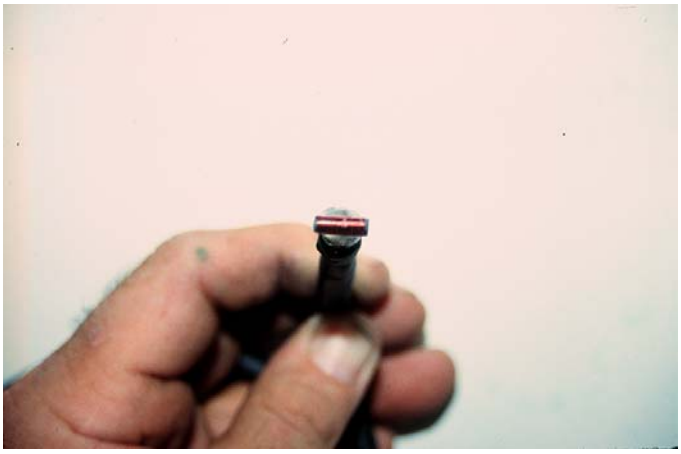

Figure 22. B-dot coil mounted on strain relief and terminated to output cable

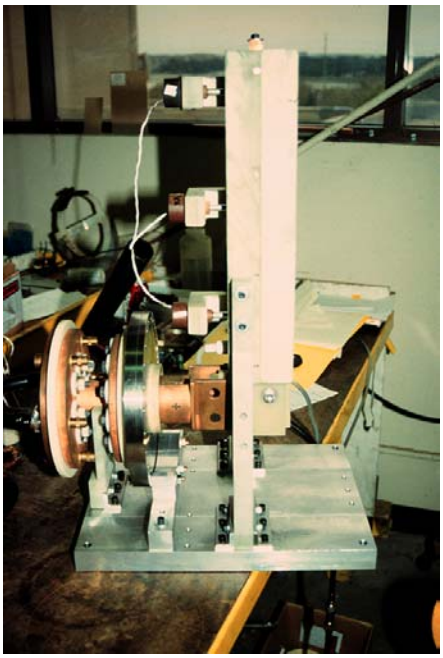

Figure 23. B-dot diagnostics attached to BTR

### *Fiber Optic Position Sensors*

The second diagnostic tool used to detect the plasma armature was fiber optics. The conducting rails of the railgun are physically separated from each other with electrical insulating members referred to as "sidewalls". One of these sidewalls was made of polycarbonate, which is transparent. Fiber optic probes were mounted to the side of this polycarbonate sidewall so that they could detect light emitted by the passing plasma sheet. Figure 24 shows the fiber optic placement on the railgun. The fiber optic probes were connected to light sensing diodes, which produce a voltage proportional to the intensity of the light picked up by the fiber optic probe.

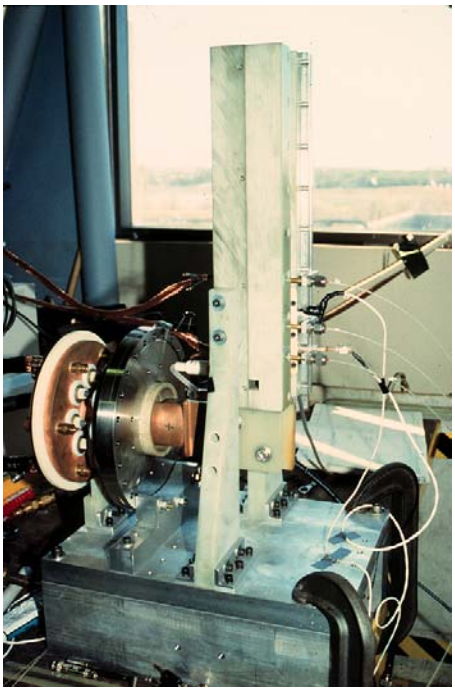

Figure 24. Fiber optic probes positioned on the transparent sidewall of the railgun

### *Pressure Transducers*

Two piezoelectric pressure transducers manufactured by PCB Company were installed to mount flush with the railgun bore. One of the transducers is shown lying next to the railgun rails in figure 25. Two transducers, a 5,000 psi model number 101A02 and a 10,000 psi model number 102A03, were used. The transducers were specified to have a fast response time.

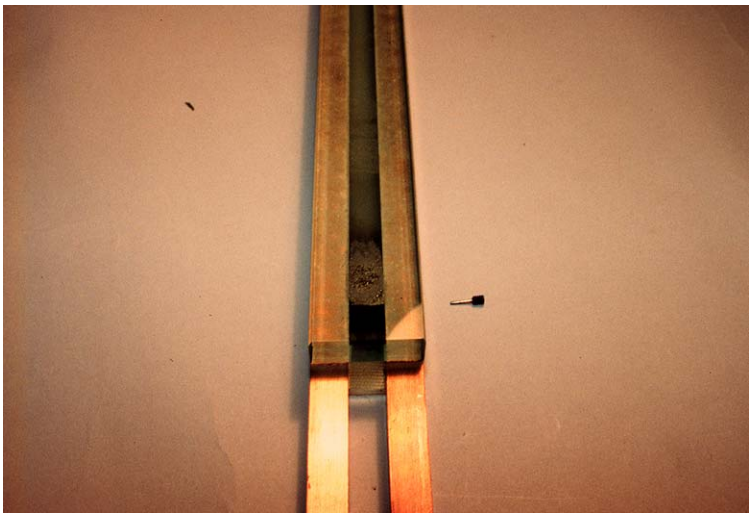

Figure 25. Pressure transducer lying next to railgun rails

In debugging, the greatest problems were experienced with the pressure transducers, an important tool for verifying the snowplow mechanism. At first, the pressure transducer traces exhibited a great deal of noise. Since the transducers where directly exposed to the plasma, it was possible that the transducer dia-

phragm was either shorting out to ground or picking up an electrical charge from the plasma. Kapton tape was placed over the face of the transducers to prohibit plasma charge coupling or at least delay coupling until after the acceleration event. With this modification most of the jagged nature of the waveform had been eliminated.

Also observed was an apparent initial pressure rise that was thought to be induced by the current pulse. Two tests were performed to determine the cause of the initial pressure increase. The pressure transducer hole was plugged with a set screw and the transducer was mounted just behind it such that no bore pressure was measured. The test was then repeated and the initial spike was due to electromagnetic (EM) noise caused by the high di/dt present at current initiation. Next, a grounded copper shield was placed around the pressure transducer lead. This reduced the induced signal by 50%.

### *High Speed Photography*

The final diagnostic used with BTR was high speed photography. An Imacon468 high speed digital framing camera was leased from Hadland Corporation. The camera was capable of taking eight exposures with a minimum of 10 ns exposure time and 20 ns inter-frame separation

**Comparison of Simulation to Experimental Results**

To evaluate the performance as measured by the different probe sets a simulation was developed to predict the performance. The system consisted of a capacitor bank discharging through bus work into a railgun. The voltage of the capacitor is

$$V_0 - \frac{1}{C}\int idt \tag{40}$$

where

$V_0$ = initial charge on the capacitor

i = pulsed current

The voltage drop across the bus work is

$$iR_B + L_B \frac{di}{dt} \tag{41}$$

where

$R_B$ = resistance of the bus

$L_B$ = bus inductance

The voltage drop across the railgun is

$$iR(x) + \frac{d[L(x)i]}{dt} + V_{arc} \tag{42}$$

where

$R(x)$ = resistance as a function of position

$L(x)$ = inductance as a function of position

$V_{arc}$ = voltage drop across the plasma arc

The inductive voltage term may be expanded

$$\frac{d[L(x)i]}{dt} = L(x)\frac{di}{dt} + i\frac{dL(x)}{dt} = L(x)\frac{di}{dt} + i\frac{dL(x)}{dx}\frac{dx}{dt} = L'x\frac{di}{dt} + iL'v \qquad (43)$$

where

$L'$ = inductance gradient of the gun

$x$ = position of the arc in the gun

$v$ = velocity of the arc

Kirkhoff's Law is written for the loop and solved for i'

$$i' = \frac{-i(R_B + R'x + L'v) - V_{arc} - (V_0 + \frac{1}{C}\int idt)}{L_B + L'x} \qquad (44)$$

where

$R'$ = resistance gradient of the gun

Equation (1) is revisited to link the railgun motion to the circuit response

$$\frac{d}{dt}(M_{gas}v) = \frac{1}{2}L'i^2 \qquad (45)$$

Utilizing equation (5)

$$v = \frac{\int \frac{1}{2} L' i^2}{M_{gas}} = \frac{\int \frac{1}{2} L' i^2}{\rho_0 A_B x} \tag{46}$$

From these equations the following state function may be written

$$F(1) = \frac{-X(1)(R_B + R'X(4) + L'v) - V_{arc} - (V_0 + \frac{1}{C}X(2))}{L_B + L'X(4)}$$

$$F(2) = i$$

$$F(3) = \frac{1}{2} L' i^2$$

$$F(4) = \frac{X(3)}{\rho_0 A_B X(4) + M_{arc}}$$

where

F(n) = state variable

X(n) = result of the time marching integration

These equations with initial conditions $F(1)=V_0/L_B$, F(2)=0, F(3)=0, F(4)=0 are solved with a time marching integrator.

The predicted current and the current from 5 representative experiments is presented in figure 26. A Pearson current transformer was used to measure railgun current and very good agreement is seen between experiment and simulation.

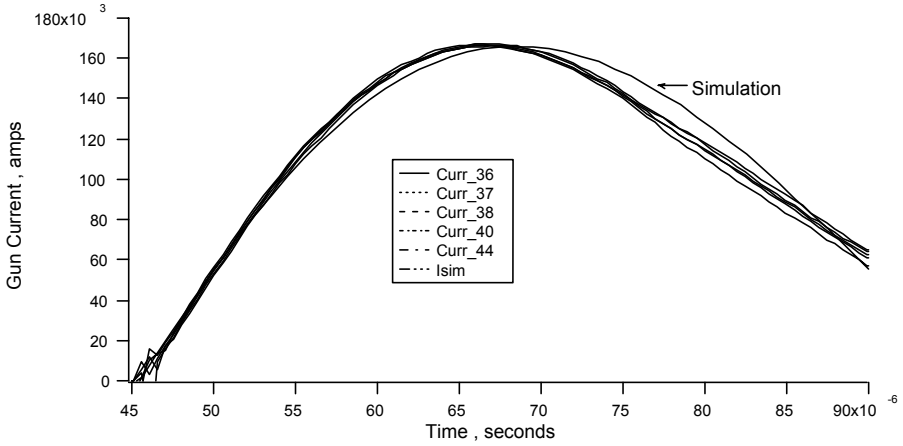


Figure 26. Current from representative experiments compared to simulation

The plasma position versus time and velocity was determined with the b-dot probes. Signals from the five experiments are presented in figure 27. These signals were divided by 10 before they were recorded. It can be seen that the output level is of the correct order as predicted in figure 21.

The signal amplitudes are stronger as the plasma passes the second b-dot position, figure 28. Here the plasma is passing the probe at the time of peak current in the railgun and the magnetic flux from the armature is stronger. The amplitude of these probes is not as important as the time of zero crossing. The zero crossing establishes the passage of the arc armature. The b-dots were repositioned on some tests to allow access to set up other diagnostics. They may not have been reinstalled in precisely the same orientation test to test. This may explain some of the amplitude variations seen in the tests.

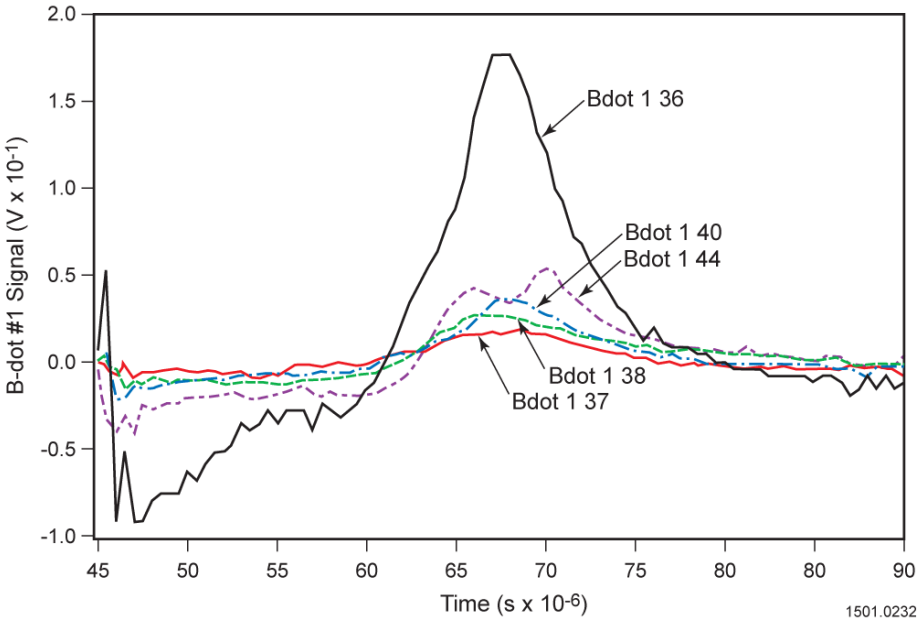


Figure 27. B-dot 1 signal comparisons for series of experiments

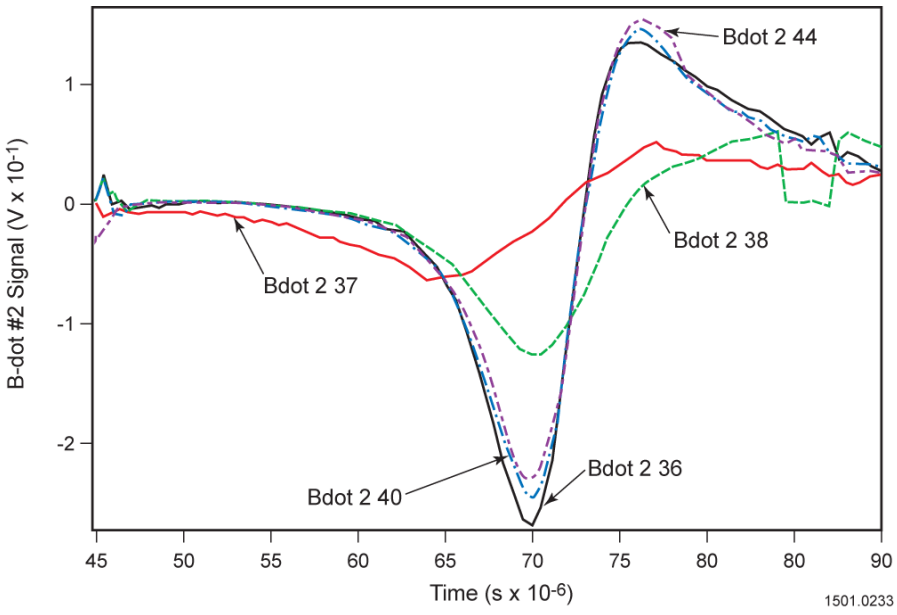


Figure 28. B-dot 2 comparisons for the series of experiments

The time of arc passage for the three fiber optic probes is presented in figures 29, 30, and 31.

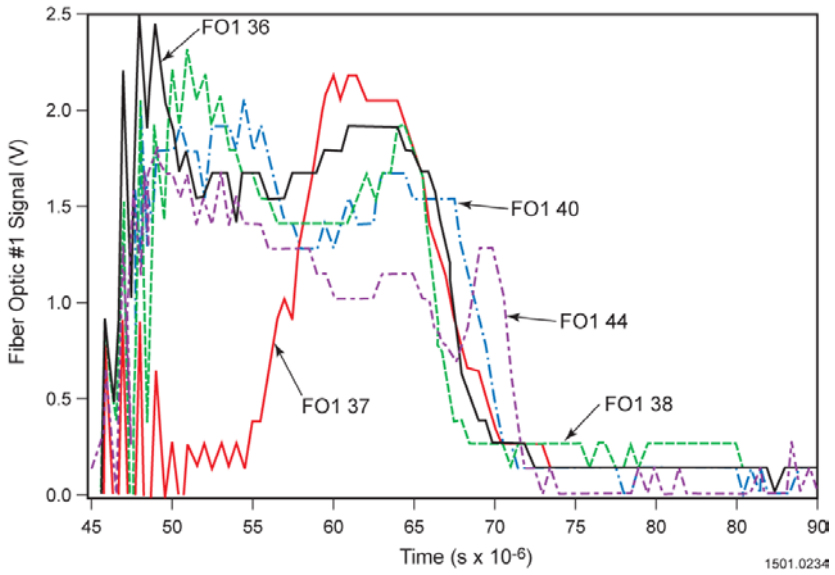


Figure 29. Recordings of arc passing fiber optic position 1

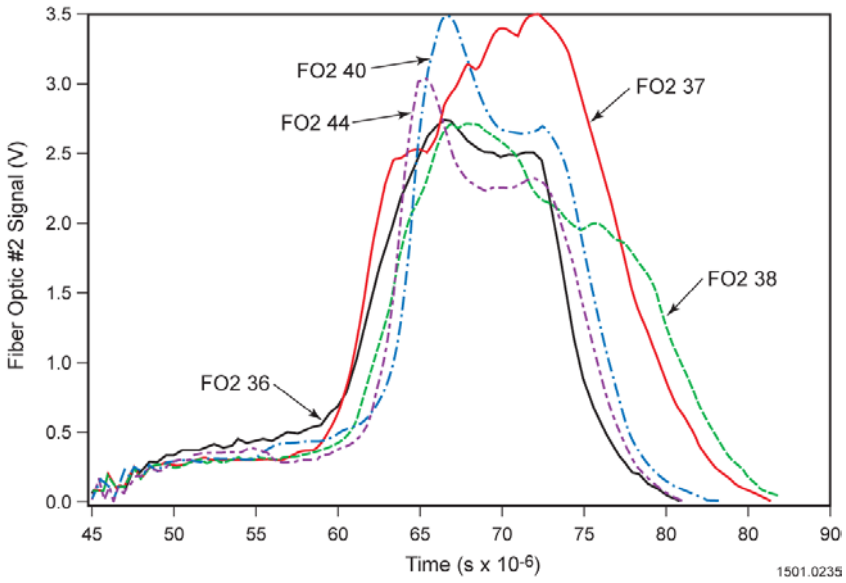


Figure 30. Recordings of arc passing fiber optic position 2

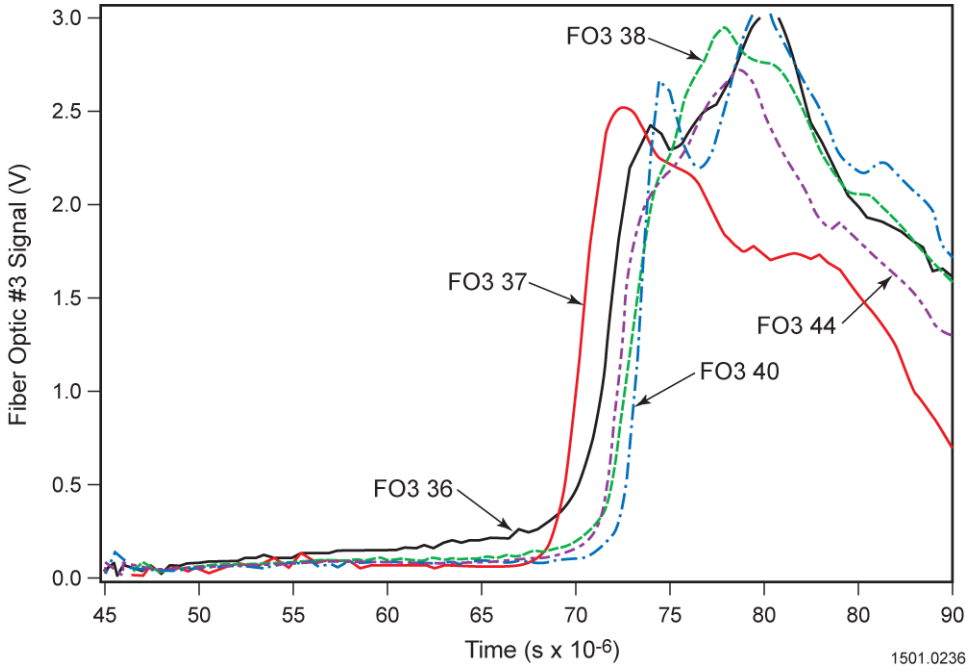


Figure 31. Recordings of arc passing fiber optic position 3

Because the position diagnostic varies slightly shot to shot a band bounding the times when the arc passed the individual diagnostics may be located on the simulated position plot to judge the repeatability of the process. In figure 32 it can be seen that each probe straddles the ideal position indicating good repeatability.

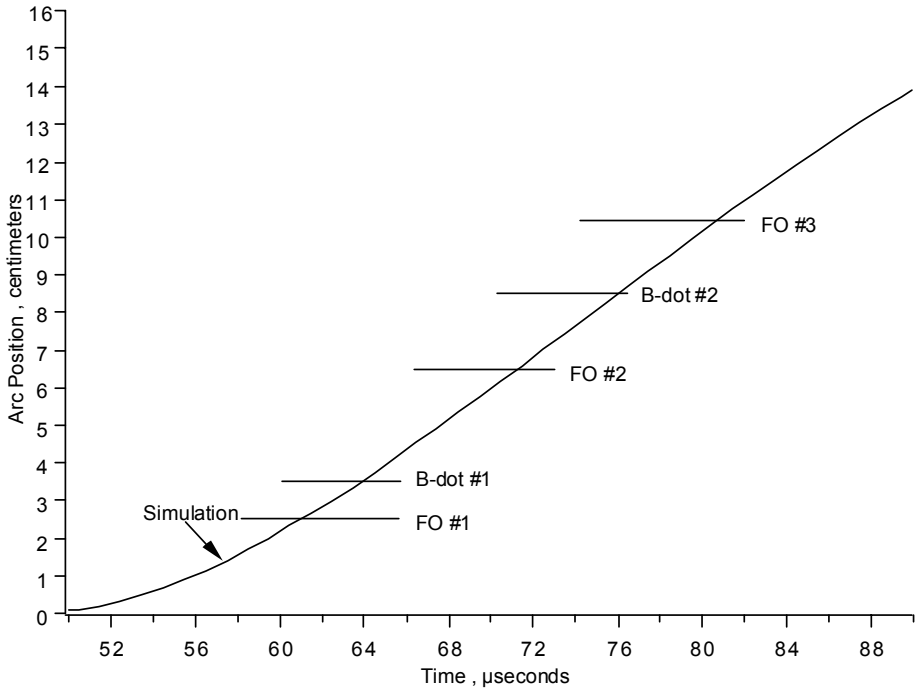


Figure 32. A range of measured arc passage time is indicated for each position diagnostic demonstrating behavior close to the ideal test to test

Discrete measure of the average velocity between the b-dot probes and between each pair of fiber optic probes may be calculated. The results are plotted with the simulated arc velocity in figure 33. Once again very good agreement is seen between simulation and experiment.

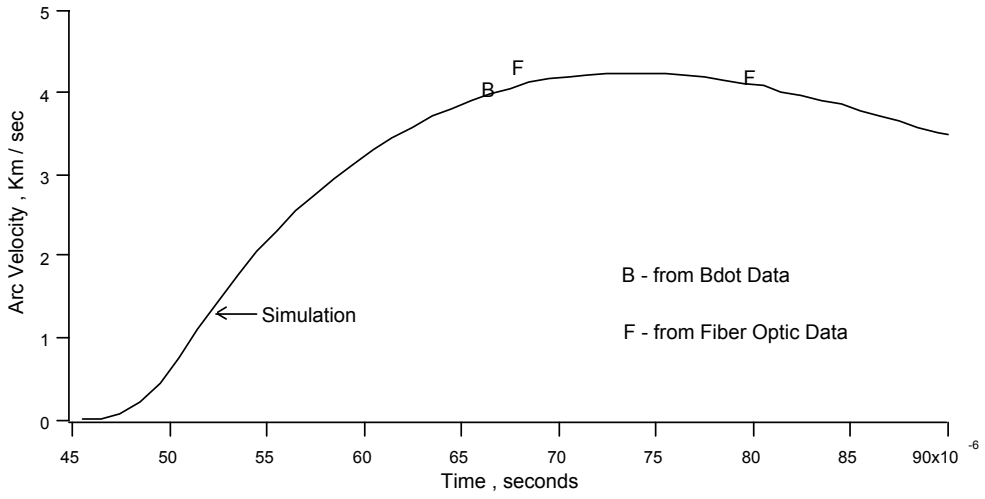


Figure 33. Calculated arc velocity versus simulated velocity

The pressure diagnostic and its comparison to simulation is shown in figure 34. The simulation assumes that the arc is an efficient snowplow and generates the pressure amplitude based on shock theory and its duration based on simulated gas column length and velocity. The longer dwell of measured pressure is not understood at this time. It well could be gas products formed by the arc heating the Lexan and G10 sidewalls. These components could well liberate gas products on heating. A sprayer designed for commercial use would have refractory materials for bore components and not be as susceptible to gas production on heating. A railgun designed for the specific requirements of the process will be discussed in the next chapter.

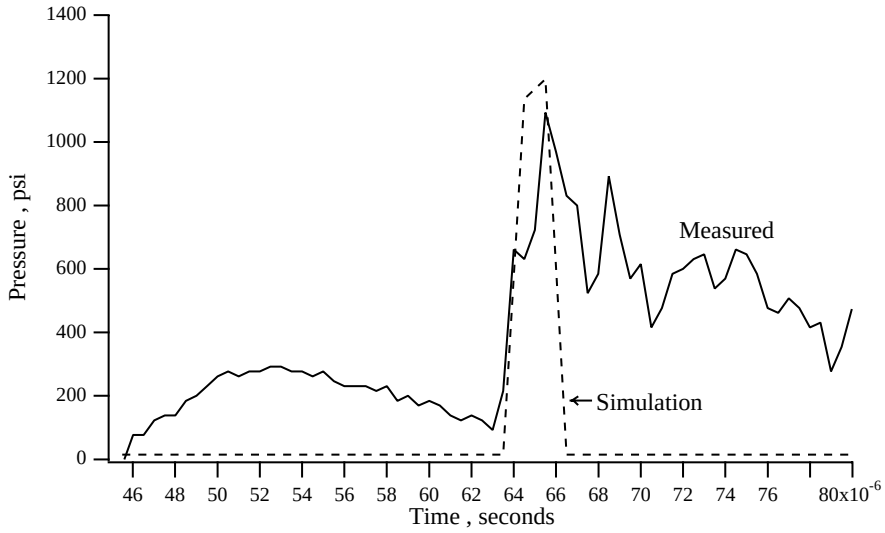


Figure 34. Pressure transducer output and comparison to experiment

The final diagnostic used to confirm the snowplow process was high speed photography. In an earlier test sequence the Hadland camera was used to photograph the plasma arc through the transparent sidewall of the railgun. In those tests the capacitor bank was charged to lower energy and the arc would just approach the first b-dot position before extinguishing. In figure 35 there are four consecutive frames from the camera. On the right of each frame is a stationary black line that is the b-dot probe. The b-dot probes were fixed to the transparent sidewall so that they would appear in the photographic frame. In frames one and two a dark line is seen to approach the probe. The frames in the location of the b-dot are expanded in figure 36 to better illustrate the dark band approaching the probe location.

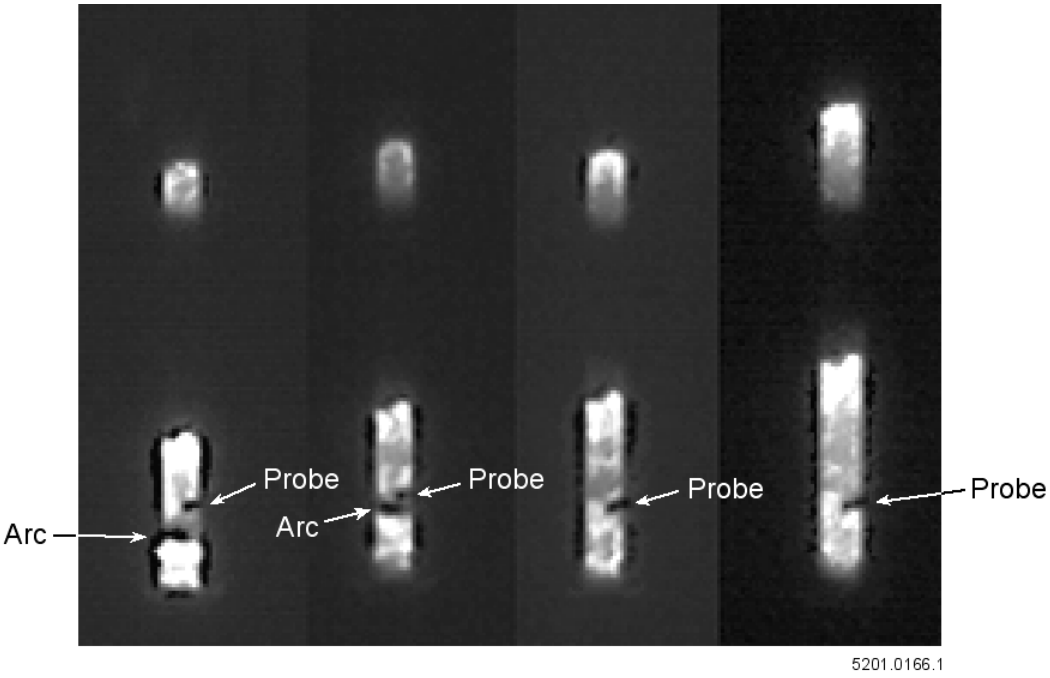


Figure 35. The stationary black mark on the right side of each frame is the b-dot and the arc is seen to approach the probe in the first two frames

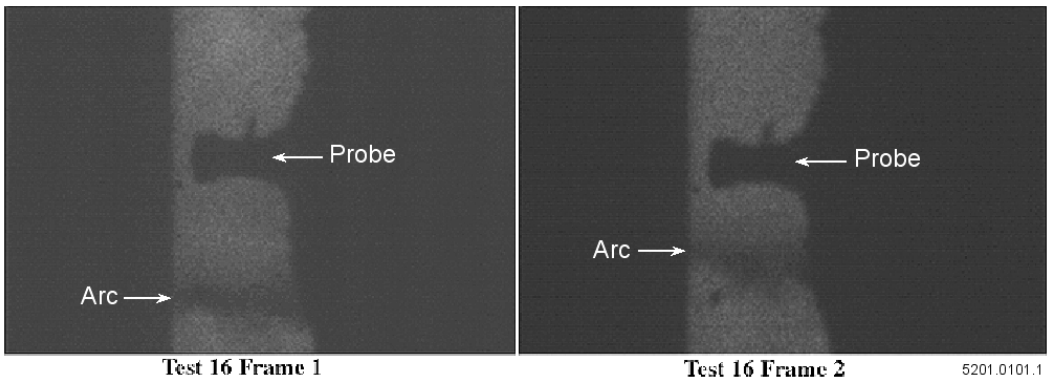


Figure 36. Blow-up showing the first two frames in the location of the b-dot probe

The dark band feature can be explained in the following way. The arc temperature is estimated to be in the 2 eV range (=20,000 C). At such a high temperature, the dense arc gas will radiate like a black body with a spectral peak falling in the ultra-violet (UV) region of the spectrum. A large amount of power is radiated in this wavelength range. The Lexan insulator will absorb some UV radiation, and then the glass in the Hadland Camera lens will strongly absorb the remaining UV. The dark band is then explained by the absorption of UV light in the camera optics. The black band is in fact to be expected.

This observation proved to be valuable in setting up fiber optic probes for the experiment. The fibers used were made of quartz, which has good transmission in the UV. Optical band pass filters were added which transmit only a narrow region in the near UV. These were used with fiber optics to only look at this portion of the light spectrum. By doing this, it becomes more plausible to assume that any intense light signals seen using a fiber optic probe probably correspond to the arc armature passing the position of the probe.

The Hadland camera outputs a voltage pulse every time a frame is captured. This data was recorded on a digital oscilloscope and downloaded to the computer. The trace contains a lot of noise because it is a low level logic grade signal, but the markers are readily identified. The camera framing markers are numbered in figure 37 and demonstrate that the b-dot probe is approaching a voltage zero at the same time the arc is approaching the probe in the photograph. This

confirmed that a nice compact arc was being maintained and that it was behaving according to classical railgun dynamics.

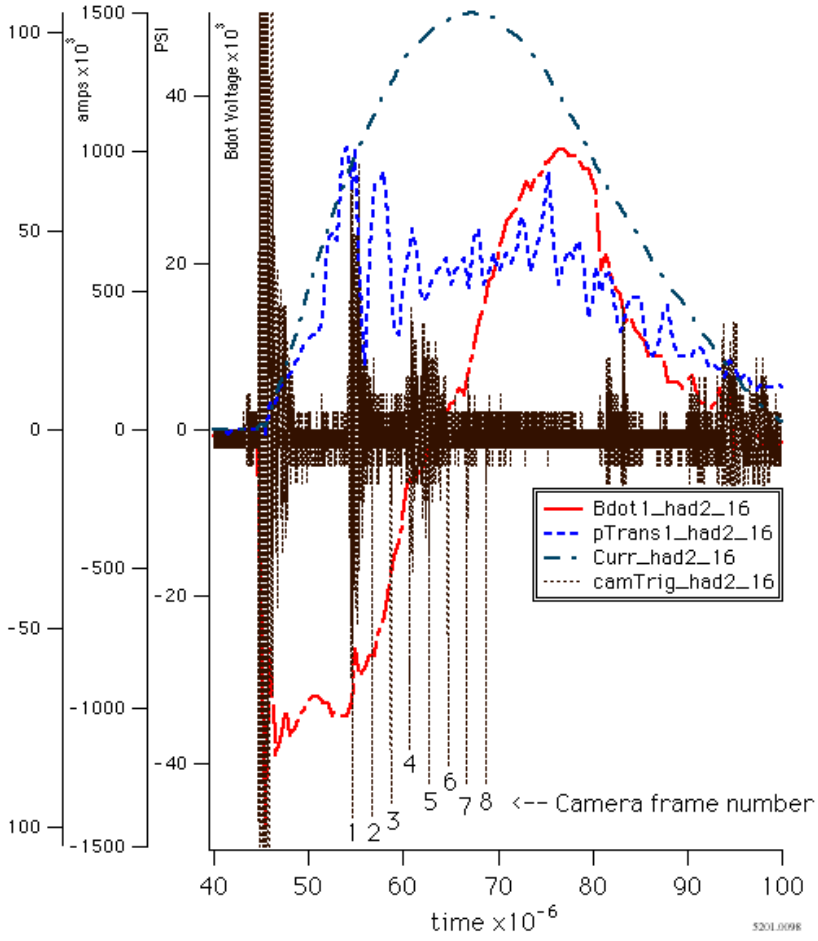


Figure 37. Correlation of camera framing markers to b-dot zero crossing confirming ideal railgun dynamics

After these early experiments correlating the photographic evidence to the b-dot diagnostics the camera was then used in the current experiments to confirm

the plasma drag theory of micro particle acceleration. As shown in figure 16 a strand of fiber optic was inserted through a sidewall insulator and stuck out into the center of the railgun bore. The fiber was coated with vacuum grease and then dipped into a supply of 300 micron diameter, 43 μg glass spheres. The railgun was then fired and the shocked gas column would flow over the glass beads and accelerate them from rest. The simulation was used to predict a final velocity based on the drag theory presented in Chapter 2. The predicted velocity was 600 m/s for this mass and diameter of particle. Figure 38 shows frames captured with the Hadland camera and camera diagnostics were used to measure the micro sphere displacement frame to frame. This combined with the inter-frame time allowed a velocity calculation. The majority of the spheres were seen to accelerate to the predicted final velocity. The slow sphere in the center of the frame could have had a stronger adherence to the fiber optic.

With this strong evidence supporting the snowplow process a laboratory system was designed and constructed to create EPD coatings.

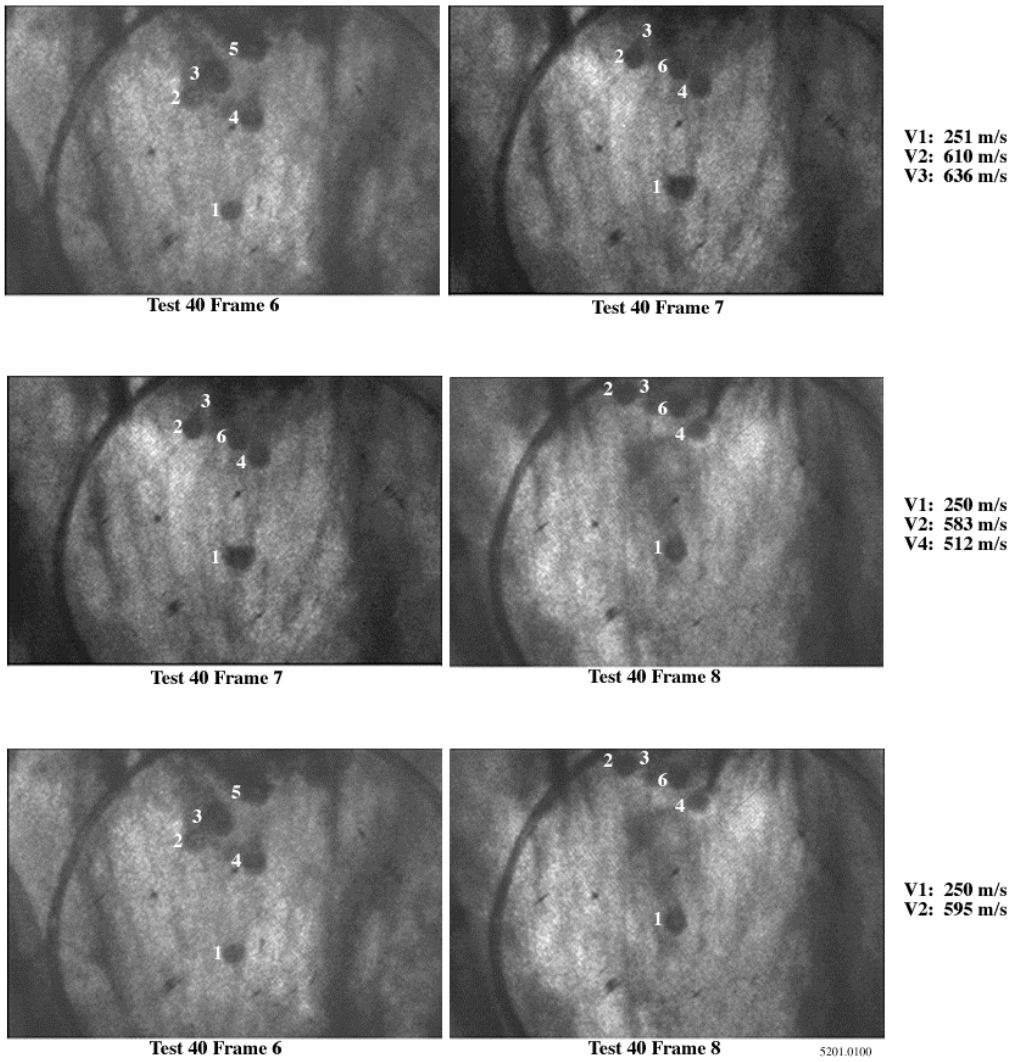


Figure 38. Micro sphere acceleration confirmed with Hadland Camera

# CHAPTER 5: MULTI SHOT SYSTEM

A rep-rate system was required to assess the adherence of the coating layer to layer, to evaluate the ability of the arc starter to reliably operate in a repetitive mode, to determine if deposition rates could be achieved, and to establish that all of the individual components performed repeatable as a system. A power supply to recharge the Pulse Forming Network (PFN) on a repetitive basis would be of high cost and a distribution bus to supply the continuous power was not available in the laboratory. For this reason a high capacitance lower voltage capacitor bank was used to store the energy for multiple shots. The output of this bank was then conditioned with power electronics to provide the repeated charge of the PFN. In Figure 39 is shown the architecture of the system and its control block diagram. Prior to a test the Argon supply into the arc starter is adjusted to a predetermined flow rate. The RF amplifier is turned on and the continuous line source of plasma is created in the coaxial cavity at the breech of the gun. A shot sequence is initiated by manually starting the powder feeder that comes to steady state in under 3 s. After this delay the fire button is pushed and the IGBTs (Integrated Gate Bipolar Transistors) close the charge capacitor bank into the inductor. The control system senses the current in the inductor and at the time of prescribed inductive energy storage the SCR switches are triggered with a pulse train on their gates. After a short delay the gate signal on the IGBT switches is removed and they open to build voltage in the inductor. This voltage charges the PFN through the

SCR switches and when a voltage set point is achieved on the PFN the Triggered Vacuum Switches (TVS) are closed to discharge the PFN into the railgun. After a delay determined by the desired repetition rate the IGBT gate command is again applied to start the sequence for the next discharge. This sequence is repeated at the inter-shot time until the energy in the recharge bank is depleted. The explosive opening switch was installed in the circuit as a fail safe mechanism in case the IGBTs failed to open.

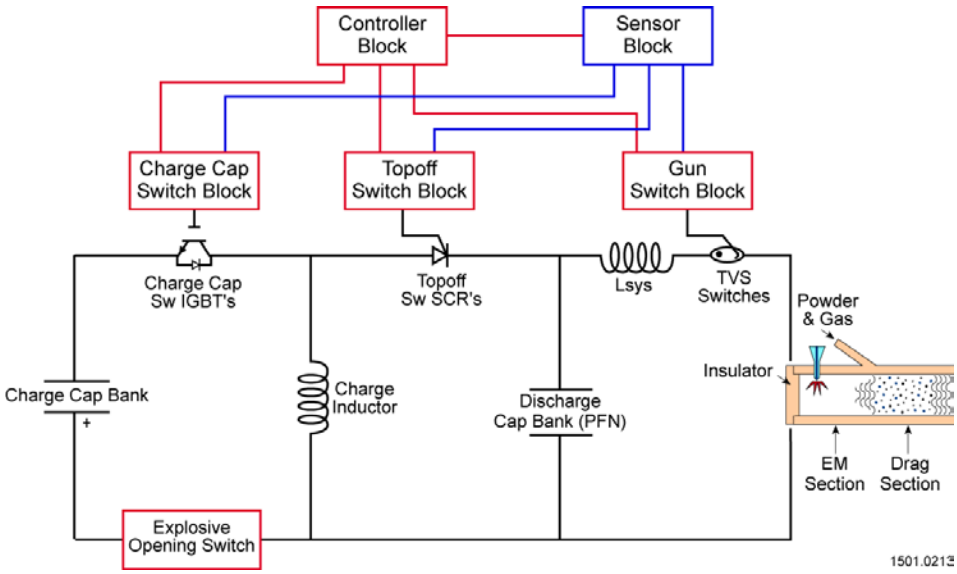


Figure 39. Multi shot system

**Pulse Forming Network**

Lessons learned from the proof of principle experiment were utilized in the rep-rate system. Instead of using paralleled capacitors in the discharge bank a

PFN was developed for the multi-shot system. It was seen earlier that the momentum of the shocked gas column is proportional to the area under the current waveform squared, equation (45). By flattening the current pulse the same momentum may be achieved while lowering the peak current. This is achieved by separating the individual capacitors in the bank with inductive elements making the bank look more like a transmission line whose natural response is a square pulse. The state variables in the simulation code were expanded to represent the extra circuit loops of the PFN and used to establish values for a more ideal current shape, figure 40. Lowering the current lowers the losses throughout the whole system, in particular the losses in the plasma armature. In addition to reducing the thermal management requirement the forces in the pulsed components are lowered proportional to the current squared.

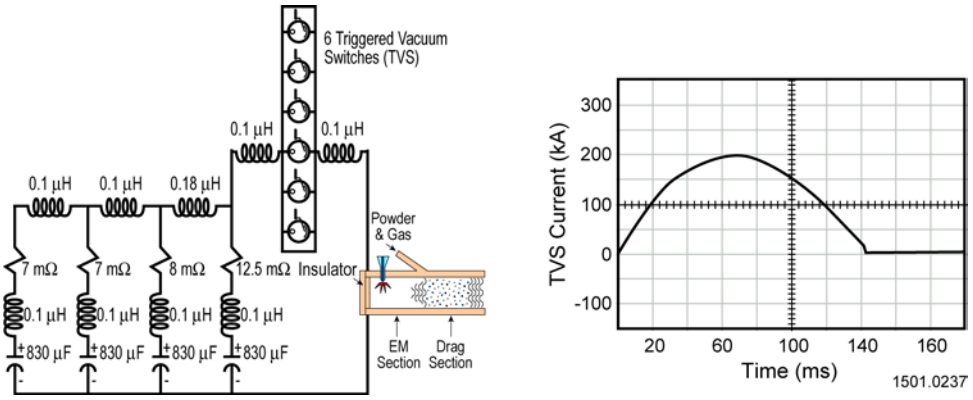


Figure 40. Pulse forming network and predicted response

Ignitrons had been used as the capacitor to railgun switching device in the bench test experiments. Ignitrons were not rated for the peak current that was required for the rep-rate railgun. Testing with ignitrons in parallel on other railgun programs had not yielded favorable results. A search was conducted for a switching device for the multi shot system. SCRs and GTOs were evaluated but it was found that a large number of these devices would be required in series and parallel to meet the switching requirements. At this time Maxwell Laboratories was marketing a Russian switch in the United States with pulsed power capability. The device was called a triggered vacuum switch and its specifications are listed in table 2. This switch was chosen because of its coulomb handling capability, ability to meet the required rep-rate, readily shared current in a parallel configuration, and the switch was very robust. Even though two switches could handle the current requirement of the railgun, six were placed in parallel to increase the probability of extinguishing the arc on a current zero. Plasma operated switches have difficulty recovering on current zero if the slope of the current is too great.

The equipment that was designed, fabricated and installed in the CEM laboratory is shown in figure 41.

Table 2. Triggered vacuum switch (TVS-40) specifications

| Parameter | Value |
|---|---|
| Operating Voltage (kV) | 0.3-25 |
| Operating Current (kA) | ≤140 |
| Charge Transfer/ Discharge Cycle (C) | 100 |
| Cumulative Charge Transfer (C) | $10^6$ |
| Repetition Rate (Hz) | $10^3$ |
| Life (shots) | $10^3$-$10^6$ |
| Trigger Voltage (kV) | 5 |
| Length (cm) | 20 |
| Diameter (cm) | 15 |
| Weight (kg) | 9 |

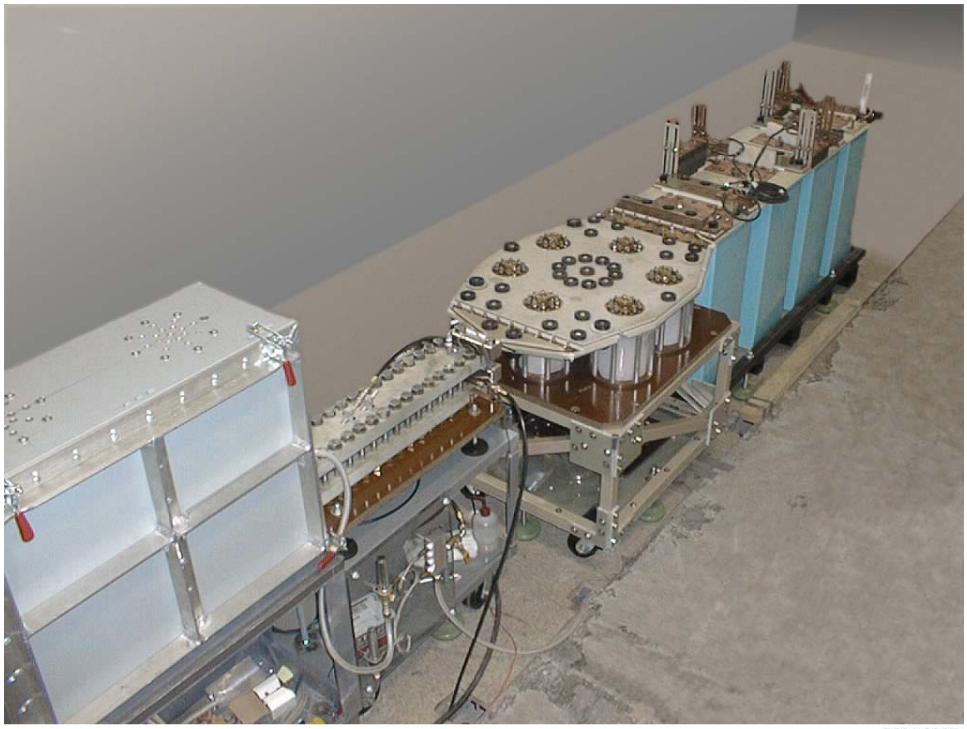


Figure 41. PFN, TVS switch module and the powder spray railgun

**Recharge Circuitry**

Figure 42 lists values of components used in the recharge circuit and the current traces for the respective charging paths. Closing the IGBTs allows current to flow from the recharge bank, charging the energy storage inductor. When the energy stored is sufficient to charge the PFN the IGBTs open and commutate current into the SCR leg. Charge flows from the inductor to the PFN until all energy has been transferred.

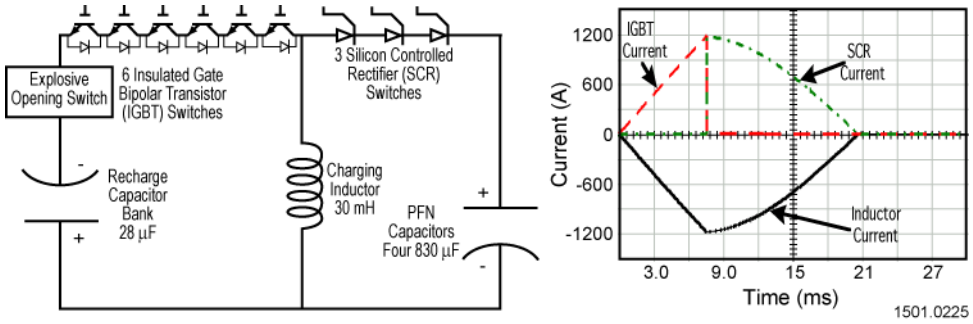


Figure 42. Recharge circuitry

When the cycle starts both the IGBTs and the SCRs are holding off the voltage of the recharge bank, figure 43. The IGBTs turn on and their voltage drops low while the SCRs continue to hold off voltage. When the control senses the inductor current set point it fires the SCRs and shortly thereafter removes the

gate signal from the IGBTs. The inductor then builds voltage on top of the re-charge bank from the perspective of the IGBTs and directly across the PFN. The IGBTs are designed to hold off the total of the recharge bank and the PFN. After the PFN is charged and the inductor current goes to zero the SCRs turn off. At this time the circuit is back to its start condition and prepared for another cycle. The control upon sensing the discharge of the PFN will restart the operation after the delay indicated by the rep-rate.

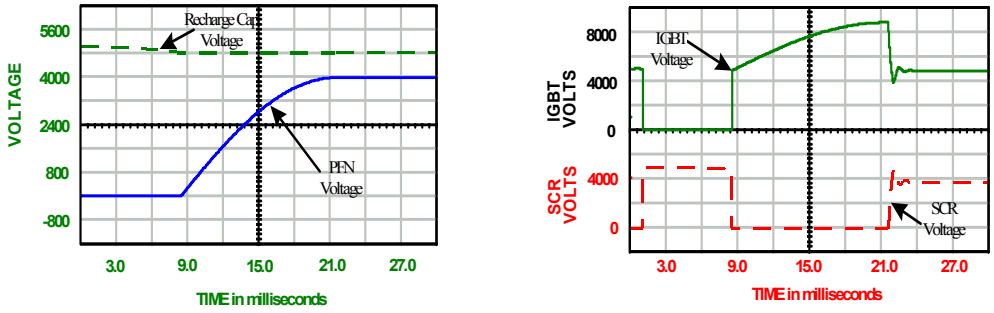


Figure 43. Voltage traces demonstrating the behavior of the recharge circuit

Figure 44 presents the components of the recharge system; in the back-ground is the recharge capacitor and the explosive opening switch. Moving for-ward is seen the box that contains the IGBTs. Next is the inductive store with the SCR module shown in the foreground.

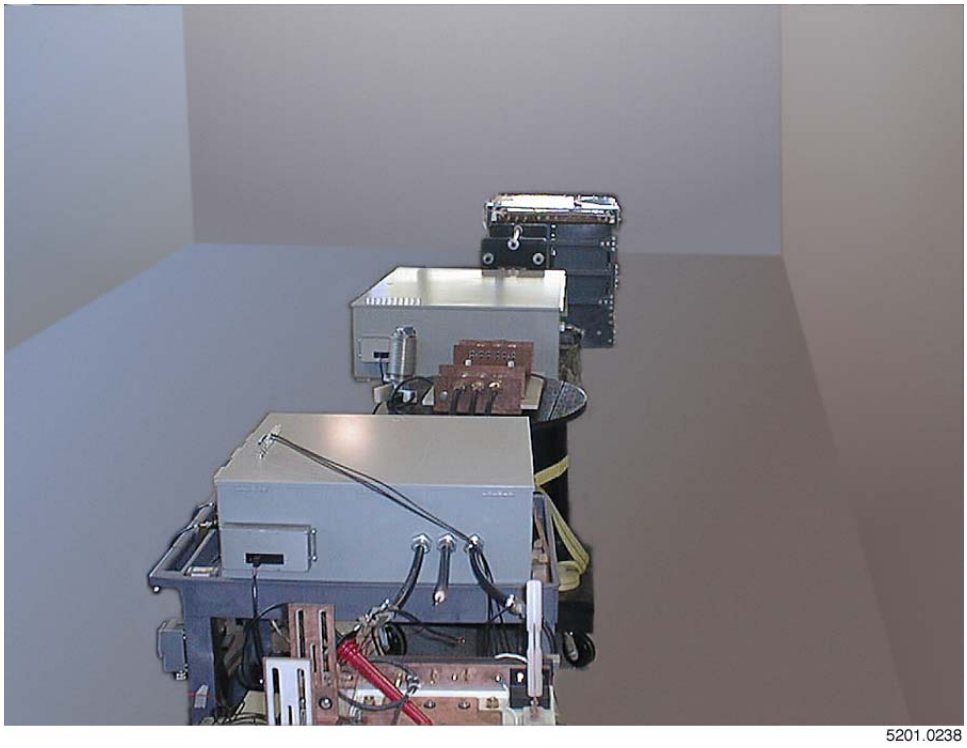


Figure 44. Recharge circuit modules including from front to back the SCR module, the energy storage inductor, the IGBT module, the explosive opening switch and the recharge capacitor bank

Observations of induced noise in the proof of principle experiment drove the design of the pulsed power circuit geometry for the rep-rate system. The power circuit would be in a coaxial geometry throughout even though many of the building blocks did not lend themselves to this architecture. In a coaxial geometry the field is contained between the inner and outer coax. Where coax bus work was not possible large flat plate bus bars were used because they emit small leakage flux near the edges of the parallel plates. Figure 45 shows a conceptual layout that

would achieve this goal. This arrangement was important to reduce pulsed fields at the instrumentation and control for the laboratory system and to demonstrate that the pulsed power technology did not have to introduce additional electrical noise to the industrial environment.

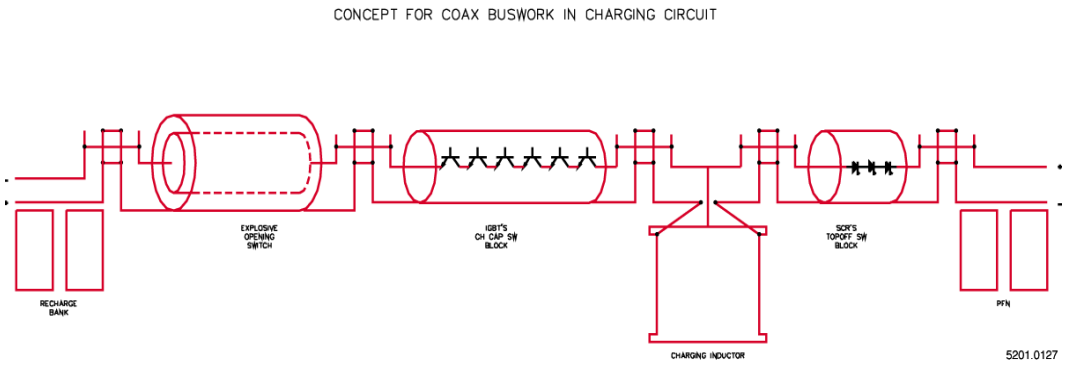


Figure 45. Concept for the coaxial arrangement of the pulsed power circuit

The IGBTs chosen were EUPEC FZ 800 R33 KF1 and their specification and required operation are presented in table 3. The IGBTs are packaged as low profile rectangular solids. They were bussed together and then placed in a metal box. The shields of coaxial cable used to connect the circuit elements together were connected to the metal box. The box carried current and was insulated from ground. The center conductors of the coax penetrated the box and were connected to the input and output bus of the IGBT string, figure 46.

Table 3. IGBT Data for FZ 800 R33 KF1 (EUPEC)

| Parameter | Operating point | Specification |
|---|---|---|
| Collector Emitter Voltage, $V_{ce}$ | 1500 V | 3300 V |
| DC Collector Current, $I_c$ | 150 A | 800 A |
| Repetitive Peak Collector Current, $I_{crm}$ | 1200 A | 1600 A |
| Total Power Dissipation, $P_{tot}$ | 600 W | 8900 W |
| Gate-Emitter Peak Voltage, $V_{ge}$ | +13 V | ± 20 V |
| DC Forward Current, $I_f$ | 0 A | 800 A |
| Repetitive Peak Reverse Current, $I_{frm}$ | 0 A | 1600 A |

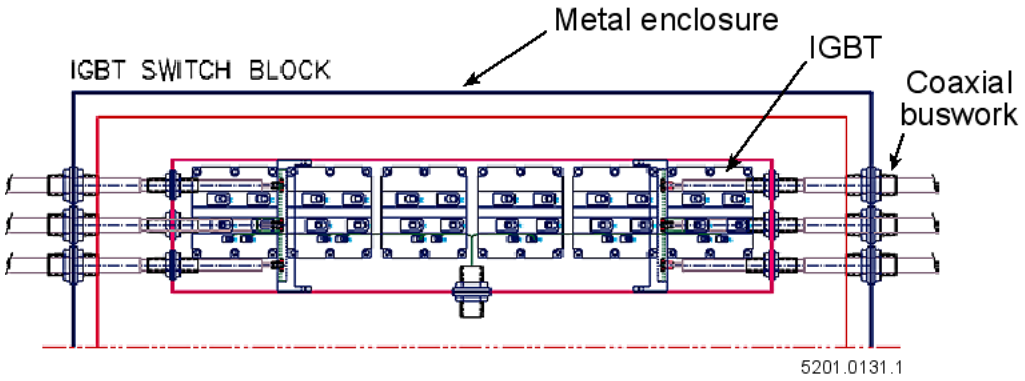


Figure 46. Packaging of IGBTs

The SCRs selected were SPCO XSPT401BGHT and their specification and operating point are presented in table 4. The SCRs are packaged as circular flat packs and must be preloaded by the bus clamping structure. Similarly to the IGBTs the SCRs were placed in a metal box and the shields of the interconnecting coaxial cables were connected to the box. The box was then isolated from ground. The center conductors of the coax penetrated the box and connected to the SCR bus work, figure 47.

Table 4. SCR Data for XSPT401BHT (SPCO)

| Parameter | Operating point | Specification |
|---|---|---|
| Repetitive Peak Off State Voltage, $V_{drm}$ | 1667 V | 5000 V |
| Repetitive Peak Reverse Voltage, $V_{rrm}$ | 1667 V | 5000 V |
| Average On-State Current, $I_t$(ave) | 150 A | 4500 A |
| External Clamping Force | | 2500 lb |
| Snubber Capacitor | | 0.5 µF |
| Snubber Resistor | | 200 ohms |

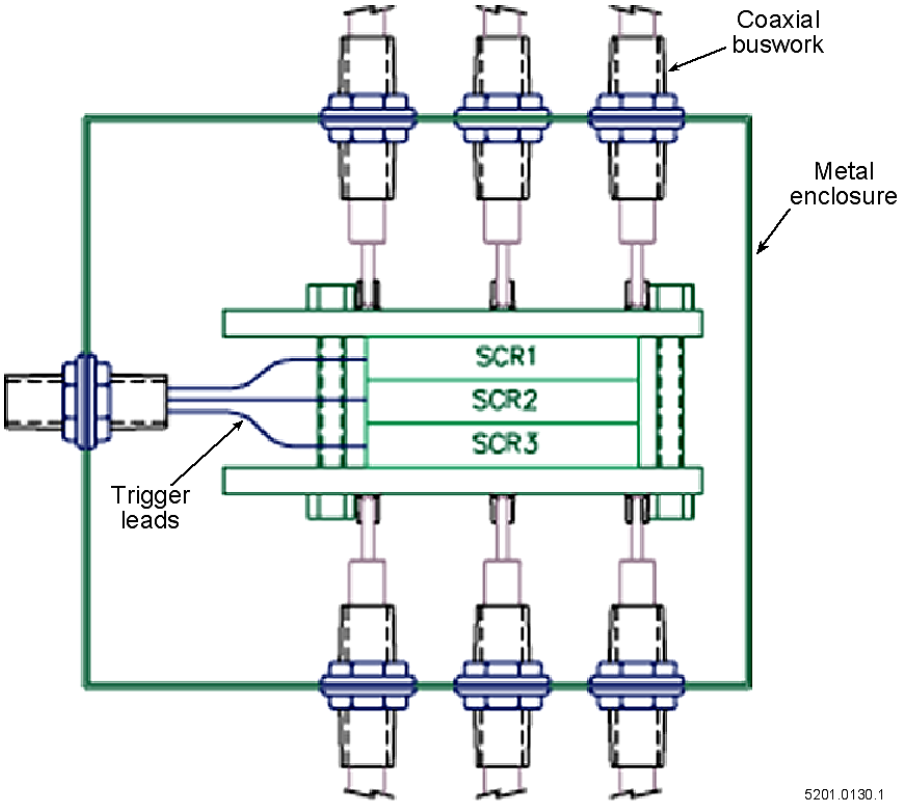


Figure 47. SCR packaging

The energy storage inductor was designed using solenoidal inductor formulas from Frederick Grover[13]. A Basic program was written to iterate on the turns per layer, the number of layers, and the conductor size until the required inductance was achieved with minimal dissipative loss. The design values are presented in table 5. The inductor was hand wrapped Essex 600 V welding cable on a reinforced spool. The outer diameter of the solenoid was banded with glass tape to support the magnetic pressure. A drawing of the inductor is presented in figure 48.

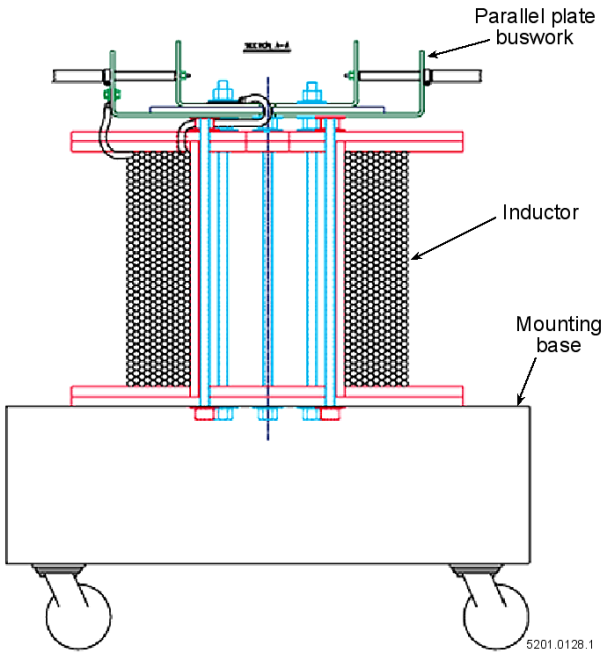


Figure 48. Energy storage inductor

Table 5. Energy storage inductor parameters

| Parameter | Value |
|---|---|
| Inductance | 31.8 mH |
| DC Resistance | 0.263 ohms |
| Number of turns | 396 |
| Number of Layers | 11 |
| Number of Turn Per Layer | 36 |
| Conductor diameter | 0.111 in. |

An explosive opening switch was installed in the charging circuit as a fail-safe device. The total electrical action that the capacitor bank would put through the energy storage inductor if the IGBTs did not receive an open command would have exceeded their rating. The control system sensed the current and if the current in the IGBTs had not gone to zero within a specified maximum charging time then the control would detonate the explosive charge in the opening switch bus work and interrupt the circuit. The opening switch is shown in figure 49. It was packaged in a containment vessel and a cage structure was built around the vessel to provide the outer coaxial conductor in the charging circuit. The inner conductor of the coax was the busbar itself.

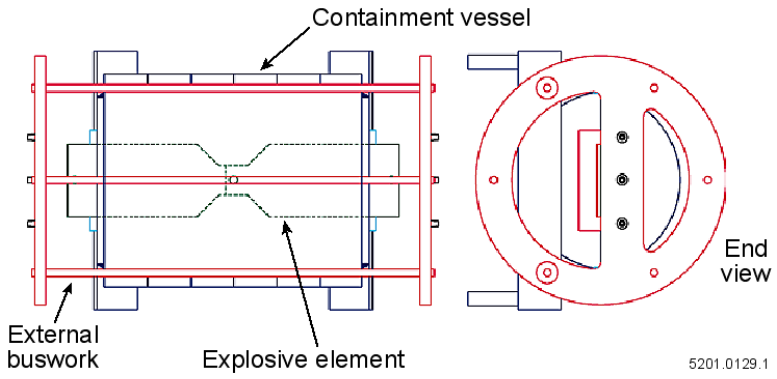


Figure 49. Explosive opening switch

**Railgun Accelerator**

This author has guided the technical evolution of electromagnetic launchers for 19 years and produced the conceptual design of the EPD railgun, figure 50. The design features a large inductance gradient for high efficiency and a favorable impedance match to pulsed power source. The importance of stiffness in high performance guns was discovered in early experiments with electromagnetic launchers. This attribute allows a precise bore shot to shot, proper pre-stress of bore components for minimum bore expansion and proper activation of plasma seals. This finding has been reported in a number of journal refereed papers [14,15,16]. Minimum bore deflection allows integration of ceramic refractory materials for long life durable sidewall insulators. In addition the preload of high stiffness sidewalls creates a plasma seal which avoids plasma leakage, a very serious instability, and the subsequent rail erosion on plasma reconstitution.

The rails are cut from a solid piece of chrome copper. The cross section of the rails is shaped like a bishops hat with laminated wings to either side.

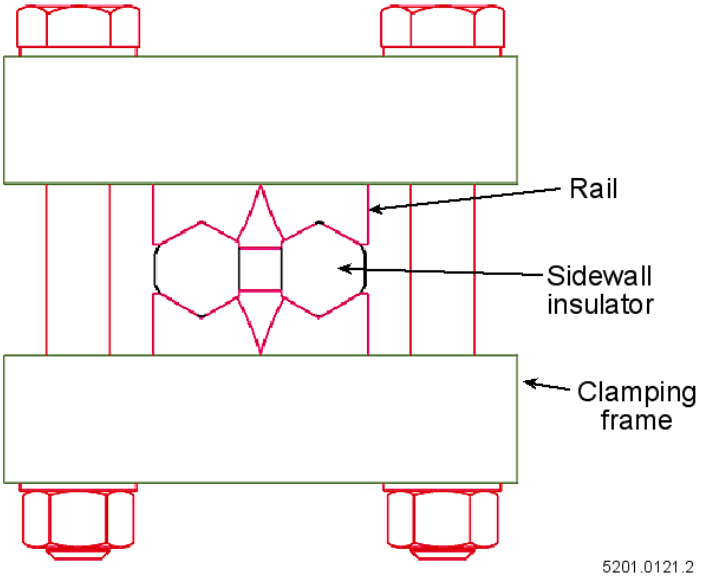


Figure 50. Powder spray railgun

The laminated wings are produced by making saw cuts from the edges of the chrome copper just leaving the triangular section in the middle, figure 51. This technique is the key to producing very stiff high inductance gradient guns. In equation (43) it was shown that one of the inductive voltage terms is iL'v. L'v has the units of ohms. The power going into this dynamic resistance is directly responsible for the acceleration of the gas column. The higher this value the greater the efficiency of the railgun. By narrowing the rail profile with the saw cuts the inductance gradient has been increased. FORTRAN codes based on the formulation of Leuer [17] were written to calculate the gradient for arbitrary rail geometries. Inductance gradients for this geometry were calculated to be 0.45 $\mu H / m$. The question should be asked, why have the laminations at all? This overhanging structure is key to use of ceramic materials in railguns. It is seen in figure 50 that

the wings directly clamp and preload the ceramic sidewalls. The large bolts in the exterior frame apply load to the rails, which in turn place the ceramic in a compressive pre-stress. The modulus of a conventional steel gun barrel is 30 Msi. The modulus of the ceramic sidewalls is 40 Msi demonstrating how the use of this material can significantly stiffen gun barrels. The clamping frame is made of G-10. It is important to keep conducting materials away from close proximity with the rails. Eddy current induced in conducting structures would lower the inductance gradient. The frame was designed for laboratory utility. It could easily be replaced with a less bulky composite structure for later industrial sprayers.

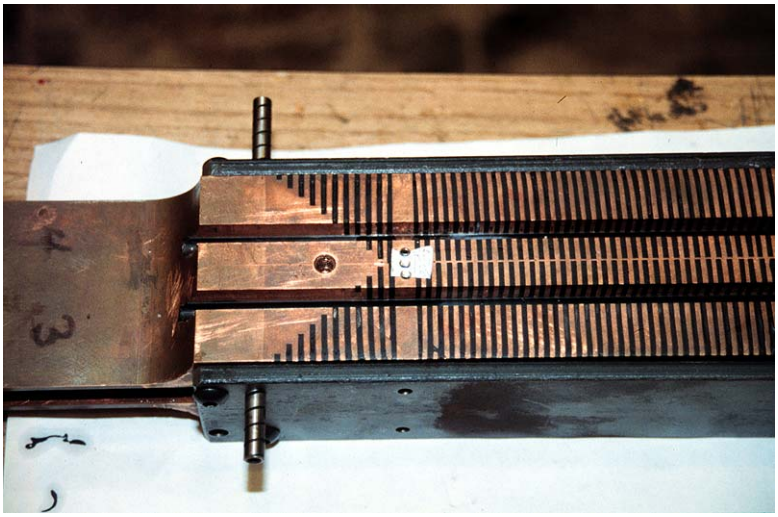

Figure 51. Actual rail set showing the saw cuts that laminate the rail

The method of integrating the arc starter into the breech of the gun is illustrated in figure 52. A series of ports are drilled and then selectively plugged to

form an Argon manifold that delivers gas at atmospheric pressure to the coaxial cavity. A hole is cross drilled through both ceramic sidewalls and just below the surface of the rail. Another machining operation then cuts through the rail surface to expose the arc starter cavity to the bore. A set of coaxial electrodes are inserted through one ceramic sidewall and the other sidewall is plugged with a quartz site glass to seal the cavity. The bore is plugged with a square ceramic block to seal the breech.

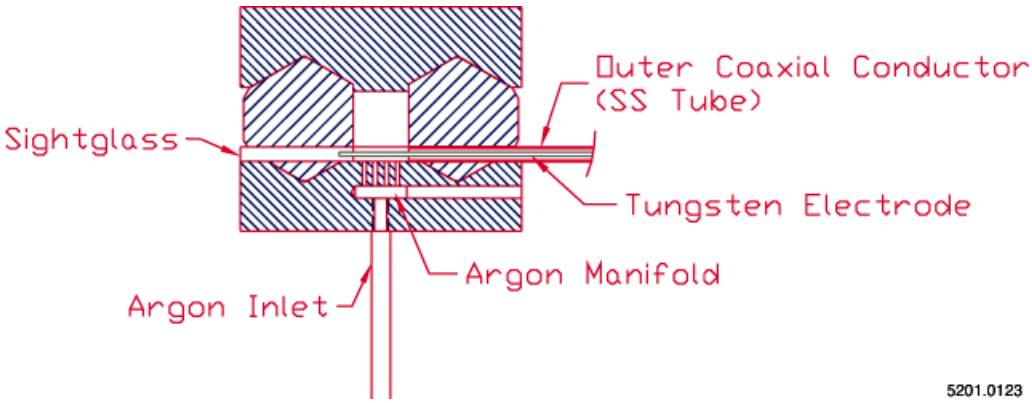


Figure 52. Integration of arc starter into the breech of the railgun

A picture looking down the bore from the muzzle in figure 53 shows the light from the arc starter plasma.

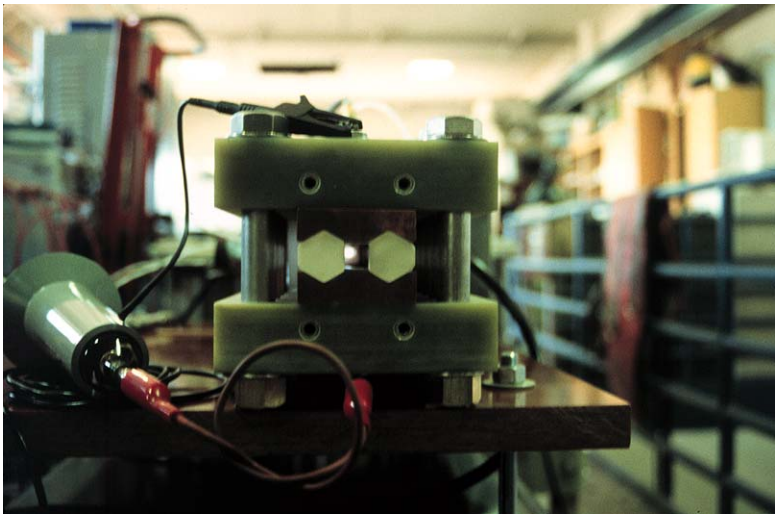

Figure 53. The light from the arc starter plasma can be seen looking into the muzzle of the gun

The gun was instrumented with b-dot probes to sense the position of the plasma armature and evaluate performance. The square bore accelerator (SBA) has the same bore dimensions as the BTR therefore W and H (fig. 20) are the same for both guns. In the SBA b-dot probes cannot be positioned as close to the bore centerline due to the thickness of the ceramic insulator. Dimension D is now 1.25 in. The decision was made to wrap the coils on 0.1 in. diameter forms for ease of manufacture and the number of turns was iterated until a large signal to noise ratio was obtained in the calculated output. Fifty turns were selected for the coils. The predicted output of 6 V peak is presented in figure 54.

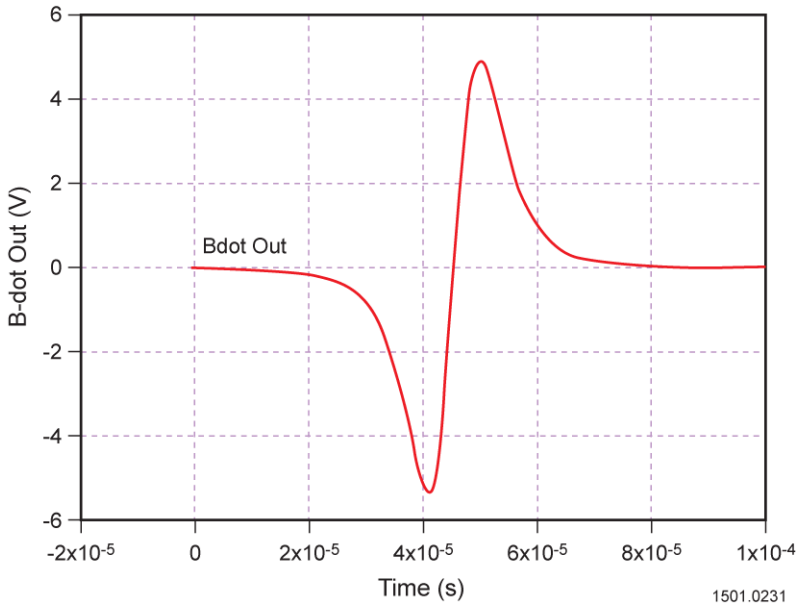


Figure 54. Calculated output of b-dot probes designed for SBA

The calculated output of this b-dot coil shows more symmetry of the positive and negative peaks of the voltage signal. Because the probe is positioned farther from the bore centerline, it is less sensitive to the distribution of current in the armature. The main information, the zero crossing of the armature flux, is well identified and velocity calculations using the probes will be accurate. There are B-dot mounting holes located every 1.72 in. down the length of the gun, figure 55. Three probes will be located along the SBA to resolve plasma armature velocity.

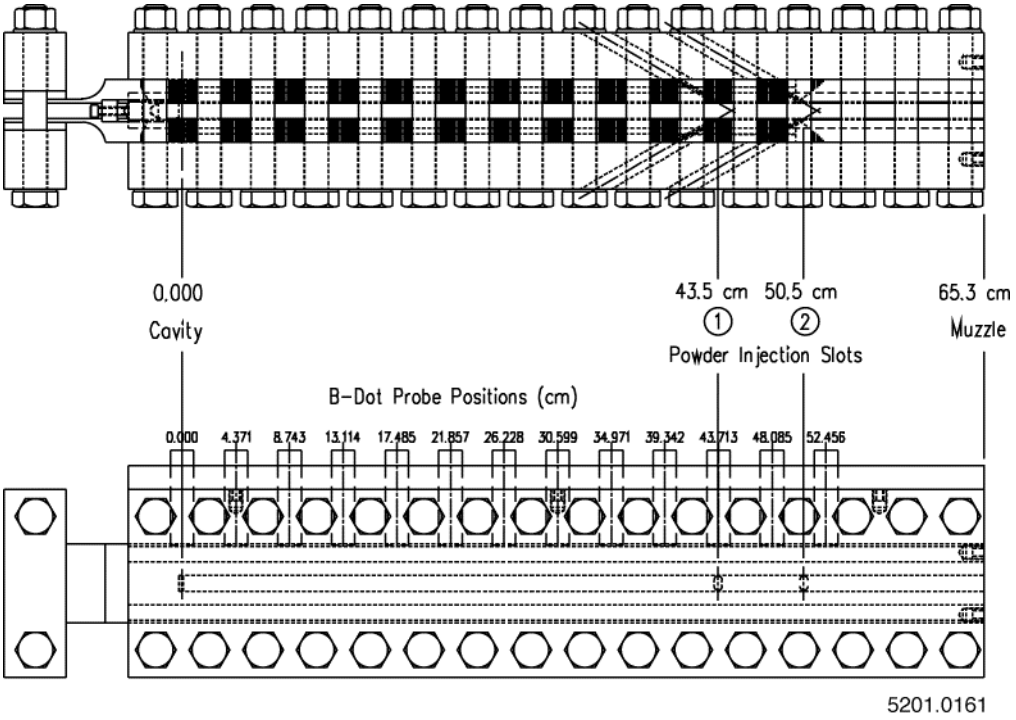


Figure 55. Instrumentation and powder port locations on SBA

Two locations for powder delivery ports were designed into the launcher. This was done to provide some adjustment between acceleration length and entrainment length. The tubes that braze into the back of the rails are shown in figure 56. A wide narrow slot is used to uniformly introduce powder into the bore.

A close-up of the slots is shown in figure 57. This photo also shows the thin layer of Inconel that is brazed to the surface of the rail. Inconel was chosen for its high melting point and the majority of the powder to be sprayed in this

launcher was Inconel. This insured any rail by-products would not contaminate the coatings.

The rails lying on the clamping structure are shown in figure 58. In an industrial rated gun this structure would be replaced with a graphite over wrap and integrated preload device.

The assembled railgun is shown in figure 59. The muzzle is sealed to the spray chamber and the rails are bolted to the PFN bus work. The clear tubing at the breech is supplying Argon the arc starter. The three equally spaced b-dots are installed against the right ceramic sidewall. The black hose on the top of the gun is connected to the powder feeder.

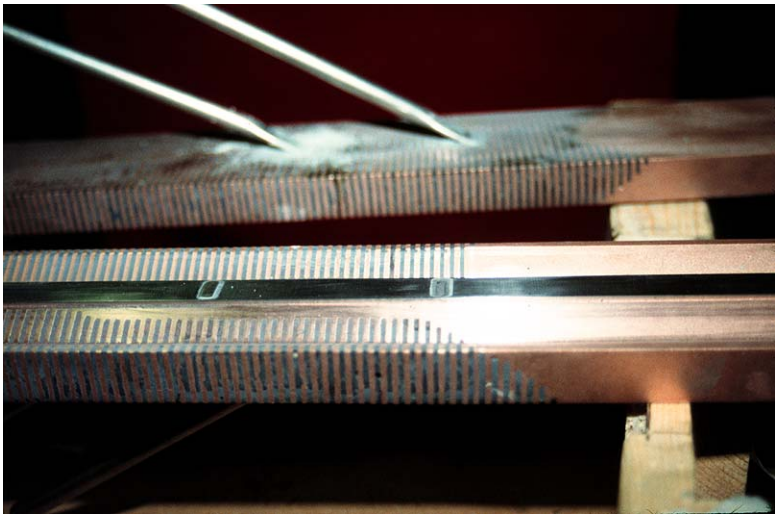

Figure 56. Flattened tubing is brazed into the backs of the rails and used to deliver powder to the bore

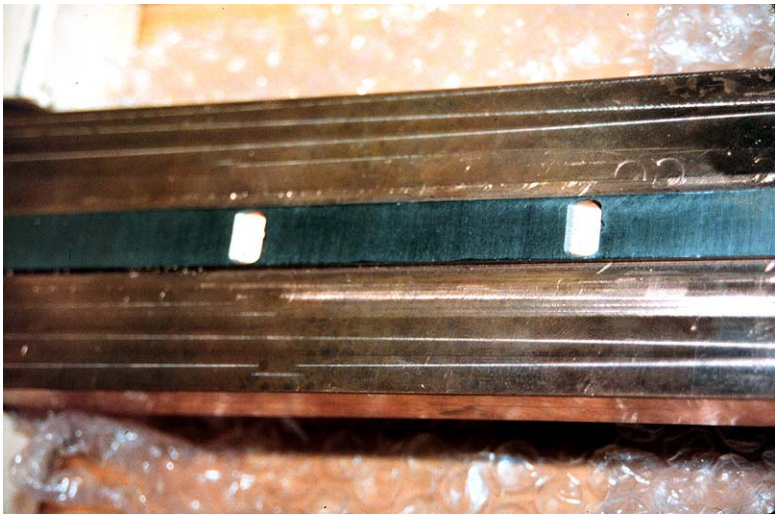

Figure 57. Photograph showing the Inconel brazed to the bore surface of the rail and the bore side of the powder ports

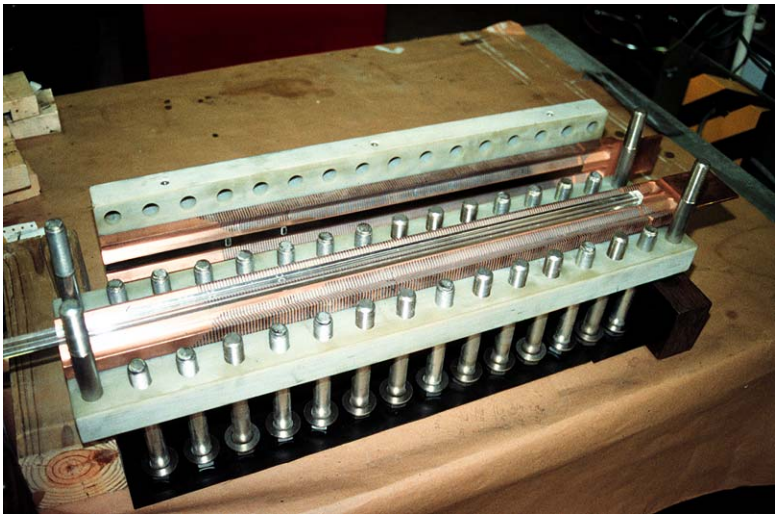

Figure 58. Railgun clamping structure

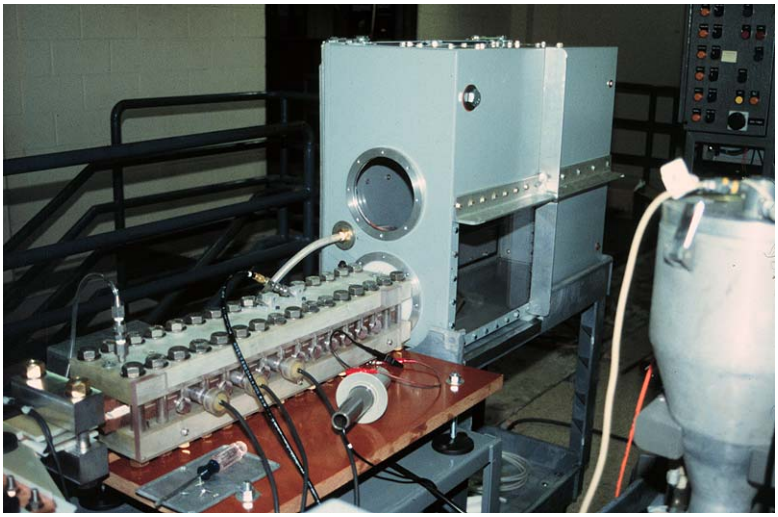

Figure 59. SBA connected to spray chamber

The spray chamber has its own argon supply to insure that the coating specimens are submerged in inert gas. The supply of argon in the chamber gives the gun the ability to fill from the muzzle as well as the argon that is introduced from the arc starter cavity at the breech of the gun. These two supplies insure that the gun bore has a supply of atmospheric argon at the start of each discharge. An open shutter photograph of the spray system creating a coupon for evaluation is shown in figure 60.

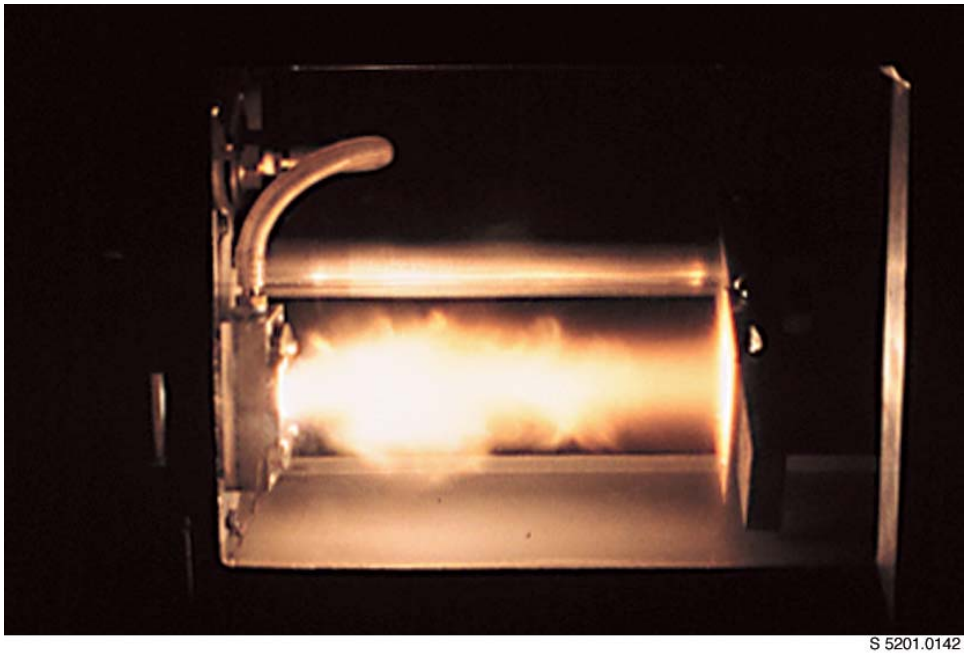


Figure 60. Open shutter photograph of railgun coating a substrate

# CHAPTER 6: MULTI SHOT CONTROL SYSTEM

A multi shot control system was designed with several aspects that would be required of an industrial system [18]. The system has a simple user interface, is noise immune and fault tolerant. In industrial use the powder sprayer will be one part of a larger system including parts manipulator, visions system and spray booth atmosphere control. The multi shot controller was designed to interface with a main process computer. For the laboratory system parts of the control were performed manually and executed from a checklist for expediency and cost savings.

## Control System Philosophy

Years of experience working with pulsed power systems were leveraged in designing the architecture of the pulsed power system and its control. First, the pulsed power system would be completely floating and designed for isolation to ground at twice the maximum voltage seen in the system. Second, the controls and instrumentation would make no galvanic connection to the pulsed power system therefore insuring no ground loops would be possible. The realization of each of these points for each block of the system will now be discussed while referring to figure 61.

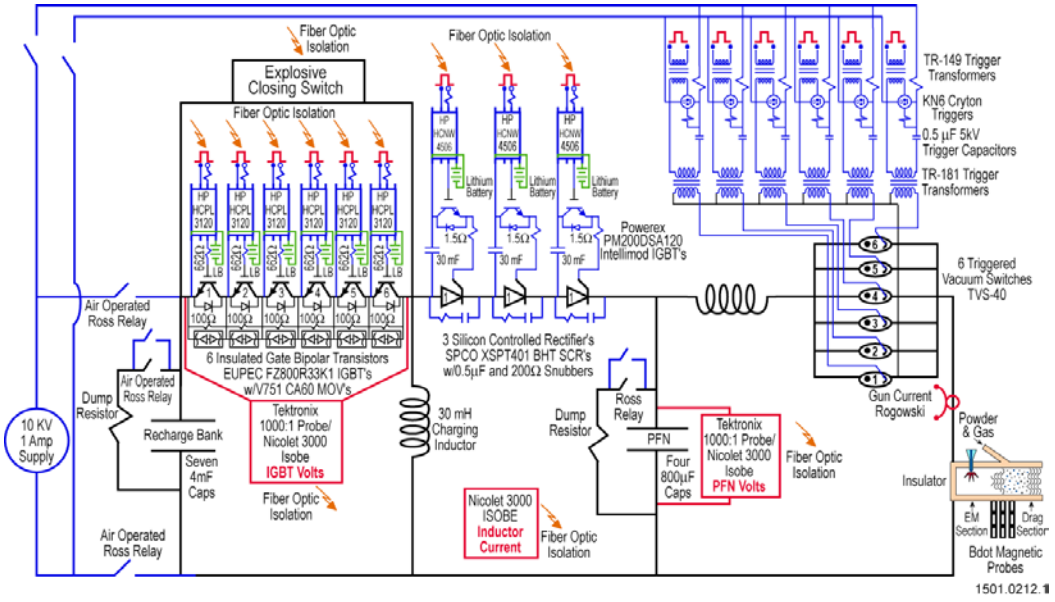


Figure 61. Pulsed power system with instrumentation and control interface points

Observations will start with the recharge capacitor bank. The recharge capacitor bank is charged manually with a 10 kV, 1 A commercial power supply. After charging the bank with sufficient energy for the expected number of shots the power supply is disconnected with dual Ross Relays isolating the bank. The next module is the IGBT switch, figure 62.

Each switch is triggered via a fiber optic coupler and the IGBT side of the coupler is powered with Lithium batteries. Each optocoupler was high potted to demonstrate 10 kV hold off. Not only are the IGBTs triggers isolated to ground they are also isolated from each other. Voltage measurements were made across the IGBTs with 1000:1 Tektronix voltage probes connected to a Nicolet Isobe

unit. The Isobe is a fiber optically isolated data acquisition module manufactured by Nicolet Company. The device consists of two units. One unit is battery powered and interfaces to the instrumentation. The second unit is wall outlet powered and interfaces to conventional data acquisition and control. The two modules are connected together with fiber optics that transmit the data real time at a 1.0 MHz rate. In parallel with the IGBTs is an explosive closing switch. If the current in the IGBT leg gets too large the control will explosively close galvanic contacts across the IGBT array and the capacitive energy will be dissipated in the energy storage inductor. The control unit to the explosive firing box is optically isolated. Earlier the explosive unit was described as an opening switch. Both units were thoroughly tested and used at different times, but fortunately were never triggered. The system had high reliability and never used this fail-safe. The next instrumentation and control point is the current through the energy storage inductor. The inductor is shown in figure 63 and the current viewing resistor is the finned device on top of the inductor behind the bus plate.

The current is measured with the current viewing resistor whose output is connected to an ISOBE instrumentation module. The next module investigated is the SCR units, figure 64.

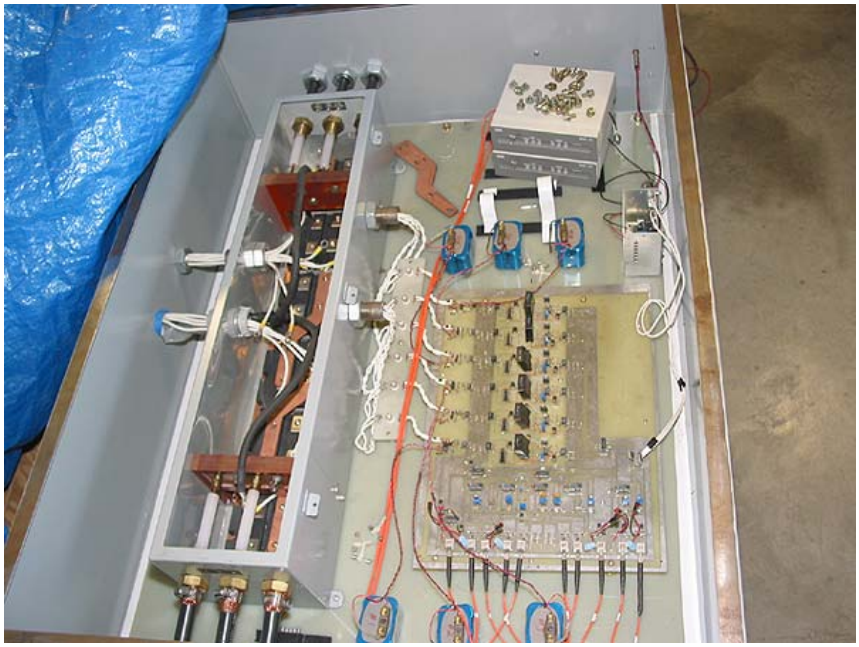

Figure 62. IGBT hardware module with IGBTs on the left and control circuits on the right

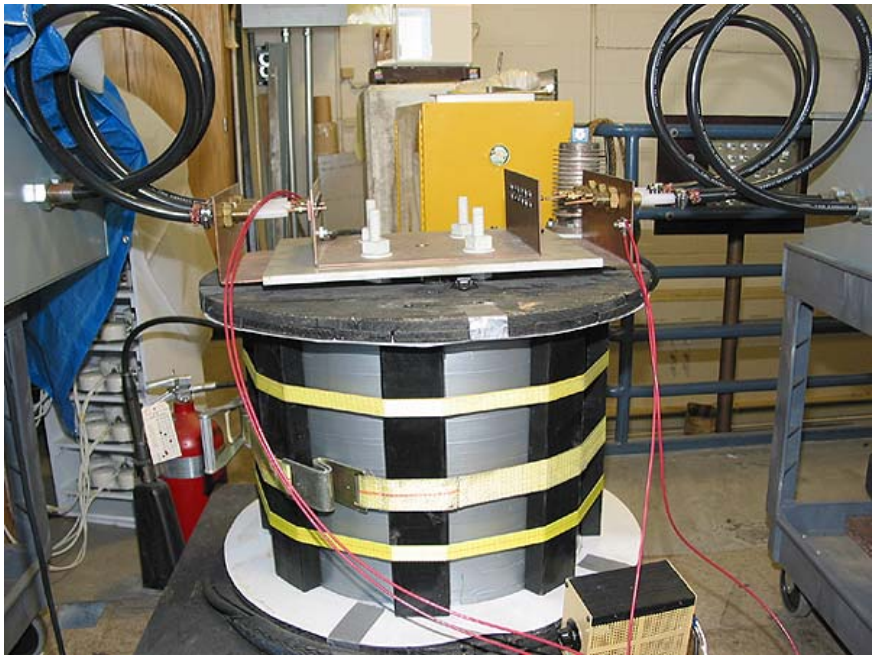

Figure 63. Energy storage inductor

Figure 64. SCR Switch module hardware with SCRs left and control circuitry right

The gate power requirement of these devices is high and could not be driven directly with optocouplers. Optocouplers provided the galvanic isolation and powered the gates of IGBT switches. The switches discharge a small capacitor bank into the SCR gate to trigger the devices. The small capacitor bank is charged and isolated before the rep-rate event and stores enough energy to fire the SCRs for the given number of shots. The capacitors and control circuits are also shown in figure 64. The next instrumentation and control point is the voltage

across the PFN. This voltage is measured with a 1000:1 Tektronix voltage probe and the output of the probe is connected to an ISOBE instrumentation module. Next in the pulsed power circuit is the TVS module, figure 65.

Figure 65. TVS trigger module with Krytron switches and isolation transformers

The TVS gates are triggered with a capacitive discharge isolated with TR-181 trigger transformers. The trigger capacitors are recharged between shots with the 10 kV, 1 amp, commercial power supply that is manually connected to the TVS firing circuits after the recharge capacitors are initially charged. The controls are isolated from the ground in this power supply with both isolation TR-149 trig-

ger transformers and first stage optocouplers. The next instrumentation and control diagnostic is the Rogowski coil measuring the gun current. Rogowski's are inductive devices that make no galvanic contact with the bus bar. The final component of the pulsed power circuit is the railgun. The railgun instrumentation is b-dot probes that make no physical contact with the circuit. The grounding and shielding techniques developed for the b-dots were discussed earlier. The commercial powder feeder is connected to the gun through a length of insulating tubing, figure 66.


Figure 66. Commercial powder feeder is connected to the railgun through insulating tubing

The only ground on the pulsed power circuit is intentionally introduced at one location and this is at the outer coax of the RF amplifier supplying the arc starter. It can be seen with this description that the pulsed power system floats until the single point ground is made at the arc starter and that all instrumentation and control signals are optically isolated from the power circuit eliminating any ground loops.

**Control Flowchart**

The logic flow of the control is presented in figure 67. The first action is to turn on isolated power. In figure 39 of the last chapter the different control modules were identified to include:

- Controller Block
- Sensor Block
- Charging Capacitor Switch Block
- Top-off Switch Block
- Gun Switch Block

Each of these modules has hard wired logic that interfaces between modules with fiber optics. The logic and optic receivers and transmitters are supplied with isolated 110 V power.

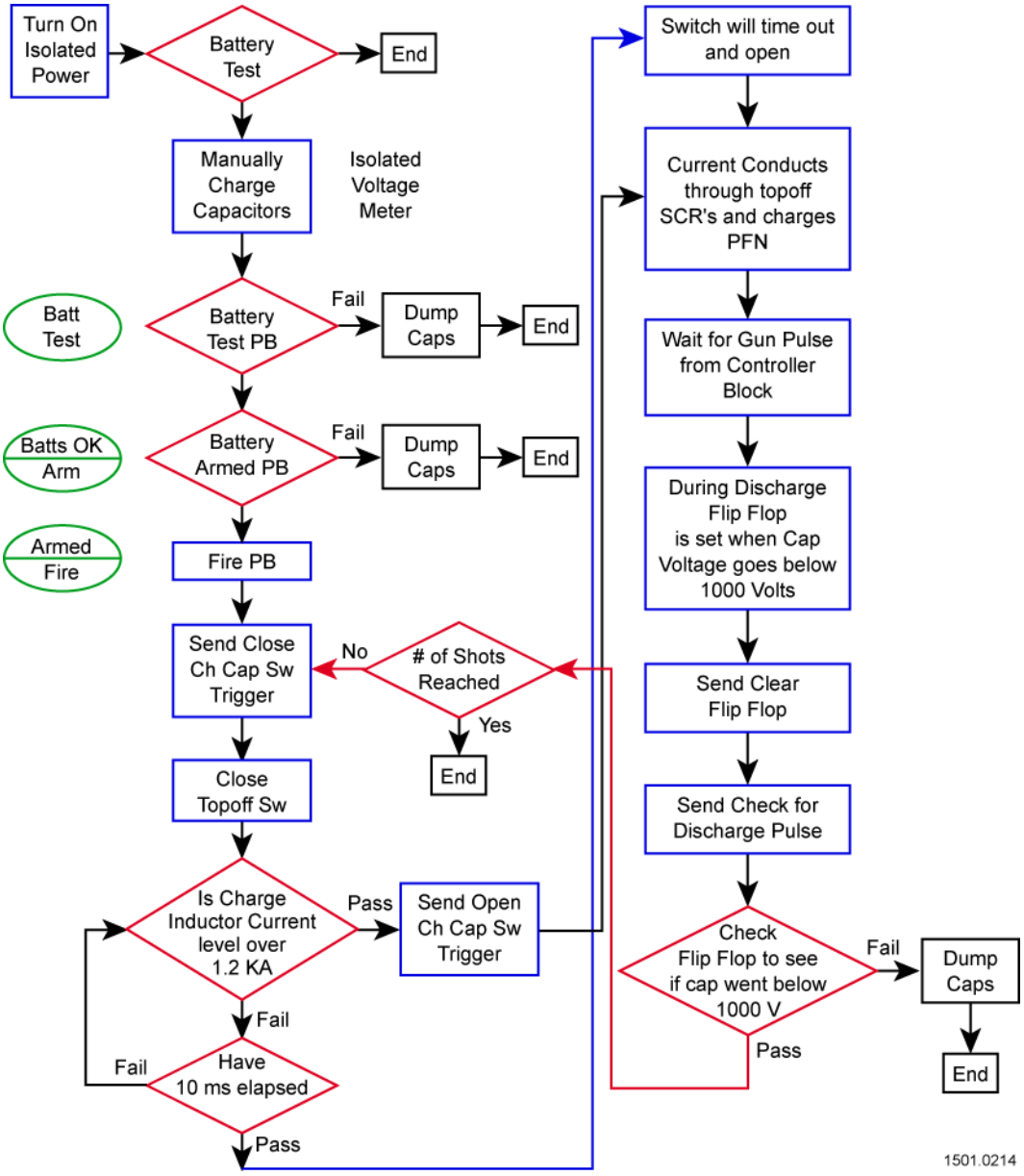


Figure 67. Control block diagram

The total isolation of this power is accomplished with an independent motor generator set mounted with each control module, figure 68. The motor is plugged into the wall with an inline switch and the generator is connected to the motor with an acrylic shaft providing high isolation to ground. These motor generator sets are turned on to supply isolated power to the control modules.

Figure 68. Isolated power is provided to each control module with a motor generator set

The next checkpoint is the battery test. It was mentioned earlier that the pulse power side of the optocouplers are powered with batteries and the experiment side of the ISOBEs are battery powered. A battery test circuit utilizes a relay

to connect a load resistor and the battery voltage is measured and compared to safe working voltage. If the batteries tested okay the control advanced to the manual activity of charging the recharge capacitor bank. After the capacitor bank was charged this activity was acknowledged on the checklist and the air actuated Ross relays were toggled to disconnect the high voltage power supply from the bank and a second set reconnects it to the TVS firing circuits. Next the small capacitors that discharge into the SCR gates are charged and isolated from their supply. Because an unknown amount of time could elapse between charging and the actual test a second battery test was conducted just prior to test. The battery test push button is pressed and if all batteries pass the load test a battery okay light comes on. Control actions are initiated from push buttons on the Control Module. Commands are routed through the Sensor Module because that is where the fault handling is sensed and managed. As the flow chart in figure 67 is explained the inter-module communications and functionality will be presented at the same time. The battery test communications is described in figure 69. Each of the control blocks is represented. In the center of the box are the hardware functions. At the edge of each block are the inter-module communications. Red boxes represent outputs; blue boxes represent inputs. In an automated system the Host Computer sends full battery test command to the Controller Block. The Controller Block then passes the command to the Sensor Block. Sensor Block sends out 3 battery test commands to Gun, Top off and Charging Capacitor Switch Blocks, while also conducting a self test. The respective modules send back a logic level response and

the Sensor Block performs a NAND operation with its self test. If all batteries pass then the Sensor Block sends the full battery test to the Controller Block, which then relays it back to the Host Computer. For manual laboratory use the battery test was initiated with a push button.

The next activity of the flowchart in figure 67 is arming the gun switch module. The high voltage capacitors in the TVS trigger circuit are checked and the system armed if the proper voltage is measured, figure 70.

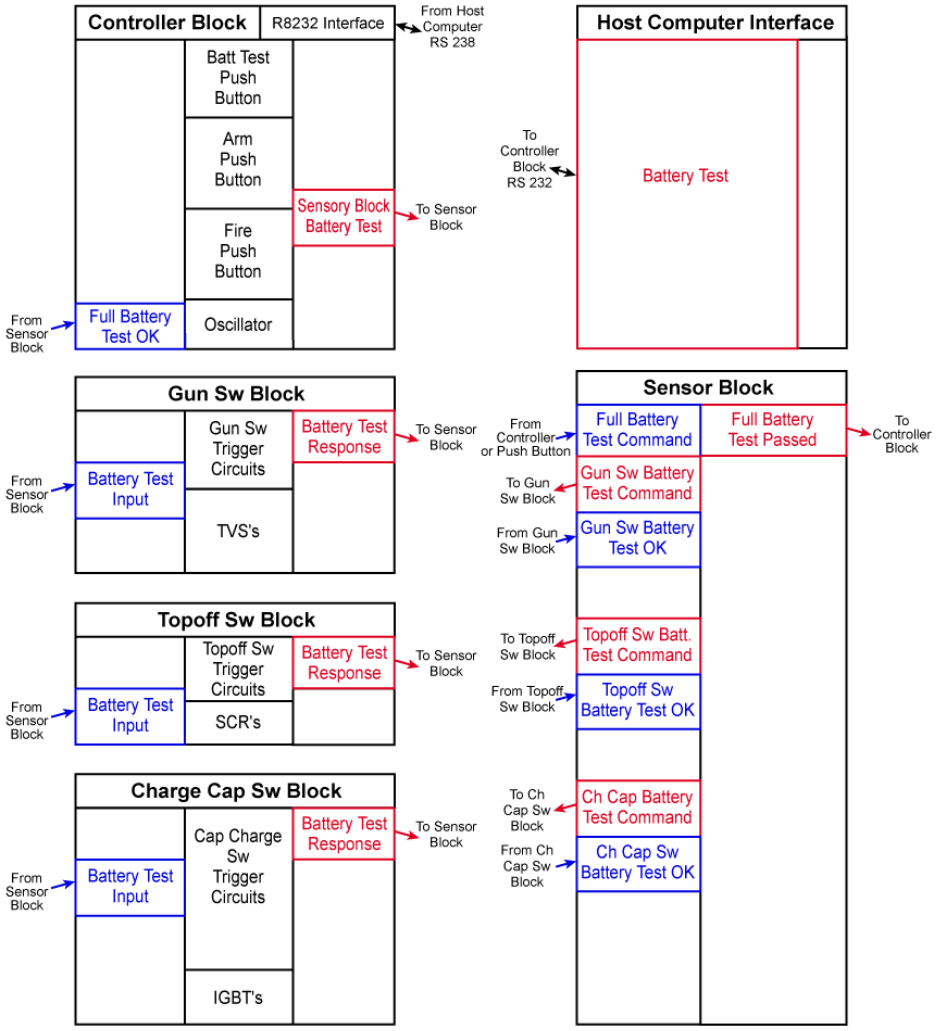


Auto Sequence

1. Host Computer send full battery test command to Controller Block.
2. Controller Block sends full battery test to Sensor Block.
3. Sensor Block sends 3 battery test commands to Gun, Topoff, and Ch Cap Sw Blocks, and also does a self test.
4. Gun, Topoff, and Ch Cap Sw Blocks sends their resective responses. The Sensor Block receives the battery test and NAND them with the self test.
5. If all battery tests pass then the Sensor Block sends the full battery test passed to the Controller Block.
6. Controller Block sends full battery passed response to Host Computer.

Manual Sequence

Skip steps 1. and 6. In step 2. the Controller Block uses the Push Button to send the battery test.

1501.0217

Figure 69. Control system communications between modules

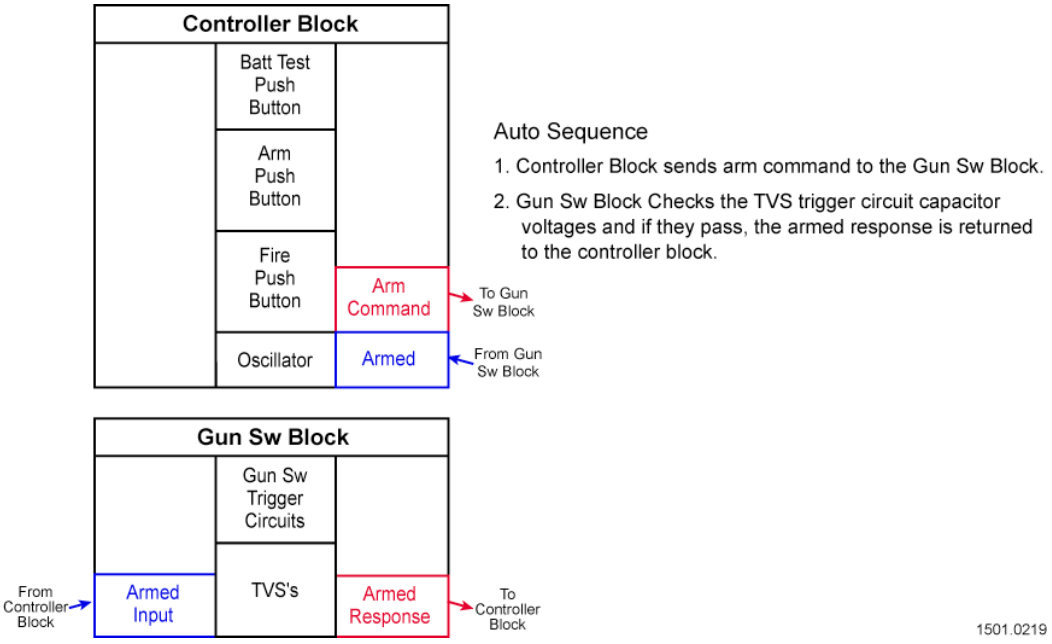


Figure 70. The gun switch module is armed from the controller block

Next in sequence is the fire command. The Host Computer has down loaded test information through an RS 232 interface. The Sensor Block holds all modules enabled if a fault is not present, figure 71. The Controller Block first closes the Charge Switch Module. After the calculated time for the inductor to reach 1200 A the Controller Block commands the Top off Switch Trigger. The Top off Switch Module receives the command and starts the pulse train of SCR gate triggers. At this point either the proper current is sensed in the inductor or a

10 ms timer times out. In response to either action the Sensor Block alerts the Charging Capacitor Switch Block and the IGBT gate signal is removed. This action causes voltage to be generated across the inductor and the PFN starts to charge. With proper circuit action, fault conditions will be discussed next, the PFN reaches voltage and if the inter-shot time has elapsed the Controller sends the Gun Switch Trigger to the Gun Switch Module. The Gun discharges and a flip flop is reset by the Control Module; if the PFN voltage drops below 1000 V the flip flop is set in the Gun Switch Module. The flip flop is interrogated and if it is not set the sequence is stopped. Another recharge into a charged PFN would over voltage the capacitors. If the flip flop is set the sequence continues until the number of shots is reached.

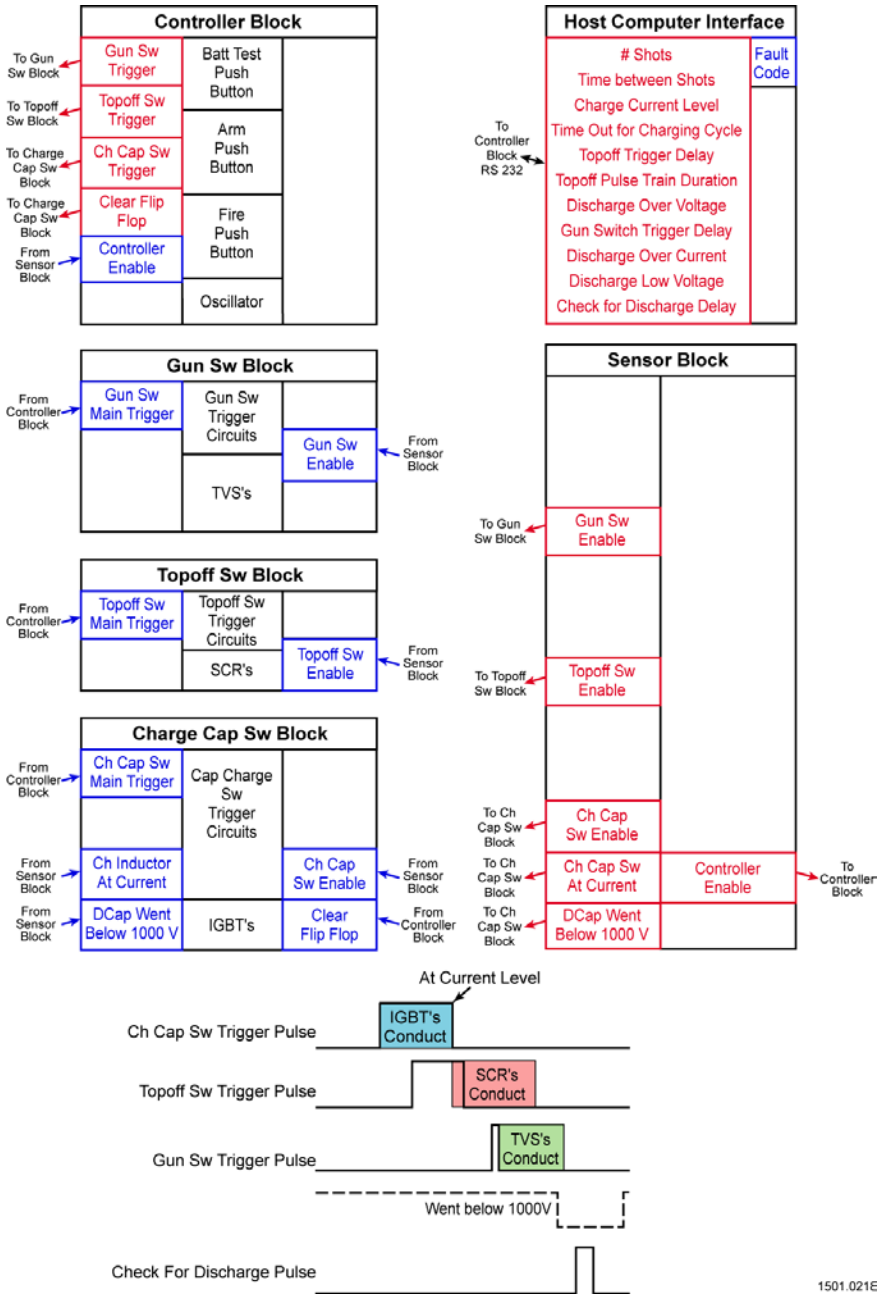


Figure 71. Firing sequence and module communications

The faults logged by the system are presented in table 6.

Table 6. System faults and their description

| Fault | Description |
|---|---|
| Discharge Capacitors (PFN) over voltage | This fault would be indicative of the charging current for the energy storage inductor not being adjusted correctly and the PFN is being overcharged. |
| PFN did not discharge | If the PFN does not discharge and the next charging cycle is initiated then the PFN will overcharge and there is the potential to have a high voltage flash over or damage to an energy storage capacitor |
| Charging Capacitor over voltage | This is a fault that is more applicable to the automated system. In the laboratory the Charging Capacitor bank was manually charged with less chance of over voltage.<br>PFN output over current |
| PFN output over current | If there was a flash over in the buswork there could be excessive current from the PFN. The repetitive cycle needs to be interrupted to prevent damage from successive discharges into the fault. |
| Charging Capacitor over current | The Charging Capacitor bank at full voltage was capable of a peak discharge current greater than 1200 A. If the controller did not open the IGBTs the current sensor would fire the explosive closing switch. |
| Charging Capacitor Switch (IGBTs) over temperature | The Charging Capacitor bank at full voltage was capable of a peak discharge current greater than 1200 A. If the controller did not open the IGBTs the current sensor would fire the explosive closing switch |
| Arc initiator extinguished | The RF amplifier had forward and reverse power meters. If the forward and reverse power were equal this was an indication that the arc starter had extinguished and failed to restart. |

The communications providing the fault handling are shown in figure 72. Once a fault is detected the enable signals are removed from the functional modules and the sequence stops. In the event of over current in the IGBT switches the Sensor Block directly fires the explosive closing switch.

The full assembled control systems communication network is presented in figure 73. The isolated power supplied to each module along with the fiber optic communications between modules prevents the transmission of noise between modules. The coaxial arrangement of the pulsed power system minimizes broadcast EM signals and the total shielding of each control module prevents any leakage from the pulsed power or RF amplifier from entering the instrumentation and control system.

**Control System Demonstration**

The success of the control philosophy is demonstrated in the data quality and repeatability of the system performing a full 10 shot sequence, figure 74. The test is at a 10 Hz rate and in each frame can be seen the inductor current, the voltage drop across the IGBT string and an individual IGBT to demonstrate voltage sharing. Also recorded is the PFN voltage. As the shots progress the charge on the Charging Capacitor bank drops and the inductor charge time increases. The control readily adapts to the extended times and holds the time shot to shot at 100 ms. No filtering was applied to this data.

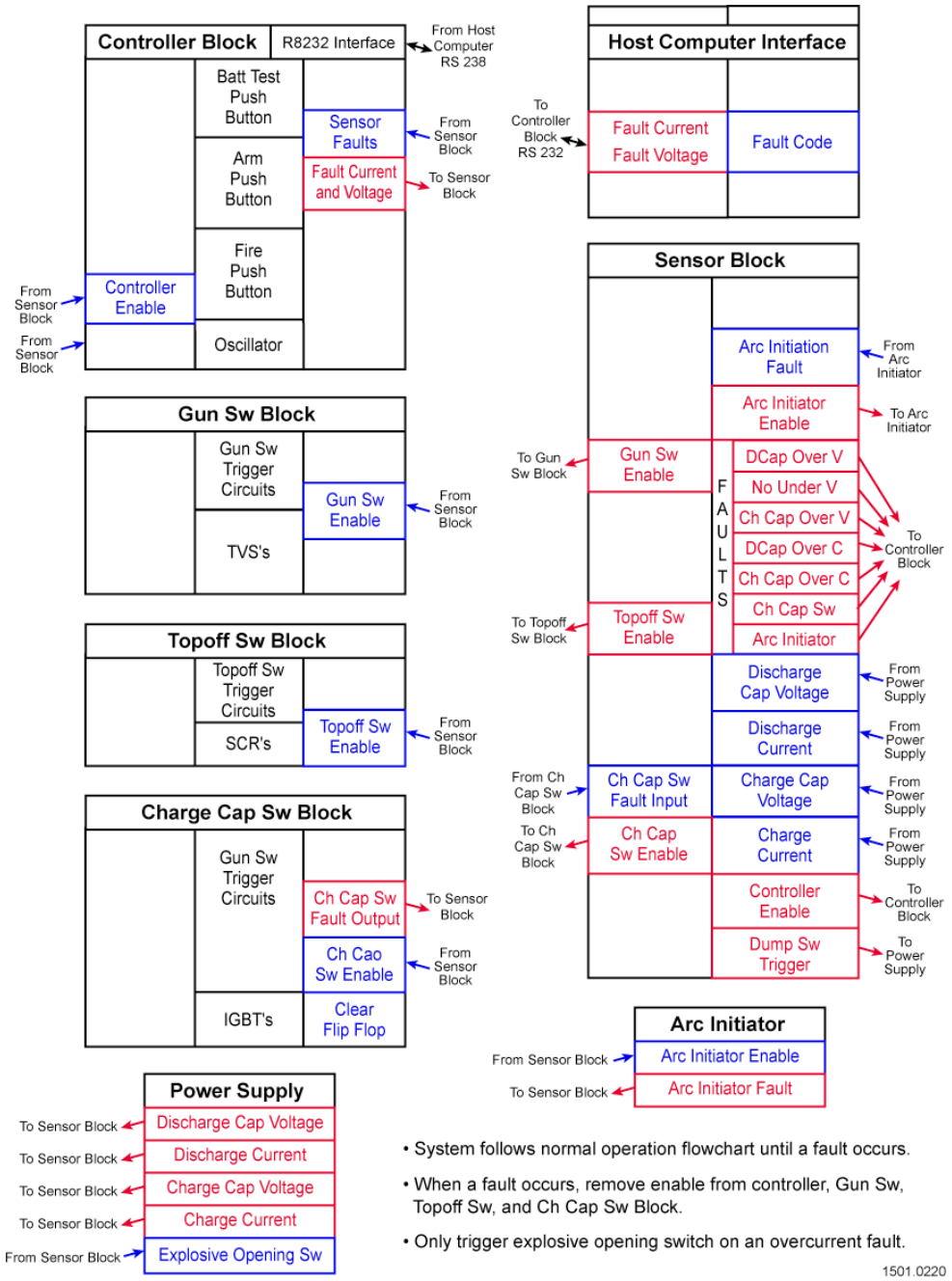


Figure 72. Inter-module communications for fault handling

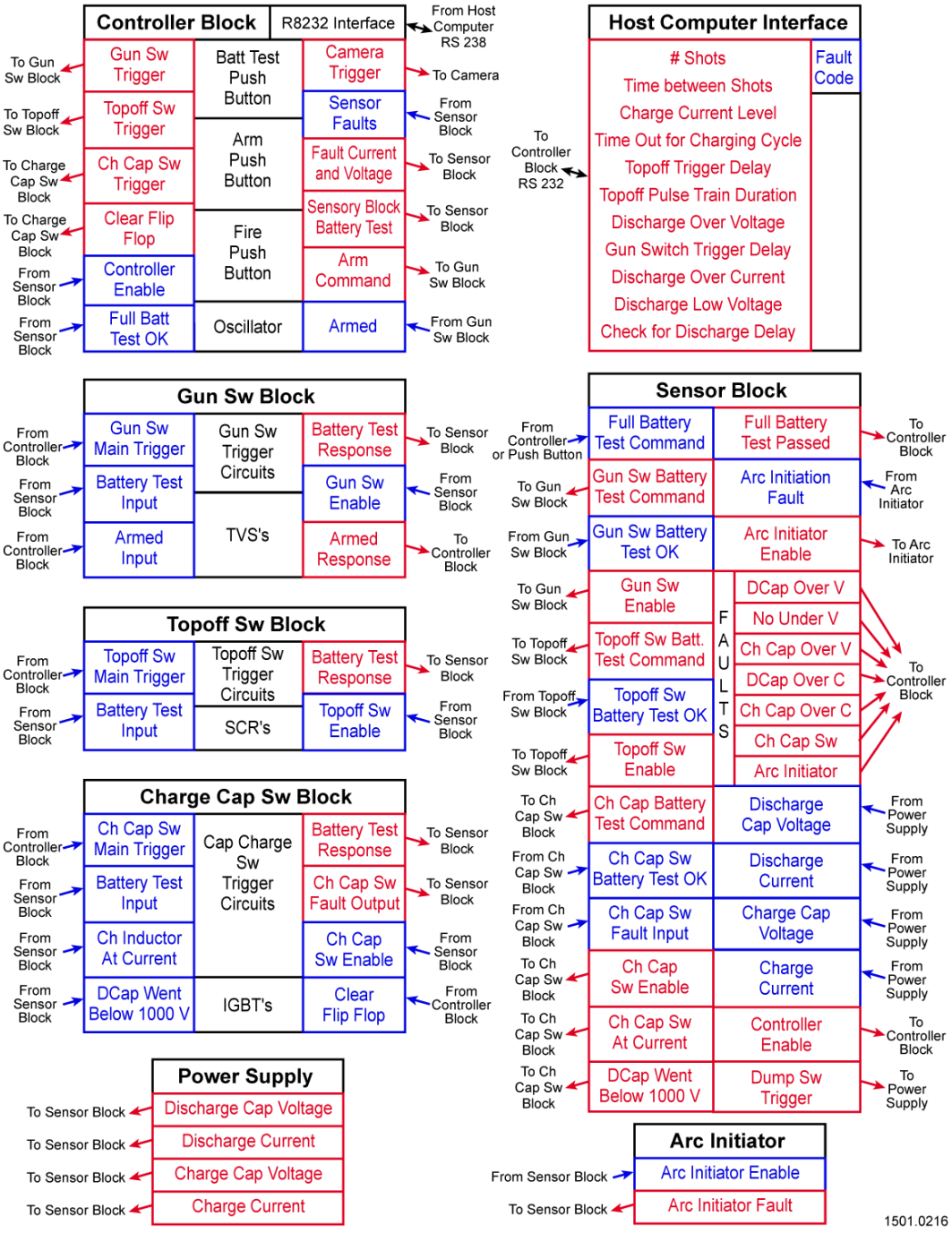


Figure 73. Communications for all system components

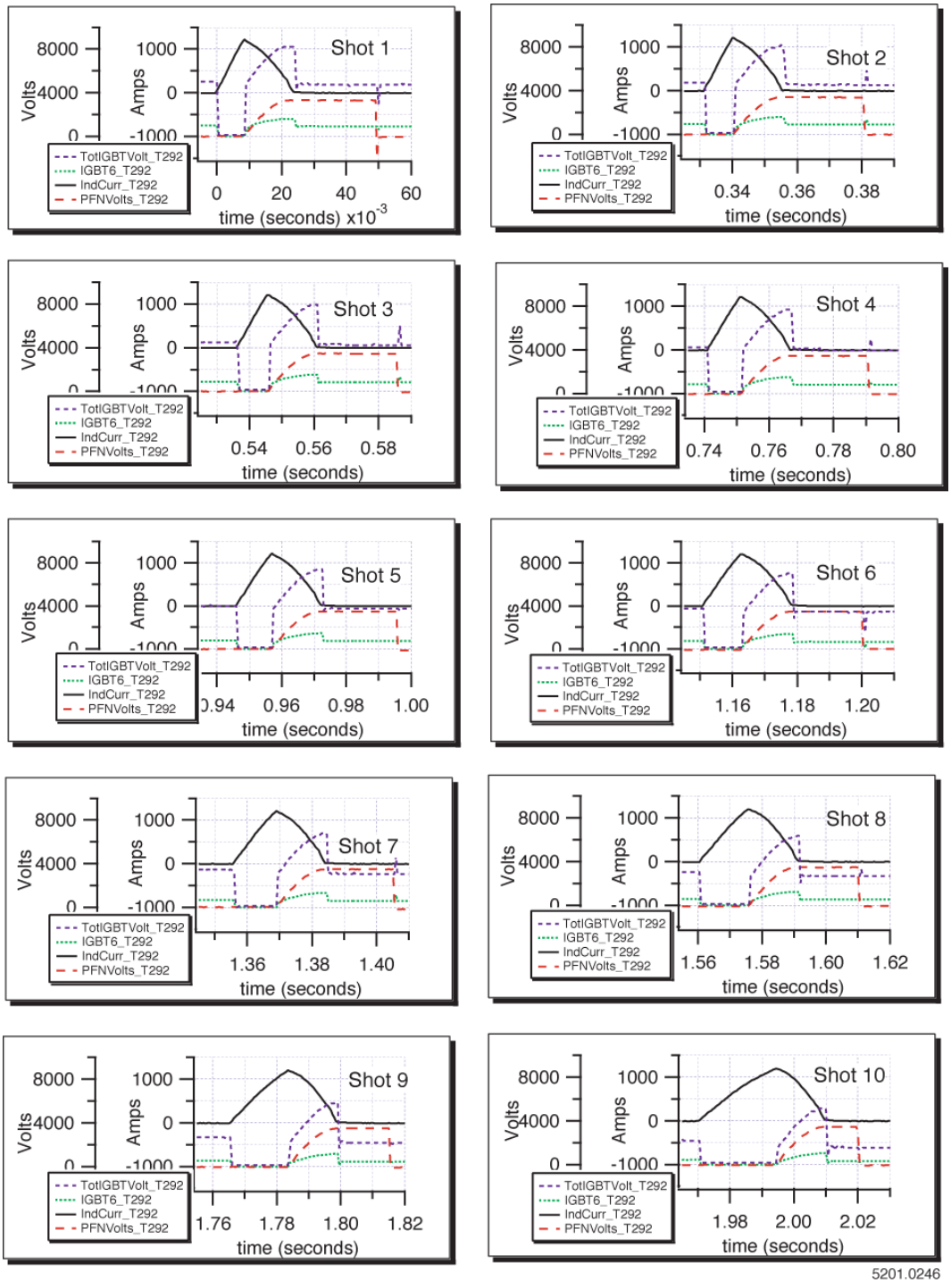


Figure 74. Pulsed power signals from 10 shot experiment

As impressive is the performance of the plasma railgun. The b-dot signals from a ten shot sequence are presented in figure 75. The arc velocity and length is very repeatable shot to shot. The arc starter reliably initiates the arc on each test. These signals are taken at the end of the acceleration section where the current is decreasing as b-dots 2 and 3 are passed.

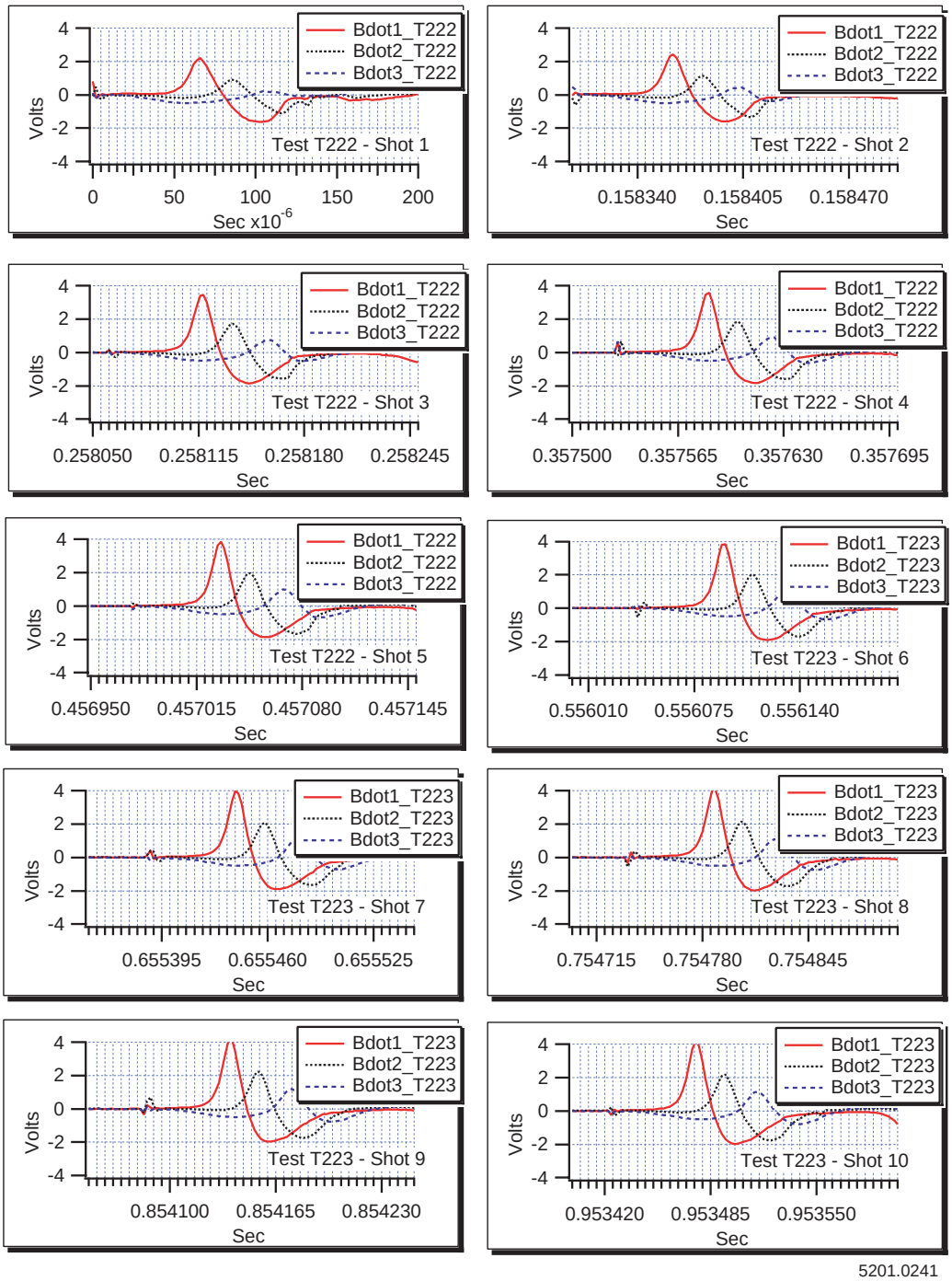


Figure 75. B-dot signals from a 10 shot sequence

Outstanding reproducibility is also seen in the current traces, figure 76.

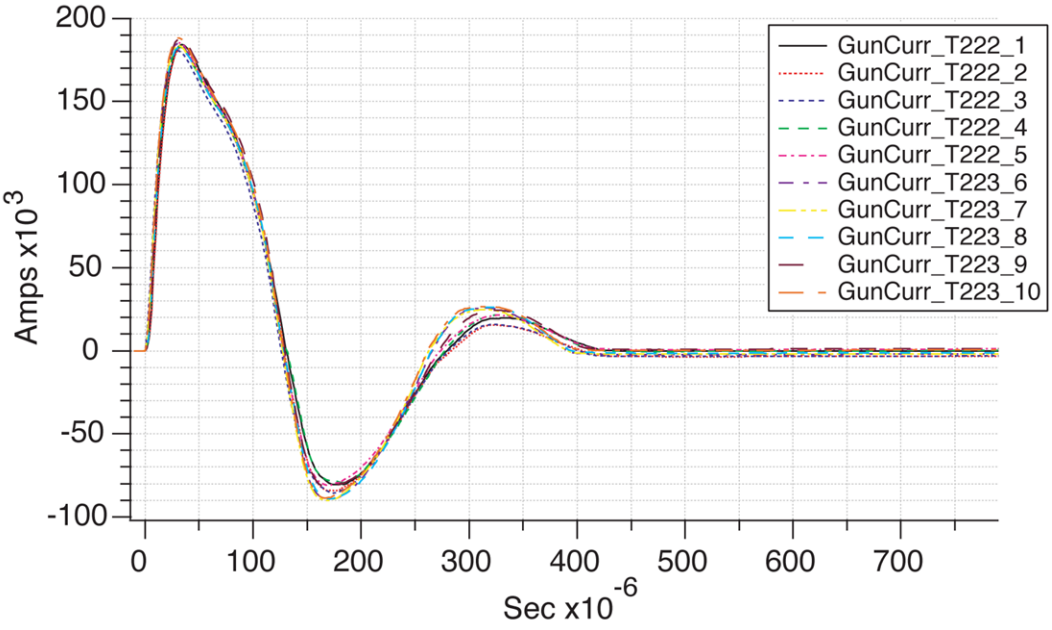


Figure 76. Current traces recorded during a ten shot test

In summary the control system was robust and supported the experimental testing reliably. A log of the tests conducted with the system are presented in Appendix A. Many aspects that would have to be carried forward to an industrial system were demonstrated.

# CHAPTER 7: RESULTS AND CONCLUSIONS

Present state of the art processes rely on the mechanical bonding of the powder to the substrate; the coatings and their bonds are a fraction of the parent material strength. To make full use of this repair process the coating has to bond to the substrate with near parent material strength and coating has to build with good strength layer to layer. The newly invented EPD thermal spray process using electromagnetic forces can accelerate powder particles to a final velocity in excess of 2 km/s. At this velocity powder particles have sufficient kinetic energy to melt their own mass and an equivalent substrate mass on impact, figure 77.

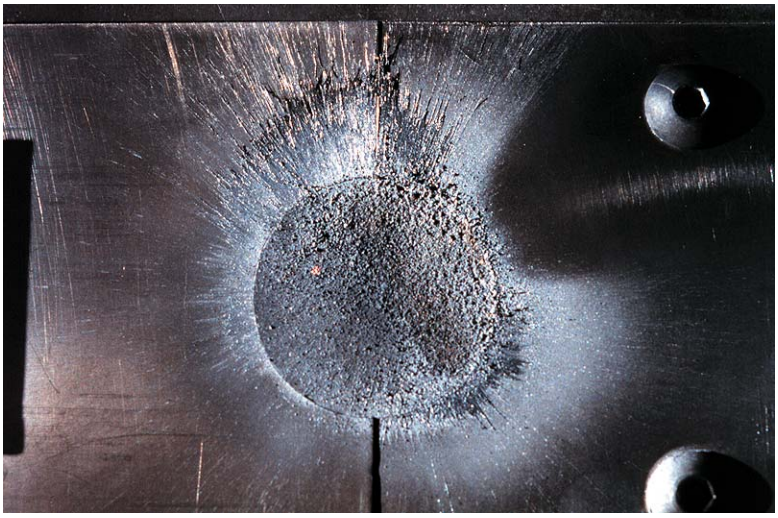

Figure 77. Example circular coupon in specimen holder demonstrating an energetic EPD process

**Metallurgical Results**

The kinetic energy of the process allow fusion bonding, figure 78, of greater strength than that created by low velocity processes as well as improved coating density.

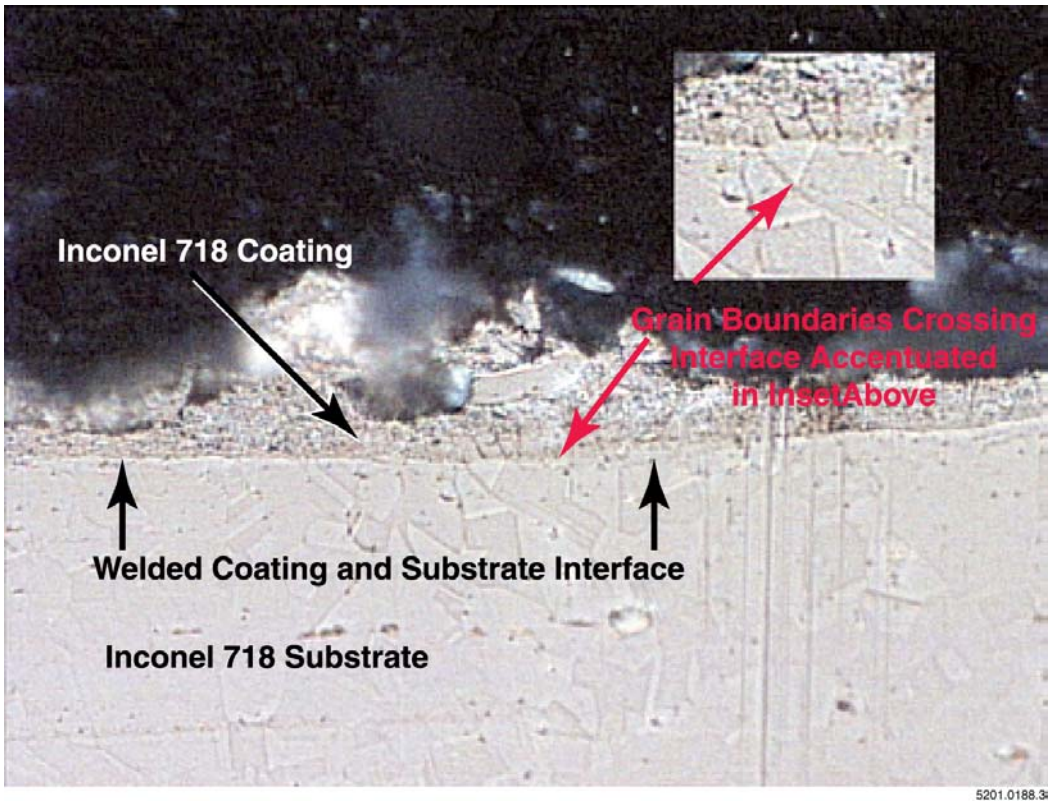


Figure 78. Micrograph of EPD produced coating demonstrating grain growth across bond interface confirming fusion bond

A close-up of the interface makes it easier to see the large grain structure growing across the interface, figure 79.

When the coating is inspected with high magnification very little void content is seen. This indicates that very dense coatings are being formed, figure 80.

The bond strength layer to layer is also very good, figure 81.

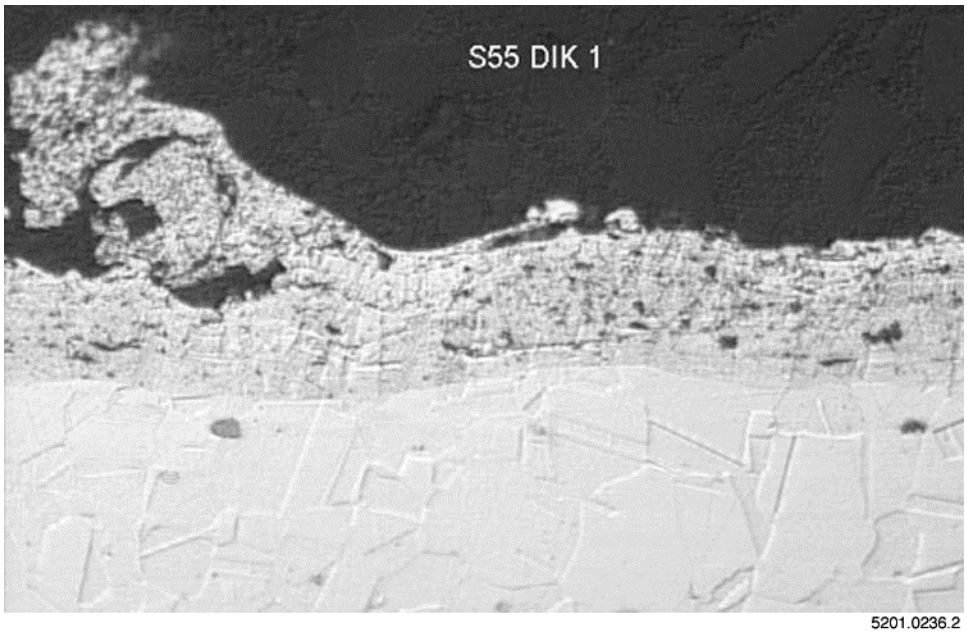


Figure 79. Close-up of coating interface

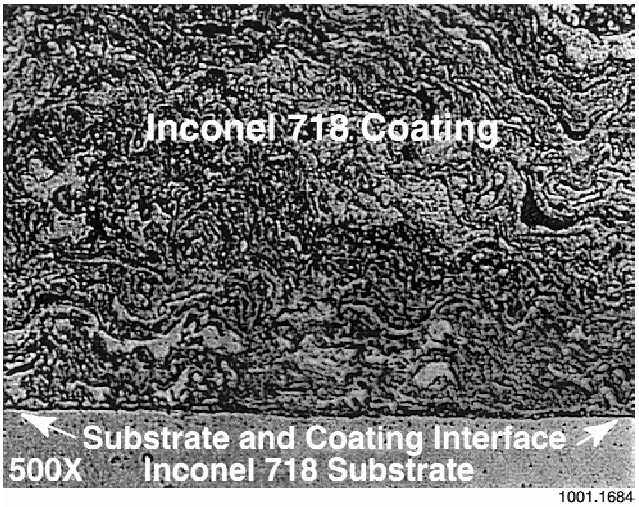


Figure 80. High magnification of the coating layer indicates low void content

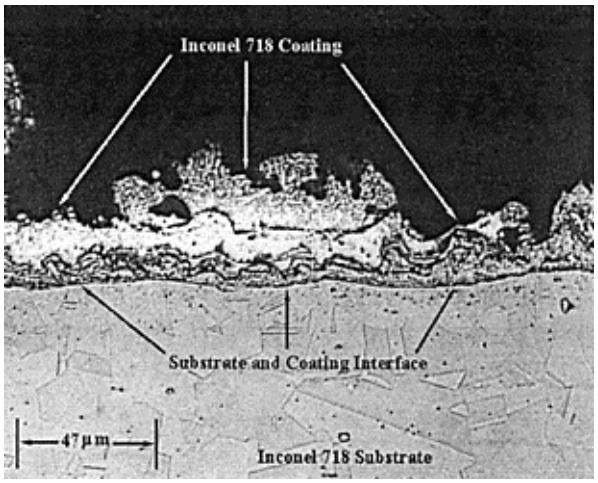


Figure 81. Multiple layer build up of Inconel 718 on Inconel 718 substrate

The mechanism resembles the hook sites introduced in explosive bonding, figure 82.

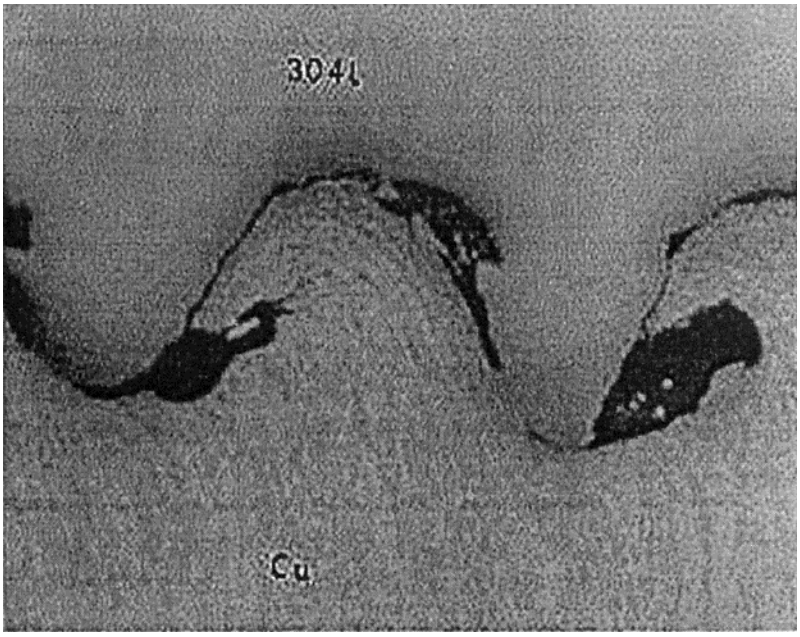


Figure 82. Example of explosively bonded metals

Coupons were also produced using chrome powder. Chrome coating were of great interest as a means of replacing the environmental problem of plating. A micrograph of chrome deposition is presented in figure 83.

For comparison a micrograph of chrome plating is shown in figure 84. The micro-cracks inherent in chrome plating are apparent in this sample. The dense EPD coating shows great promise for eliminating these cracks which provide oxidation paths to the substrate.

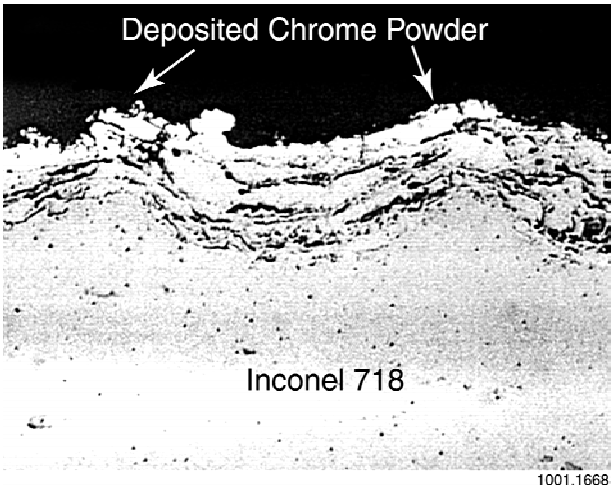


Figure 83. EPD coating of Chrome on Inconel 718

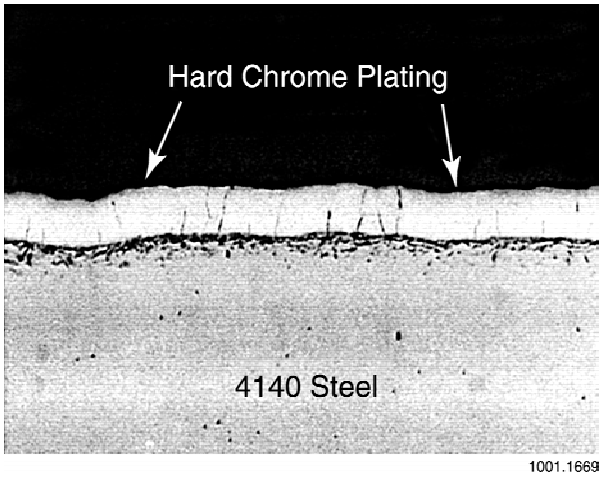


Figure 84. Micrograph of Chrome Plating on steel

**Deposition Efficiency**

In addition to these results outstanding deposition efficiency was achieved. The powder that was entering the gun was being swept into the gas column and of the powder striking the substrate the majority was bonding. A sample calculation demonstrates this fact.

***Calculation of Deposition Efficiency of S51***

Mass flow rate of powder feeder was determined using the bag collection method. Before the test the powder feeder nozzle was placed in a pre-weighed plastic bag and powder was collected for 30 seconds, the mass flow rate was:

36.76 g/min (0.61267 g/s)

Powder velocity was measured using the vertical flight method. The powder feeder nozzle was held vertical and the maximum upward projection of the powder stream measured. Vertical trajectory peak observed:

27-1/8 in. (0.68898 m)

Injector exit velocity calculated:

$v = (2sg)^{0.5} = 3.6748$ m/s

Available mass m of powder available in entrainment section was calculated:

Powder injection to muzzle distance = 0.20198 m

Bore area A = 1.6129 E-4 $m^2$

Entrainment volume = 3.2577 E-5 $m^3$

Average density d of the powder was calculated from the mass flow rate equation mass flow = dAv:

d = mass flow / (Av) = 1033.7 $g/m^3$

m = (d)(Entrainment volume) = 0.03674 g

For 10 shots, available mass was = 0.3674 g

DE: Target mass gain = 3.6411 g - 3.3545 g = 0.2866 g

DE = 100%(0.2866/0.3674) = 85%

**Industrial Systems**

As the technology matures and future direction moves towards identifying a production system, the research effort will center around trying to identify a power supply that can drive the process on a continuous basis. The challenge will be to minimize the total energy required per pulse so that upon rep rating the power requirements remain reasonable. The time marching simulation has been used to outline the fundamental energy requirements of the system. Quantities required of the process are: kinetic energy of the compressed gas and powder, 1.179 kJ; arc resistive energy, 2.25 kJ; rail resistive energy, 0.87 kJ; for a total energy of 4.299 kJ.

If the source is power-matched to the load, then an additional 4.299 kJ is absorbed by the power supply. The EPD process is rep rated at 30 shots a second to obtain the mass deposition rate required which indicates a process requiring

just over 250 kW of prime power. This is the average power required of the supply. During the railgun pulse, a peak power of 80 MW is required. The challenge is to identify a continuous rated pulsed power source capable of this power output which is properly impedance-matched to the load. In Chapter 5 it was pointed out that modifying the current wave shape could lower the peak current while maintaining the momentum of the gas. Similarly, as seen from equation (45), if the inductance gradient of the gun is increased the system current may be decreased while maintaining the momentum of the gas column. A method of increasing the inductance gradient is called augmenting. A rail topology that maintains the force of the launcher while lowering the current is shown in figure 85. It can be seen that a set of auxiliary rails are positioned around the primary rails to augment the magnetic flux in the bore of the launcher. This increase of magnetic field allows reducing the current density in the armature while maintaining the desired force.

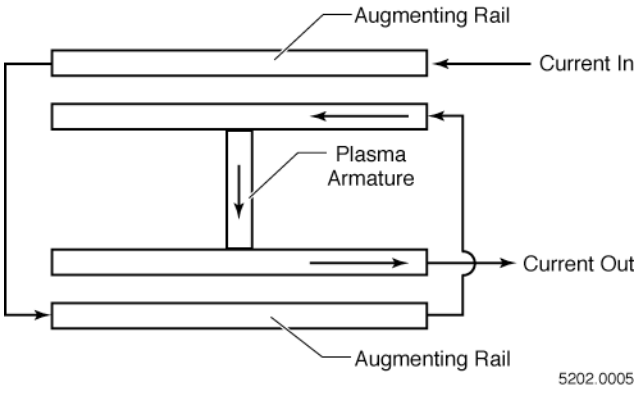


Figure 85. Topology of augmented railgun

The cross section of the square bore accelerator was modified as shown in figure 86. Two slots were cut in the back of the rail and augmenting current conductors were installed inside insulating inserts. The L' Code was used to predict the inductance gradient of this geometry and a value of 1.1 $\mu H / m$ was calculated. The augmenting conductors were manufactured from tubing. This allows them to perform a double function of railgun cooling. For an industrial steady state process the heat has to be removed from the gun and this may be accomplished by using the augmenting conductors as cooling tubes.

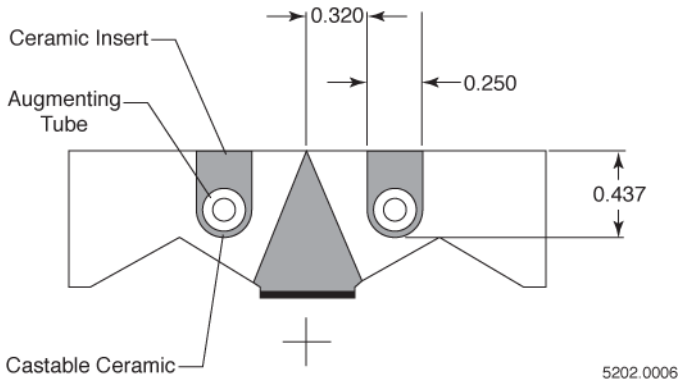


Figure 86. Modification of SBA to include augmenting conductors

The new current path through the launcher may be traced in figure 87. Current from the PFN enters the top breech bus bar tab and flows down the top primary rail. It crosses the bore using the plasma armature and flows back to the breech on the bottom primary rail. At this point it uses the crossover strap to enter the top augmenting tubes. The current flows to the muzzle and back on the lower augmenting tubes. The tubes attach to the lower augmenting tab termination block which in turn is the return path to the PFN.

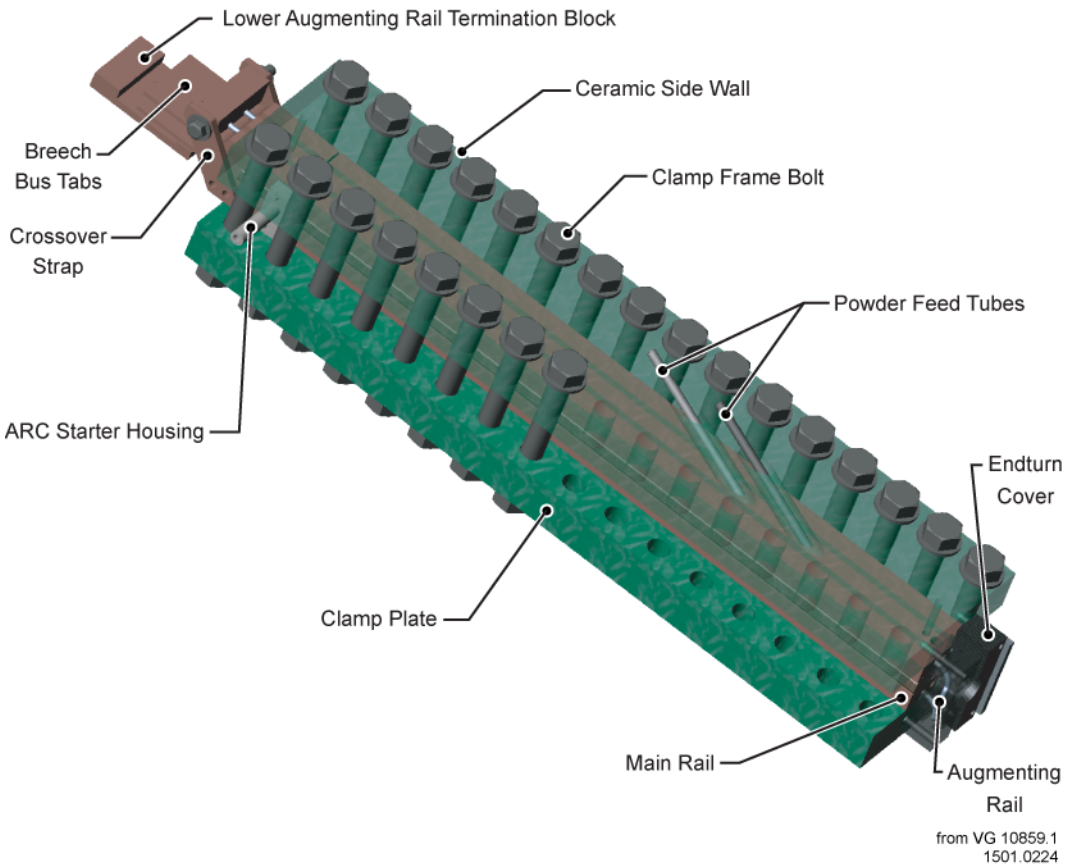


Figure 87. Solid body model of augmented railgun

The SBA rails were modified and the augmenting tubes installed, figure 88.

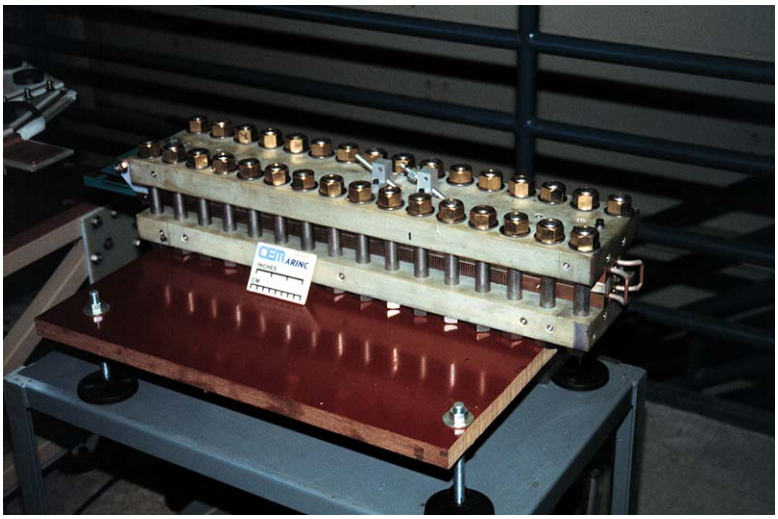

Figure 88. Augmented powder spray railgun

This launcher was fired with the PFN and snowplow performance confirmed. Data from a typical experiment is presented in figure 89. It can be seen that the same performance is achieved in this launcher at half the current required of the SBA. Reducing the current in the launcher reduces the energy dissipated in the plasma arc proportionately. This in turn reduces the steady power required by the system from 250 kW to 200 kW.

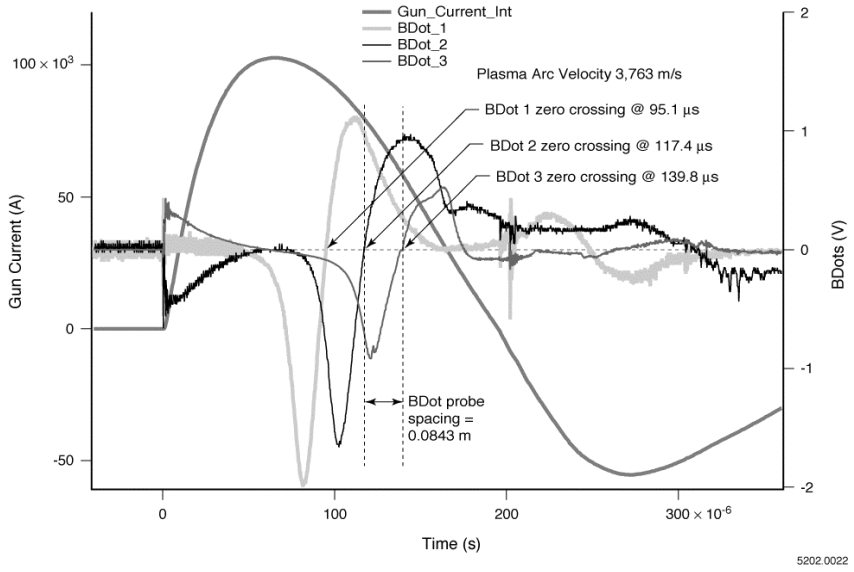


Figure 89. Test data from the augmented square bore accelerator (ASBA)

In addition to the railgun improvement other components were investigated for use in an industrial system. Single capacitor modules were purchased and placed into test loops to confirm lifetimes in the one million cycles at the current shape and rep rate required of a steady state coating process. Two different capacitor vendors, Maxwell Laboratories and Aerovox Incorporated, supplied units that met the life requirements. Robicon Incorporated was contacted and supplied quotations for a steady state high voltage power supply that could recharge the PFN to 5000 V at the required repetition rate. The DOD EM Gun Program in the United States was developing Silicon Controlled Rectifier switches of the specification required of the powder spray system. The identification of these components allowed the development of the conceptual industrial spray system shown in figure 90.

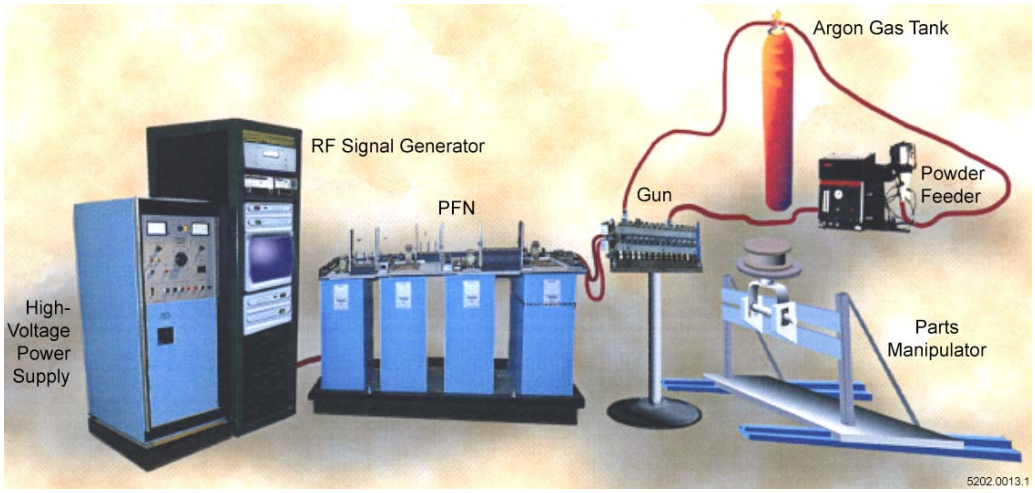


Figure 90. Conceptual industrial spray system

## Conclusion

In this research the EPD process was invented and analyzed. Proof of principle experiments were used to confirm the operational theory. A repetitive system was built to demonstrate fusion bonding and good bond strength layer to layer. A control system with aspects applicable to an industrial service was built and controlled the rep rate experiment. Metallurgical results confirmed that fusion bonding was achieved. Work was performed to optimize the efficiency of critical system components reducing operating power requirements. An industrial system has been proposed and early component development has identified no impedi-ments to realizing that system.

# APPENDIX A: EPD SYSTEM TESTS

Table A-1 presents tests performed with the EPD system. Early tests started with system check out and single shot experiments with the railgun. Testing then moved to multi-shot testing where the system was demonstrated in 3, 5 and 10 shot modes. During the testing two important test sequences were completed. The first utilized the Taguchi method to identify the system operating variables that showed the greatest influence on target mass gain. The second set of tests was a formal Acceptance Test Plan (ATP) executed for the Air Force to demonstrate all aspects of system operation in a formal review process.

Tests performed for Taguchi evaluation were 135 through 160. The quality characteristic for the test sequence was target mass gain. The control factors were powder size, time between shots, powder mass flow rate, spray distance, PFN voltage. It was determined that powder mass flow rate had the greatest effect on mass gain and spray distance had the second highest effect.

Table A-1. EPD system tests

| Shot No. | Date | Re-charge Bank Charge (V) | Approx PFN Charge (V) | Shot Reps | Powder Size (mi-crons) | Purpose | Mass Gain (mg) |
|---|---|---|---|---|---|---|---|
| Testing week of 10/20/97: | | | | | | | |
| **Double Shot Tests: shots at 0 and 70 ms** | | | | | | | |
| RF modulated: 5 ms @ 0.24V, 200 us @ 0.86 V | | | | | | | |
| 8cfh seed gas. No shield gas or aux. flow. | | | | | | | |
| T63 | 10/20/1997 | **1000** | 1700 | 2 | 0 | achieve 2 dschrges | |
| T64 | 10/20/1997 | **1500** | 2500 | 2 | 0 | achieve 2 dschrges | |
| T65 | 10/20/1997 | **1800** | 3050 | 2 | 0 | achieve 2 dschrges | |
| Dschrg. on current, not time. Changed RF modulation time to 2 ms low, 200us high | | | | | | | |
| T66 | 10/20/1997 | **500** | 760 | 2 | 0 | achieve 2 dschrges | |
| Replaced arc init paint insulation with Kapton/Teflon wrap | | | | | | | |
| T67 | 10/20/1997 | **500** | 760 | 2 | 0 | achieve 2 dschrges | |
| T68 | 10/20/1997 | **1000** | 1400 | 2 | 0 | achieve 2 dschrges | |
| T69 | 10/20/1997 | **1500** | 2600 | 2 | 0 | achieve 2 dschrges | |
| Increased RF input to .30V during the low cycle, high cycle also increased | | | | | | | |
| T70 | 10/21/1997 | **500** | - | 2 | 0 | achieve 2 dschrges | |
| T71 | 10/21/1997 | **1000** | 1700 | 2 | 0 | achieve 2 dschrges | |
| T72 | 10/21/1997 | **1500** | 2600 | 2 | 0 | achieve 2 dschrges | |
| T73 | 10/21/1997 | **1800** | 2580 | 2 | 0 | achieve 2 dschrges | |
| Increased SCR-TVS delay from 45 to 50 ms | | | | | | | |
| T74 | 10/21/1997 | **500** | 1000 | 2 | 0 | achieve 2 dschrges | |
| T75 | 10/21/1997 | **1800** | 2580 | 2 | 0 | achieve 2 dschrges | |
| T76 | 10/21/1997 | **1800** | 2540 | 2 | 0 | look for snowplows | |
| Moved B-dots and Total Current to Pro 40. | | | | | | | |
| T77 | 10/21/1997 | **100** | 170 | 2 | 0 | system checkout | |
| T78 | 10/21/1997 | **500** | 1000 | 2 | 0 | system checkout | |
| T79 | 10/21/1997 | **1800** | 2540 | 2 | 0 | system checkout | |
| T80 | 10/21/1997 | **500** | 1000 | 2 | 0 | system checkout | |
| T81 | 10/21/1997 | **2000** | 3140 | 2 | 0 | system checkout | |

Table A-1. EPD system tests (contd.)

| Shot No. | Date | Re-charge Bank Charge (V) | Approx PFN Charge (V) | Shot Reps | Powder Size (mi-crons) | Purpose | Mass Gain (mg) |
|---|---|---|---|---|---|---|---|
| Introduce powder, feeder at 3.75 turns (42 g/min for 30 s or 17 g/min for 3 s) | | | | | | | |
| T82, S61 | 10/21/1997 | **2100** | 3150 | 2 | **45-90** | double shot coating | 97.9 |
| T83, S62 | 10/21/1997 | **2100** | 3150 | 2 | **45-90** | double shot coating | 1506.2 |
| T84, S63 | 10/21/1997 | **2100** | 3150 | 2 | **45-90** | double shot coating | 208.0 |
| T85, S64 | 10/21/1997 | **2100** | 3150 | 2 | **45-90** | double shot coating | 205.0 |
| Introducing auxiliary flow to minimize powder pooling; indicated flow 45 scfh air; shield gas 70 cfh | | | | | | | |
| T86 | 10/22/1997 | **500** | 1070 | 2 | 0 | system checkout | |
| T87, S65 | 10/22/1997 | **2200** | 3300 | 2 | **45-90** | double shot coating | -35.4 |
| Reduced aux flow to 20 scfh, increased RF input to .40 V, seed gas flow to 12 cfh | | | | | | | |
| T88, S66 | 10/22/1997 | **2200** | 3300 | 2 | **45-90** | double shot coating | 74.0 |
| T89, S67 | 10/22/1997 | **2200** | 3300 | 2 | **45-90** | double shot coating | 30.2 |
| Changed to finest powder at 30.9 g/min | | | | | | | |
| T90, S68 | 10/22/1997 | **2200** | 3300 | 2 | **15-45** | double shot coating | 42.0 |
| T91 | 10/22/1997 | **2200** | 3300 | 2 | **15-45** | double shot coating | |
| T92, S69 | 10/22/1997 | **2200** | 3300 | 2 | **15-45** | double shot coating | 46.4 |
| T93, S70 | 10/22/1997 | **2200** | 3300 | **1** | **15-45** | single shot coating | 34.3 |
| **Triple Shot Tests: shots at 0, 85, and 140 ms** | | | | | | | |
| no shield or aux flow, RF back to 0.30V, 12 CFH | | | | | | | |
| T94 | 10/22/1997 | **100** | 200 | 3 | 0 | achieve 3 dschrges | |
| T95 | 10/22/1997 | **500** | 1000 | 3 | 0 | achieve 3 dschrges | |
| T96 | 10/22/1997 | **2200** | 1900 | 3 | 0 | achieve 3 dschrges | |
| RF back up to .40V, 12 CFH | | | | | | | |
| T97 | 10/22/1997 | **2200** | 1900 | 3 | 0 | achieve 3 dschrges | |
| T98 | 10/22/1997 | **2400** | 2300 | 3 | 0 | achieve 3 dschrges | |
| Testing week of 11/03/97: | | | | | | | |
| **Triple Shot Tests: shots at 0, 85, and 140 ms** | | | | | | | |
| no shield or aux flow, RF back to 0.30V, 12 CFH | | | | | | | |
| T100 | 11/4/1997 | **100** | | 3 | 0 | checkout | |
| T101 | 11/4/1997 | **500** | | 3 | 0 | checkout | |
| T102 | 11/4/1997 | **500** | | 3 | 0 | checkout | |
| T103 | 11/4/1997 | **2400** | | 3 | 0 | 3 dschrges | |
| T104 | 11/5/1997 | **100** | | 3 | 0 | checkout | |
| T105 | 11/5/1997 | **500** | | 3 | 0 | checkout | |
| T106 | 11/5/1997 | **2400** | | 3 | 0 | 3 dschrges | |

Table A-1. EPD system tests (contd.)

| Shot No. | Date | Re-charge Bank Charge (V) | Approx PFN Charge (V) | Shot Reps | Powder Size (mi-crons) | Purpose | Mass Gain (mg) |
|---|---|---|---|---|---|---|---|
| RF back up to 0.40V, 12 CFH | | | | | | | |
| T107 | 11/5/1997 | **100** | | 3 | 0 | checkout | |
| T108 | 11/5/1997 | **2500** | | 3 | 0 | 3 dschrges | |
| RF back down to 0.30V, replaced initiator rod, cleaned cavity w/ alcohol | | | | | | | |
| T109 | 11/5/1997 | **500** | | 3 | 0 | checkout | |
| next test performed with explosive switch loaded and armed | | | | | | | |
| T110 | 11/5/1997 | **3000** | | 3 | 0 | 3 dschrges | |
| T111 | 11/5/1997 | **500** | | 3 | 0 | checkout | |
| T112 | 11/5/1997 | **1000** | | 3 | 0 | checkout | |
| **5-Shot Tests** | | | | | | | |
| Explosive switch armed | | | | | | | |
| Changed RF power scope time per pt from 100 to 200 us. Still no shield or aux gas. RF @ 0.30V | | | | | | | |
| T113 | 11/5/1997 | 3500 | 3200 | 5 | 0 | 5 dschrges | |
| Introduce powder same settings as T82, shield gas 70 cfh, aux gas 20 scfh | | | | | | | |
| T114, S71 | 11/5/1997 | 3500 | 3200 | 5 | **45-90** | 5 dschrges | 42.0 |
| **Taguchi Matrix** | | | | | | | |
| T115 | 11/6/1997 | 100 | | 5 | 0 | checkout | |
| T116 | 11/6/1997 | 1000 | | 5 | 0 | checkout | |
| T117, S72 | 11/6/1997 | 3500 | **3120** | 5 | **45-90** | Taguchi 1: 50ms, 3", feed 1 | **27.7** |
| T118, S73 | 11/6/1997 | 3500 | **3120** | 5 | **45-90** | Taguchi 1 | **26.9** |
| T119, S74 | 11/6/1997 | 3500 | **3120** | 5 | **45-90** | Taguchi 1 | **29.0** |
| T120 | 11/6/1997 | 100 | | 5 | 0 | checkout | |
| T121 | 11/6/1997 | 1000 | | 5 | 0 | checkout | |
| T122, S75 | 11/6/1997 | 3700 | **3400** | 5 | **45-90** | Taguchi 3: 100ms, 3", feed 1 | 47.5 |
| T123, S76 | 11/6/1997 | 3700 | **3400** | 5 | **45-90** | Taguchi 3 | **51.0** |
| T124, S77 | 11/6/1997 | 3700 | **3400** | 5 | **45-90** | Taguchi 3 | **54.6** |
| T125, S78 | 11/6/1997 | 3700 | **3400** | 5 | **45-90** | Taguchi 3 | **53.4** |

Table A-1. EPD system tests (contd.)

| Shot No. | Date | Re-charge Bank Charge (V) | Approx PFN Charge (V) | Shot Reps | Powder Size (mi-crons) | Purpose | Mass Gain (mg) |
|---|---|---|---|---|---|---|---|
| T126 | 11/7/1997 | 100 | | 5 | 0 | checkout | |
| T127 | 11/7/1997 | 1000 | | 5 | 0 | checkout | |
| T128, S79 | 11/7/1997 | 3700 | **3120** | 5 | **45-90** | Taguchi 4: 100ms, 5", feed 2 | **62.2** |
| T129, S80 | 11/7/1997 | 3700 | **3120** | 5 | **45-90** | Taguchi 4 | **68.0** |
| T130, S81 | 11/7/1997 | 3700 | **3120** | 5 | **45-90** | Taguchi 4 | **67.8** |
| T131, S82 | 11/7/1997 | 3700 | **3400** | 5 | **45-90** | Taguchi 2: 50ms, 5", feed 2 | **28.8** |
| T132, S83 | 11/7/1997 | 3700 | **3400** | 5 | **45-90** | Taguchi 2 | **32.0** |
| T133, S84 | 11/7/1997 | 3700 | **3400** | 5 | **45-90** | Taguchi 2 | **26.4** |
| Testing week of 11/10/97 (Taguchi contin-ued): | | | | | | | |
| Changed to 15-45 powder and performed powder feed rate tests. | | | | | | | |
| T134 | 11/10/1997 | 1000 | | 5 | 0 | checkout | |
| T135, S85 | 11/10/1997 | 3700 | **3120** | 5 | **15-45** | Taguchi 6: 50ms, 3", feed 2 | **127.5** |
| T136, S86 | 11/10/1997 | 3700 | **3120** | 5 | **15-45** | Taguchi 6: no bdot trigger | 63.6 |
| T137, S87 | 11/10/1997 | 3700 | **3120** | 5 | **15-45** | Taguchi 6 | 102.6 |
| T138, S88 | 11/10/1997 | 3700 | **3120** | 5 | **15-45** | Taguchi 6 | 83.6 |
| T139, S89 | 11/10/1997 | 3700 | **3120** | 5 | **15-45** | Taguchi 6 | 84.6 |
| T140 | 11/11/1997 | 1000 | | 5 | 0 | checkout | |
| T141, S90 | 11/11/1997 | 3700 | **3120** | 5 | **15-45** | Taguchi 6 | **117.8** |
| T142, S91 | 11/11/1997 | 3700 | **3120** | 5 | **15-45** | Taguchi 6 | 124.9 |
| T143 | 11/11/1997 | 1000 | | 5 | 0 | checkout | |
| T144, S92 | 11/11/1997 | 3700 | **3120** | 5 | **15-45** | Taguchi 6 | 57.6 |
| T145, S93 | 11/11/1997 | 3700 | **3120** | 5 | **15-45** | Taguchi 6 | 60.5 |
| - | 11/11/1997 | 3700 | **3120** | 5 | 0 | checkout | |
| T146 | 11/11/1997 | 3700 | **3120** | 5 | 0 | checkout | |

Table A-1. EPD system tests (contd.)

| Shot No. | Date | Re-charge Bank Charge (V) | Approx PFN Charge (V) | Shot Reps | Powder Size (mi-crons) | Purpose | Mass Gain (mg) |
|---|---|---|---|---|---|---|---|
| T147 | 11/11/1997 | 3700 | **3120** | 5 | 0 | checkout | |
| T148, S94 | 11/11/1997 | 3700 | **3120** | 5 | **15-45** | Taguchi 6 | 83.5 |
| T149, S95 | 11/11/1997 | 3700 | **3120** | 5 | **15-45** | Taguchi 6 | **91.6** |
| - | 11/11/1997 | 1000 | | 5 | 0 | checkout | |
| T150, S96 | 11/11/1997 | 3700 | **3400** | 5 | **15-45** | Taguchi 8: 100ms, 3", feed 2 | **112.4** |
| T151, S97 | 11/11/1997 | 3700 | **3400** | 5 | **15-45** | Taguchi 8 | **88.9** |
| T152, S98 | 11/11/1997 | 3700 | **3400** | 5 | **15-45** | Taguchi 8 | **71.2** |
| T153 | 11/12/1997 | 1000 | | 5 | 0 | checkout | |
| T154, S99 | 11/12/1997 | 3700 | **3120** | 5 | **15-45** | Taguchi 7: 100ms, 5", feed 1 | 49.6 |
| T155, S100 | 11/12/1997 | 3700 | **3120** | 5 | **15-45** | Taguchi 7 | **27.2** |
| T156, S101 | 11/12/1997 | 3700 | **3120** | 5 | **15-45** | Taguchi 7 | **26.0** |
| T157, S102 | 11/12/1997 | 3700 | **3120** | 5 | **15-45** | Taguchi 7 (repeat of T154) | **32.5** |
| - | 11/12/1997 | 1000 | | 5 | 0 | checkout | |
| T158, S103 | 11/12/1997 | 3700 | **3400** | 5 | **15-45** | Taguchi 5: 50ms, 5", feed 1 | **24.3** |
| - | 11/12/1997 | 1000 | | 5 | 0 | checkout | |
| T159, S104 | 11/12/1997 | 3700 | **3400** | 5 | **15-45** | Taguchi 5 | **17.1** |
| T160, S105 | 11/12/1997 | 3700 | **3400** | 5 | **15-45** | Taguchi 5 | **18.6** |
| **Build-up Tests: Two 5-shot salvos** | | | | | | 100ms, 3", feed 2 with 45-90 powder | |
| T161, S106 | 11/12/1997 | 3700 | **3400** | 5 | **45-90** | | - |
| T162, S106 | 11/12/1997 | 3700 | **3400** | 5 | **45-90** | | - |
| | | | | | | | **166.2** |
| T163, S107 | 11/12/1997 | 3700 | **3400** | 5 | **45-90** | Weight lost in strip-ping, 0.7 mg | 77.3 |
| T164, S107 | 11/12/1997 | 3700 | **3400** | 5 | **45-90** | | 96.8 |
| | | | | | | | **174.1** |

Table A-1. EPD system tests (contd.)

| Shot No. | Date | Re-charge Bank Charge (V) | Approx PFN Charge (V) | Shot Reps | Powder Size (mi-crons) | Purpose | Mass Gain (mg) |
|---|---|---|---|---|---|---|---|
| **Build-up Tests: 5-shot salvos until buildup is 16 mils** | | | | | | 100ms, 3", feed 2 (22.5 g/min) | |
| T165, S108 | 11/14/1997 | 3700 | **3400** | 5 | **45-90** | | |
| **Start over with new target (punched target)** | | | | | | | |
| T166, S109 | 11/14/1997 | 3700 | **3400** | 5 | **45-90** | | 84.3 |
| T167, S109 | 11/14/1997 | 3700 | **3400** | 5 | **45-90** | | 80.8 |
| T168, S109 | 11/14/1997 | 3700 | **3400** | 5 | **45-90** | | 79.8 |
| T169, S109 | 11/14/1997 | 3700 | **3400** | 5 | **45-90** | | 81.4 |
| T170, S109 | 11/14/1997 | 3700 | **3400** | 5 | **45-90** | | 87.6 |
| T171, S109 | 11/14/1997 | 3700 | **3400** | 5 | **45-90** | | 73.0 |
| T172, S109 | 11/14/1997 | 3700 | **3400** | 5 | **45-90** | | 79.1 |
| T173, S109 | 11/14/1997 | 3700 | **3400** | 5 | **45-90** | | 94.8 |
| T174, S109 | 11/14/1997 | 3700 | **3400** | 5 | **45-90** | | 86.6 |
| | | | | | | **TOTAL (9 salvos):** | **747.4** |
| | | | | | | **Average per salvo:** | **135.0** |
| **Work System up to 10-Shot salvos** | | | | | | | |
| T175 | 11/18/1997 | **3700** | 3400 | 10 | 0 | Try to achieve 10 dis-charges | |
| T176 | 11/18/1997 | **4000** | 3400 | 10 | 0 | | |
| T177 | 11/18/1997 | **4500** | 3400 | 10 | 0 | | |
| **Build-up Test: 10-shot salvos until buildup is 16 mils** | | | | | | 100ms, 3", feed 2 (22.5 g/min) | |
| T178, S110 | 11/18/1997 | **4600** | 3400 | 10 | **45-90** | | 125.3 |
| T179, S110 | 11/18/1997 | **4600** | 3400 | 10 | **45-90** | | - |
| T180, S112 | 11/18/1997 | **4600** | 3400 | 10 | **45-90** | | 140.5 |
| T181, S112 | 11/18/1997 | **4600** | 3400 | 10 | **45-90** | | 146.8 |
| T182, S112 | 11/18/1997 | **4600** | 3400 | 10 | **45-90** | | 134.8 |

Table A-1. EPD system tests (contd.)

| Shot No. | Date | Re-charge Bank Charge (V) | Approx PFN Charge (V) | Shot Reps | Powder Size (mi-crons) | Purpose | Mass Gain (mg) |
|---|---|---|---|---|---|---|---|
| T183, S112 | 11/18/1997 | **4600** | 3400 | 10 | **45-90** | | 126.1 |
| T184, S112 | 11/18/1997 | **4600** | 3400 | 10 | **45-90** | | 126.6 |
| | | | | | | **TOTAL (5 salvos):** | **674.8** |
| | | | | | | **Average per salvo:** | **135.0** |
| **Removable coating test: shoot at ceramic tile** | | | | | | 100ms, 3", feed 2 (22.5 g/min) | |
| T185, tile | 11/18/1997 | **4600** | 3400 | 10 | **45-90** | | - |
| Testing week of 12/01/97: | | | | | | | |
| Still using RF signal generator setting of 0.30V (plasma on), 12 CFH seed gas. 20 SCFH aux. gas. 70 CFH shield. | | | | | | | |
| Check-outs: | | | | | | | |
| T186 | 12/2/1997 | **1000** | | 10 | 0 | checkout shot | |
| T187 | 12/2/1997 | **1000** | | 10 | 0 | checkout shot | |
| T188 | 12/2/1997 | **1000** | | 10 | 0 | checkout shot | |
| T189 | 12/2/1997 | **3700** | | 10 | 0 | checkout shot | |
| T190 | 12/2/1997 | **4600** | 3400 | 10 | 0 | checkout shot | |
| T191 | 12/2/1997 | **4600** | 3400 | 10 | 0 | checkout shot | |
| T192 | 12/2/1997 | **1000** | | 10 | 0 | checkout shot | |
| T193 | 12/2/1997 | **4600** | 3400 | 10 | 0 | checkout shot | |
| **First Build-up Coating for Tensile Tests** | | | | | | Build-up 20 mils minimum (measured at edge) | |
| T194, S1t | 12/2/1997 | **4600** | 3400 | 10 | **45-90** | | 146.7 |
| T195, S1t | 12/2/1997 | **4600** | 3400 | 10 | **45-90** | | |
| **Started over with new substrate, S2t** | | | | | | | |
| T196, S2t | 12/2/1997 | **4600** | 3400 | 10 | **45-90** | | 138.1 |
| T197, S2t | 12/2/1997 | **4600** | 3400 | 10 | **45-90** | | |
| **Started over with new substrate, S3t** | | | | | | | |
| T198, S3t | 12/2/1997 | **4600** | 3400 | 10 | **45-90** | | 137.8 |
| T199, S3t | 12/2/1997 | **4600** | 3400 | 10 | **45-90** | | 138.9 |
| T200, S3t | 12/3/1997 | **4600** | 3400 | 10 | **45-90** | | 132.0 |
| T201, S3t | 12/3/1997 | **4600** | 3400 | 10 | **45-90** | | 156.6 |
| T202, S3t | 12/3/1997 | **4600** | 3400 | 10 | **45-90** | | 136.6 |
| T203, S3t | 12/3/1997 | **4600** | 3400 | 10 | **45-90** | | 144.0 |
| T204, S3t | 12/3/1997 | **4600** | 3400 | 10 | **45-90** | | 120.0 |

Table A-1. EPD system tests (contd.)

| Shot No. | Date | Re-charge Bank Charge (V) | Approx PFN Charge (V) | Shot Reps | Powder Size (mi-crons) | Purpose | Mass Gain (mg) |
|---|---|---|---|---|---|---|---|
| T205, S3t | 12/3/1997 | **4600** | 3400 | 10 | **45-90** | | 146.9 |
| T206, S3t | 12/3/1997 | **4600** | 3400 | 10 | **45-90** | | 144.9 |
| T207, S3t | 12/3/1997 | **4600** | 3400 | 10 | **45-90** | | 139.0 |
| T208, S3t | 12/3/1997 | **4600** | 3400 | 10 | **45-90** | | 124.1 |
| | | | | | | **TOTAL (11 bursts):** | **1520.8** |
| | | | | | | **Average per burst:** | **138.3** |
| **Second Build-up Coating for Tensile Tests, S4t** | | | | | | | |
| T209, S4t | 12/3/1997 | **4600** | 3400 | 10 | **45-90** | | 138.7 |
| T210, S4t | 12/3/1997 | **4600** | 3400 | 10 | **45-90** | | 139.1 |
| T211, S4t | 12/3/1997 | **4600** | 3400 | 10 | **45-90** | | 127.8 |
| T212, S4t | 12/3/1997 | **4600** | 3400 | 10 | **45-90** | | 135.0 |
| T213, S4t | 12/3/1997 | **4600** | 3400 | 10 | **45-90** | | 127.8 |
| T214, S4t | 12/3/1997 | **4600** | 3400 | 10 | **45-90** | | 115.1 |
| T215, S4t | 12/3/1997 | **4600** | 3400 | 10 | **45-90** | | 128.0 |
| T216, S4t | 12/3/1997 | **4600** | 3400 | 10 | **45-90** | | 120.6 |
| T217, S4t | 12/4/1997 | **4600** | 3400 | 10 | **45-90** | | 176.6 |
| T218, S4t | 12/4/1997 | **4600** | 3400 | 10 | **45-90** | | 155.8 |
| T219, S4t | 12/4/1997 | **4600** | 3400 | 10 | **45-90** | | 139.8 |
| T220, S4t | 12/4/1997 | **4600** | 3400 | 10 | **45-90** | | 121.2 |
| | | | | | | **TOTAL (12 bursts):** | **1625.5** |
| | | | | | | **Average per burst:** | **135.5** |

Testing week of 12/08/97:

Removed powder from hopper and added more to it, dried in oven, and refilled hopper.

**ATP:**

**D Series: SBA (auxiliaries)**

**Tests**

| | | | | | | | |
|---|---|---|---|---|---|---|---|
| D.4 | 12/8/1997 | RFPG: Plasma start-up was slow but full width. 49 MHz. Power traces printed out. Base Forward = 122 W, Reverse = 76 W. | | | | | |
| D.2 Trial 1 | 12/8/1997 | Powder Feed 6 sec: Incorrect measurement of 0.37g/min was due to no aux. flow and/or first run of the refilled hopper. | | | | | |
| D.2 Trial 2 | 12/8/1997 | Powder Feed 6 sec (gun): | | | 15.3 g/min | Pooling at 0.712 g | 22.4 g/min |

Table A-1. EPD system tests (contd.)

| Shot No. | Date | Re-charge Bank Charge (V) | Approx PFN Charge (V) | Shot Reps | Powder Size (mi-crons) | Purpose | Mass Gain (mg) |
|---|---|---|---|---|---|---|---|
| D.2 Trial 3 | 12/8/1997 | Powder Feed 6 sec (gun): | | | 17.2 g/min | Pooling at 1.1519 g | 28.7 g/min |
| D.2 Trial 4 | 12/8/1997 | Powder Feed 6 sec (gun): | | | 20.0 g/min | Pooling at 1.3448 g | 33.4 g/min |
| D.3 | 12/8/1997 | Cleaned around chamber and verified no powder leaking. | | | | | |
| D.1 | 12/8/1997 | Zinc-air battery test of shield gas showed less than 2% air present after 5 min of shield gas flow. | | | | | |
| **E Series: Multi-Shot Tests** | | | | | | | |
| T221, S117 | 12/8/1997 | 4600 | 3400 | 10 | 45-90 | E.1,100ms, 3", feed setting #2 (3.5 turns, nominally 22.5 g/min) | 305.6 |
| T222, S118 | 12/9/1997 | 4600 | 3400 | 10 | 45-90 | E.1, Better resolution on Bdots;1st 5. | 157.8 |
| T223, S119 | 12/9/1997 | 4600 | 3400 | 10 | 45-90 | E.1, Better resolution on Bdots;2nd 5. | 152.1 |
| **F Series: Parametric Adjustment Tests** | | | | | | | |
| Changed powder feed setting and meas-ured: | | | | | | powder feed setting #1 (3.75 turns, nominally 15 g/min) | |
| | 12/9/1997 | Powder Feed 6 sec (injctr): | | | 18.1 g/min | | |
| | 12/9/1997 | Powder Feed 6 sec (gun): | | | 10.7 g/min | Pooling at 0.2750 g | 13.4 g/min |
| T224, S120 | 12/9/1997 | 4600 | 3400 | 10 | 45-90 | F.1.1, Reduced feed rate; Bdot moved to #1 position (4.37 cm from cavity) | 178.6 |
| Changed powder feed back to setting #2 (3.5 turns). Changed time between shots to 50ms. | | | | | | | |
| T225, S121 | 12/9/1997 | 4600 | 3400 | 10 | 45-90 | F.1.2, Shot to shot time 50 ms | 105.7 |
| T226, S122 | 12/9/1997 | 4600 | 3400 | 10 | 45-90 | F.1.2, Shot to shot time 55 ms | 66.5 |
| T227, S123 | 12/9/1997 | 4600 | **2840** | 10 | 45-90 | F.1.3, Ability to change PFN voltage | 72.7 |
| T228, S124 | 12/9/1997 | 3700 | 3400 | **5** | 45-90 | Ability to change no. of shots | 49.4 |
| **G Series: MSPS Safety Features Tests** | | | | | | | |
| T229 | 12/9/1997 | 800 | - | - | 0 | G.1.1, Overcurrent fault test | |
| T230 | 12/9/1997 | 800 | - | - | 0 | repeat w/ RF plasma on | |
| T231 | 12/9/1997 | 2200 | - | - | 0 | G.2.1 | |
| T232 | 12/9/1997 | 2200 | - | - | 0 | G.3.1 | |

Table A-1. EPD system tests (contd.)

| Shot No. | Date | Re-charge Bank Charge (V) | Approx PFN Charge (V) | Shot Reps | Powder Size (mi-crons) | Purpose | Mass Gain (mg) |
|---|---|---|---|---|---|---|---|
| **E Series repeats using higher frequency B-dot sampling to get more precise velocity data** | | | | | | | |
| T233, S125 | 12/10/1997 | 4600 | 3400 | 10 | 45-90 | | 138.3 |
| T234, S126 | 12/10/1997 | 4600 | 3400 | 10 | 45-90 | | 93.9 |
| T235, S127 | 12/10/1997 | 4600 | 3400 | 10 | 45-90 | | 113.7 |
| T236, S128 | 12/10/1997 | 4600 | 3400 | 10 | 45-90 | | 117.3 |
| T237, S129 | 12/10/1997 | 4600 | 3400 | 10 | 45-90 | | 114.2 |
| T238, S130 | 12/10/1997 | 4600 | 3400 | 10 | 45-90 | | 119.7 |
| **Sample Coatings for TEM** | | | | | | | |
| T238, S131 | 12/11/1997 | 4600 | 3400 | 10 | 45-90 | Normal substrate; took extra care to not contaminate | - |
| T240 | 12/11/1997 | 4600 | 3400 | 10 | 0 | Plasma only to clear any possible cleaning debris. | - |
| T241, S-Ice | 12/11/1997 | 4600 | 3400 | 10 | 45-90 | Ice substrate | - |
| Testing week of 12/15/97: | | | | | | | |
| **Coatings to study effects of surface finish and target thickness** | | | | | | | |
| T242, S5t-g | 12/17/1997 | 4600 | 3400 | 10 | 45-90 | Coat onto ground surface | 230.4 |
| T243, S5t-l | 12/17/1997 | 4600 | 3400 | 10 | 45-90 | Coat onto lathe mchn'd surface | 145.6 |
| T244, S2t-g | 12/17/1997 | 4600 | 3400 | 10 | 45-90 | Coat onto ground surface | 134.0 |
| T245, S132 | 12/17/1997 | 4600 | 3400 | 10 | 45-90 | Coat onto thin target | 117.0 |

In tests 221-238 the ATP was executed for the Air Force. The purpose was to verify Prototype EPD System integration and operation. These tests verify the proper integration and operation of the subsystems supporting the Square Bore Accelerator (SBA), the single-shot and multi-shot powder deposition capabilities of the Prototype EPD System as well as the flexibility of the multi-shot power supply (MSPS). All available diagnostics were used to verify system operation. The metallurgical properties of the coatings produced by the Prototype EPD System during these acceptance tests were fully evaluated.

Proper integration and operation of the subsystems supporting the SBA includes verification of integration and operation for the radio frequency plasma generator (RFPG) subsystem, and the powder feeder (PF) subsytem as well as the proper application of argon shield gas to the target substrate. In addition, the operation of the powder containment chamber (PCC) attached to the end of the SBA were verified.

Powder velocity was provided by simulation results using plasma velocity based on b-dot data. A single shot test was performed to verify that powder velocities of 2 km/s ( plus or minus error band) were produced by the system. In addition, supporting data from gun current and b-dot coils was provided for tracking system performance against the expectations of the snowplow.

A multi-shot test was performed to demonstrate the multiple impact deposition capabilities of the Prototype EPD System. All of the diagnostics used in the single-shot test were applied to the multi-shot test. The measurements of most

importance acquired evidence of 2 km/s (plus or minus error band) powder velocities for each shot, and the creation of a snowplowing plasma armature for each shot. Finally, plasma re-strike for the RFPG were verified by the b-dot probe voltage traces.

Parametric adjustment tests were performed to demonstrate the flexibility and safety features of the MSPS and other subsystems. Flexibility of operation is intended to provide the capability to optimize system operation based on a given performance criteria for the resulting coatings such as mass gain, or bond strength. The safety features of the MSPS were intended to eliminate risk to personnel and equipment during system operation.

When the Augmented Square Bore Accelerator (ASBA) was introduced to lower the power demand of the process it was necessary to show that the augmenting field had no influence on the snowplow process. Table A-2 presents tests conducted with the ASBA and demonstrate that it produced required arc velocities at greatly reduced currents.

Table A-3 lists results from coating tests with the augmented square bore railgun.

Table A-2. ASBA test results

| Test Number | Shot Number | Inductor Current (A) | PFN Voltage (V) | Gun Current (kA) | Velocity (m/s) | Time Btw Shots (ms) |
|---|---|---|---|---|---|---|
| **T360** | 1 | 1,092 | 2,947 | 104.3 | 4,167 | 150 |
| | 2 | 1,109 | 3,043 | 106.9 | 4,268 | |
| | 3 | 1,078 | 2,947 | 102.4 | 4,487 | |
| | 4 | 1,099 | 3,018 | 105.1 | 4,861 | |
| | 5 | 1,067 | 2,928 | 100.5 | 4,487 | |
| | 6 | 1,087 | 3,008 | 103.5 | 4,375 | |
| | 7 | 1,058 | 2,918 | 99.6 | 4,070 | |
| | 8 | 1,051 | 2,928 | 100.0 | 4,167 | |
| | 9 | 1,044 | 2,925 | 99.9 | 4,268 | |
| | 10 | 1,040 | 2,922 | 99.4 | 4,268 | |
| **T361** | 1 | 1,077 | 2,902 | 103.5 | 3,723 | 200 |
| | 2 | 1,081 | 2,896 | 102.4 | 4,167 | |
| | 3 | 1,068 | 2,896 | 101.5 | 4,375 | |
| | 4 | 1,090 | 2,973 | 104.3 | 4,487 | |
| | 5 | 1,060 | 2,947 | 109.1 | 4,605 | |
| | 6 | 1,056 | 2,877 | 99.9 | 4,167 | |
| | 7 | 1,051 | 2,874 | 99.0 | 4,070 | |
| | 8 | 1,045 | 2,886 | 99.3 | 4,320 | |
| | 9 | 1,040 | 2,944 | 107.1 | 4,268 | |
| | 10 | 1,066 | 2,954 | 102.2 | 4,375 | |
| **T362** | 1 | 1,073 | 2,890 | 102.9 | 3,977 | 200 |
| | 2 | 1,070 | 2,906 | 102.3 | 3,977 | |
| | 3 | 1,075 | 2,896 | 101.3 | 4,375 | |
| | 4 | 1,060 | 2,880 | 100.9 | 4,375 | |
| | 5 | 1,082 | 2,960 | 103.7 | 4,487 | |
| | 6 | 1,077 | 2,950 | 103.4 | 4,730 | |
| | 7 | 1,046 | 2,867 | 99.5 | 4,167 | |
| | 8 | 1,042 | 2,864 | 99.5 | 4,070 | |
| | 9 | 1,037 | 2,870 | 98.5 | 4,070 | |
| | 10 | 1,060 | 2,934 | 101.7 | 4,375 | |
| **T363** | 1 | 1,083 | 2,931 | 104.4 | 3,646 | 150 |
| | 2 | 1,086 | 2,922 | 102.3 | 4,268 | |
| | 3 | 1,075 | 2,950 | 101.3 | 4,375 | |
| | 4 | 1,098 | 3,024 | 104.2 | 4,730 | |
| | 5 | 1,063 | 2,915 | 101.7 | 4,268 | |

Table A-2. ASBA test results (contd.)

| Test Number | Shot Number | Inductor Current (A) | PFN Voltage (V) | Gun Current (kA) | Velocity (m/s) | Time Btw Shots (ms) |
|---|---|---|---|---|---|---|
| **T364** | 1 | 1,083 | 2,938 | 104.2 | 3,723 | 150 |
| | 2 | 1,105 | 3,024 | 106.6 | 4,375 | |
| | 3 | 1,077 | 2,922 | 101.1 | 4,605 | |
| | 4 | 1,072 | 2,931 | 101.0 | 4,375 | |
| | 5 | 1,060 | 2,918 | 100.4 | 4,605 | |
| | 6 | 1,090 | 2,989 | 103.1 | 4,605 | |
| | 7 | 1,090 | 3,002 | 103.1 | 4,375 | |
| | 8 | 1,083 | 2,989 | 102.9 | 4,375 | |
| | 9 | 1,078 | 2,963 | 102.2 | 4,268 | |
| | 10 | 1,034 | 2,877 | 98.2 | 4,268 | |
| **T365** | 1 | 1,089 | 2,934 | 104.1 | 3,889 | 100 |
| | 2 | 1,081 | 2,922 | 102.8 | 4,487 | |
| | 3 | 1,080 | 2,944 | 101.5 | 4,487 | |
| | 4 | 1,073 | 2,922 | 100.4 | 4,375 | |
| | 5 | 1,097 | 2,995 | 99.2 | 4,431 | |
| | 6 | 1,067 | 2,922 | NA | NA | |
| | 7 | 1,085 | 2,979 | NA | NA | |
| | 8 | 1,056 | 2,906 | NA | NA | |
| | 9 | 1,046 | 2,973 | NA | NA | |
| **T368** | 1 | 1,162 | 3,146 | 110.7 | 4,487 | 175 |
| | 2 | 1,162 | 3,152 | 109.9 | 4,605 | |
| | 3 | 1,158 | 3,155 | 108.5 | 4,861 | |
| | 4 | 1,173 | 3,222 | 111.2 | 5,303 | |
| | 5 | 1,148 | 3,123 | 106.9 | 5,000 | |
| | 6 | 1,169 | 3,206 | 110.0 | 5,303 | |
| | 7 | 1,132 | 3,126 | 106.3 | 5,000 | |
| | 8 | 1,158 | 3,200 | 108.9 | 4,730 | |
| | 9 | 1,124 | 3,107 | 105.5 | 5,000 | |
| | 10 | 1,126 | 3,107 | 105.1 | 4,730 | |
| **T370** | 1 | 1,256 | 3,386 | 124.3 | 5,000 | 175 |
| | 2 | 1,250 | 3,411 | 119.1 | 4,861 | |
| | 3 | 1,244 | 3,392 | 117.0 | 5,303 | |
| | 4 | 1,234 | 3,398 | 115.8 | 5,303 | |
| | 5 | 1,232 | 3,395 | 115.8 | 5,303 | |
| | 6 | 1,247 | 3,456 | 117.9 | 5,645 | |
| | 7 | 1,251 | 3,459 | 117.9 | 6,034 | |
| | 8 | 1,249 | 3,453 | 117.4 | 5,303 | |
| | 9 | 1,209 | 3,363 | 114.1 | 5,645 | |
| | 10 | 1,217 | 3,424 | 139.4 | NA | |

Table A-2. ASBA test results (contd.)

| Test Number | Shot Number | Inductor Current (A) | PFN Voltage (V) | Gun Current (kA) | Velocity (m/s) | Time Btw Shots (ms) |
|---|---|---|---|---|---|---|
| **T401** | 1 | 982 | 2,608 | 96.4 | 3,540 | 175 |
| | 2 | 1,005 | 2,726 | 99.5 | 4,083 | |
| | 3 | 1,005 | 2,707 | 99.8 | 4,142 | |
| | 4 | 1,007 | 2,733 | 99.0 | 4,046 | |
| | 5 | 968 | 2,598 | 94.2 | 3,768 | |
| | 6 | 993 | 2,698 | 97.6 | 3,851 | |
| | 7 | 963 | 2,573 | 93.4 | 3,752 | |
| | 8 | 986 | 2,675 | 96.9 | 3,973 | |
| | 9 | 953 | 2,566 | 93.2 | 3,801 | |
| | 10 | 950 | 2,602 | 93.5 | 3,705 | |
| **T402** | 1 | 986 | 2,634 | 97.2 | 3,818 | 175 |
| | 2 | 1,014 | 2,761 | 100.5 | 4,142 | |
| | 3 | 1,014 | 2,739 | 100.4 | 4,065 | |
| | 4 | 981 | 2,627 | 95.4 | 3,955 | |
| | 5 | 1,002 | 2,733 | 98.8 | 4,009 | |
| | 6 | 974 | 2,618 | 94.8 | 4,009 | |
| | 7 | 999 | 2,707 | 98.8 | 4,046 | |
| | 8 | 999 | 2,733 | 98.8 | 3,991 | |
| | 9 | 994 | 2,701 | 98.3 | 4,103 | |
| | 10 | 957 | 2,598 | 93.6 | 3,801 | |
| **T403** | 1 | 983 | 2,608 | 97.2 | 3,430 | 175 |
| | 2 | 1,006 | 2,720 | 99.3 | 3,991 | |
| | 3 | 1,006 | 2,707 | 100.7 | 4,181 | |
| | 4 | 1,007 | 2,730 | 99.7 | 4,065 | |
| | 5 | 998 | 2,707 | 98.9 | 4,046 | |
| | 6 | 966 | 2,579 | 94.0 | 3,991 | |
| | 7 | 988 | 2,698 | 98.1 | 4,142 | |
| | 8 | 959 | 2,586 | 94.2 | 3,991 | |
| | 9 | 981 | 2,669 | 97.5 | 4,028 | |
| | 10 | 984 | 2,682 | 98.0 | 4,122 | |
| **T404** | 1 | 973 | 2,582 | 95.5 | 3,658 | NA |
| **T405** | 1 | 966 | 2,554 | 94.7 | 3,628 | 175 |
| | 2 | 989 | 2,653 | 97.4 | 3,902 | |
| | 3 | 989 | 2,662 | 97.9 | 3,991 | |
| | 4 | 985 | 2,656 | 97.5 | 4,142 | |
| | 5 | 952 | 2,554 | 92.7 | 3,736 | |
| | 6 | 978 | 2,630 | 96.7 | 3,801 | |
| | 7 | 979 | 2,650 | 96.7 | 3,955 | |
| | 8 | 939 | 2,544 | 91.8 | 3,817 | |

Table A-2. ASBA test results (contd.)

| Test Number | Shot Number | Inductor Current (A) | PFN Voltage (V) | Gun Current (kA) | Velocity (m/s) | Time Btw Shots (ms) |
|---|---|---|---|---|---|---|
| | 9 | 970 | 2,627 | 95.6 | 3,768 | |
| | 10 | 932 | 2,525 | 91.5 | 3,752 | |
| **T406** | 1 | 959 | 2,560 | 93.2 | 3,569 | 175 |
| | 2 | 982 | 2,646 | 96.0 | 3,955 | |
| | 3 | 953 | 2,554 | 92.8 | 3,955 | |
| | 4 | 979 | 2,643 | 96.2 | 3,584 | |
| | 5 | 976 | 2,650 | 96.1 | 3,955 | |
| | 6 | 976 | 2,659 | 95.6 | 3,643 | |
| | 7 | 973 | 2,669 | 95.8 | 3,818 | |
| | 8 | 937 | 2,531 | 91.0 | 3,736 | |
| | 9 | 935 | 2,608 | 99.9 | 3,705 | |
| | 10 | 931 | 2,541 | 90.5 | 3,658 | |
| **T407** | 1 | 964 | 2,563 | 94.0 | 3,498 | 175 |
| | 2 | 988 | 2,656 | 97.0 | 3,937 | |
| | 3 | 986 | 2,672 | 97.5 | 3,885 | |
| | 4 | 985 | 2,669 | 96.8 | 4,009 | |
| | 5 | 950 | 2,560 | 91.8 | 3,587 | |
| | 6 | 974 | 2,637 | 95.5 | 3,674 | |
| | 7 | 978 | 2,653 | 95.6 | 3,817 | |
| | 8 | 971 | 2,630 | 95.5 | 3,851 | |
| | 9 | 938 | 2,528 | 91.0 | 3,555 | |
| | 10 | 935 | 2,538 | 91.1 | 3,584 | |
| **T408** | 1 | 967 | 2,582 | 94.6 | 3,555 | 175 |
| | 2 | 994 | 2,672 | 97.6 | 4,142 | |
| | 3 | 962 | 2,573 | 93.5 | 4,028 | |
| | 4 | 986 | 2,666 | 96.7 | 4,103 | |
| | 5 | 984 | 2,669 | 96.5 | 3,885 | |
| | 6 | 949 | 2,557 | 92.2 | 3,851 | |
| | 7 | 948 | 2,566 | 92.2 | 3,834 | |
| | 8 | 946 | 2,557 | 92.1 | 3,885 | |
| | 9 | 973 | 2,627 | 95.6 | 3,973 | |
| | 10 | 971 | 2,659 | 95.8 | 3,920 | |

Table A-3. Augmented square bore coupon results

| Shot # | Substrate # | Sub. Mat | Powder | Powd. Delay | Shot Delay | Current | Mass Gain |
|---|---|---|---|---|---|---|---|
| T401 | S158 | Ti 6Al-4V | Ti 6Al-4V | 3 s | 175 ms | 100 kA | 373.5 mg |
| T402 | S159 | Ti 6Al-4V | Ti 6Al-4V | 1 s | 175 ms | 100 kA | 163 mg |
| T403 | S160 | Ti 6Al-4V | Ti 6Al-4V | 1 s | 175 ms | 100 kA | 293 mg |
| T404 | S161 | Ti 6Al-4V | Ti 6Al-4V | 1 s | 175 ms | 100 kA | 16.8 mg |
| T405 | S162 | Ti 6Al-4V | Ti 6Al-4V | 1 s | 175 ms | 100 kA | 331.7 mg |
| T406 | S163 | Ti 6Al-4V | Ti 6Al-4V | 1 s | 175 ms | 100 kA | 473.5 mg |
| T407 | S164 | Ti 6Al-4V | Ti 6Al-4V | 1 s | 175 ms | 100 kA | 330.6 mg |
| T408 | S165 | Ti 6Al-4V | Ti 6Al-4V | 1 s | 175 ms | 100 kA | 284.7 mg |
| T412 | S169 | Inconel | Chrome | 1 s | 175 ms | 100 kA | 132.0mg |
| T413 | S170 | Inconel | Chrome | 1 s | 175 ms | 100 kA | 1086.0 mg |
| T415 | S171 | Inconel | Chrome | 1 s | 175 ms | 100 kA | 242.3 mg |
| T416 | S172 | Inconel | Chrome | 1 s | 175 ms | 100 kA | 499.4 mg |
| T417 | S173 | Inconel | Chrome | 1 s | 175 ms | 100 kA | 391.1 mg |
| T418 | S174 | Inconel | Chrome | 1 s | 175 ms | 100 kA | 568.6 mg |
| T419 | S175 | Inconel | Chrome | 1 s | 175 ms | 100 kA | 383.6 mg |
| T420 | S176 | Inconel | Chrome | 1 s | 175 ms | 100 kA | 264.1 mg |
| T421 | S177 | Inconel | Chrome | 1 s | 175 ms | 100 kA | 169.5 mg |

# REFERENCES


[1] R. McCune, "An Exploration of the Cold Gas-Dynamic Spray Method for Several Materials Systems," *Proc. of the 8th National Thermal Spray Conf.*, 1995.

[2] J.L. Bacon, D.G. Davis, R.J. Polizzi, R.L. Sledge, J.R. Uglum, W.F. Weldon, R.C. Zowarka, "Method and Apparatus for Electromagnetic Powder Deposition", U.S. Patent No. 6,329,025.

[3] J. W. Shearer, "Xenon Shock Waves Driven by High Magnetic Fields," Proc. 2nd International Conf. on Megagauss Magnetic Fields", 1979.

[4] R.C. Zowarka, J.R. Uglum, J.L. Bacon, M.D. Driga, R.L. Sledge, D.G Davis, "Electromagnetic Powder Deposition Experiments", United Thermal Spray Conference, September 1997.

[5] J.R. Uglum, J.L.. Bacon, D.G. Davis, R.J. Polizzi, R.L. Sledge, R.C. Zowarka, "Scaling Analysis of the Electromagnetic Powder Deposition Gun", United Thermal Spray Conference, September 1997.

[6] Seigel, A.E., "The Theory of High Speed Guns, North Atlantic Treaty Organization Advisory Group for Aerospace Research and Development, AGARDograph 91", May 1965.

[7] Plapp, John E., "Engineering Fluid Mechanics", Prentice-Hall, Inc. Englewood Cliffs, New Jersey, 1968.

[8] H. Schlichting, "Boundary Layer Theory," Fourth Edition, McGraw-Hill Book Co., New York, NY, 1960.

[9] R.L. Sledge, J.L. Bacon, D.G. Davis, R.J. Polizzi, J.R. Uglum, R.C. Zowarka, "Arc Initiation for an Electromagnetic Deposition (EPD) Gun", United Thermal Spray Conference, September 1997.

[10] J.L. Bacon, J.R. Uglum, D.G Davis, R.J. Polizzi, R.L. Sledge, R.C. Zowarka, "The Diagnostic History of a New Electromagnetic Power Deposition System", United Thermal Spray Conference, September 1997.

[11] Jerald V. Parker, "Magnetic-Probe Diagnostics for Railgun Plasma Armatures", IEEE Transactions on Plasma Science, Vol. 17, No. 3, June 1989.

[12] K.A. Jamison, M.Marquez-Reines, and Henry S. Burden, "Measurements of the Spatial Distributions of Current in a Rail Gun Arc Armature," *IEEE Transactions on Magnetics*, Vol. Mag-20, No. 2, March 1984.

[13] Frederick W. Grover, “Inductance Calculations: Working Formulas and Tables”, Dover Publications Inc., New York, New York, 1946.

[14] W.F. Weldon, J.L. Bacon, D.A. Weeks, R.C. Zowarka, Jr., “Stiff Railguns”, IEEE Transactions on Magnetics, Vol. 27, No.1, January 1991.

[15] D.R. Peterson, D.A. Weeks, R.C. Zowarka, Jr., R.W. Cook, W.F. Weldon, “Testing of a High Performance, Precision Bore Railgun”, IEEE Transactions on Magnetics, Vol. Mag-22, No.6, November 1986.

[16] D.A. Weeks, W.F. Weldon, R.C. Zowarka, Jr., Hypervelocity Macroparticle Accelerator Experiments at CEM-UT”, IEEE Transactions on Magnetics, Vol. 27, No. 1, 1991.

[17] J.A. Leuer, “Electromagnetic Modeling of Complex Railgun Geometries”, IEEE Transactions on Magnetics, Vol. Mag-22, No. 6, November 1986.

[18] D.G. Davis, J.L. Bacon, R.L. Sledge, R.J. Polizzi, R.C. Zowarka, J.R. Uglum, “Multi-Shot Power Supply Using Capacitors for an Electromagnetic Powder Deposition (EPD) Gun”, 11th IEEE Pulsed Power Conference, Baltimore, Maryland, June 29-July 2, 1997.

# VITA

Raymond Charles Zowarka, Jr. was born in March 1950 in San Antonio, Texas, the son of Raymond C. Zowarka, Sr. and Mary Louise Buckholdt. He graduated from Antonian High School in San Antonio in 1968, and received Bachelor of Science in Engineering Science from Trinity University in San Antonio, Texas in 1972 and Master of Science degrees in Electrical Engineering from the University of Texas at Austin in 1980. Since then, he has worked in university research. He has held the positions of Research Engineer from 1974 to 1984, Research Associate from 1984 to 1989, and became Research Scientist in 1989. He is currently employed as a Research Scientist with the Center for Electromechanics at the University of Texas in Austin. In January 1995 he re-entered the Graduate School at the University of Texas.

Permanent address: 8900 N.I.H. 35, #1086, Austin, Texas 78753

This dissertation was typed by the author.